

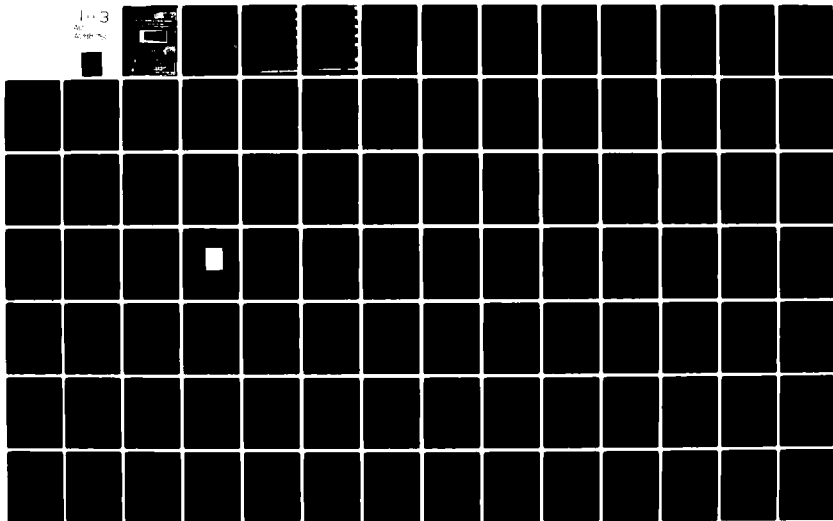
AD-A088 750

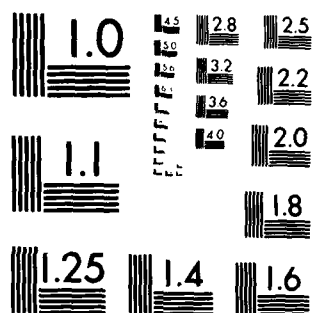
PURDUE UNIV LAFAYETTE IND RAY W HERRICK LABS F/G 20/4  
COHERENT STRUCTURES IN THE SIMILARITY REGION OF A TWO-DIMENSION--ETC(U)  
MAR 80 J W OLER, V W GOLDSCHMIDT N00014-75-C-1048  
HL-80-6 NL

UNCLASSIFIED

1-3

2-10-80





MICROCOPY RESOLUTION TEST CHART  
NATIONAL BUREAU OF STANDARDS 1963 A

Prepared Partly Under ONR N0014-75-C-1048  
And NSF (GK 19317A3, Eng 74-20780)

15) N00014-75-C-1048  
✓ NSF-ENG 74-20780

12) 198

6) COHERENT STRUCTURES IN THE SIMILARITY  
REGION OF A TWO-DIMENSIONAL TURBULENT  
JET: A VORTEX STREET,

11) Mar 80  
Sponsored by  
Office of Naval Research  
and  
National Science Foundation

14) HL-80-6

10) James Walter/Oler  
Victor W. Goldschmidt

DTIC  
ECTE  
AUG 28 1980  
D  
C

Submitted by:

James W. Oler, Graduate Research Assistant  
Victor W. Goldschmidt, Principal Investigator

Approved by:

Raymond Cohen, Director  
Ray W. Herrick Laboratories

March 1980

This document has been approved  
for public release and sale; its  
distribution is unlimited.

407205 xlt

REPORT DOCUMENTATION PAGE		READ INSTRUCTIONS BEFORE COMPLETING FORM
1. REPORT NUMBER	2. GOVT ACCESSION NO. <b>AD-A088750</b>	3. RECIPIENT'S CATALOG NUMBER <b>750</b>
4. TITLE (and Subtitle) <b>Coherent Structures in the Similarity Region of a Two-Dimensional Turbulent Jet: A Vortex Street</b>		5. TYPE OF REPORT & PERIOD COVERED
7. AUTHOR(s) <b>J.W. Oler and V.W. Goldschmidt</b>		8. PERFORMING ORG. REPORT NUMBER <b>HL 80-6</b>
9. PERFORMING ORGANIZATION NAME AND ADDRESS <b>School of Mechanical Engineering/ Ray W. Herrick Laboratories Purdue University West Lafayette, IN 47907</b>		6. CONTRACT OR GRANT NUMBER(s) <b>N00014-75-C-1048</b>
11. CONTROLLING OFFICE NAME AND ADDRESS <b>Fluid Dynamics Program Office of Naval Research Arlington, Virginia 22217</b>		10. PROGRAM ELEMENT, PROJECT, TASK AREA & WORK UNIT NUMBERS <b>N66005</b>
14. MONITORING AGENCY NAME & ADDRESS (if different from Controlling Office)		12. REPORT DATE <b>March 1980</b> 13. NUMBER OF PAGES <b>Distributed 6/1980 4 microfiche -196 pp.</b>
		15. SECURITY CLASS. (of this report) <b>Unclassified</b>
16. DISTRIBUTION STATEMENT (of this Report)		15a. DECLASSIFICATION/DOWNGRADING SCHEDULE <b>N/A</b>
<div style="border: 1px solid black; padding: 5px; transform: rotate(-2deg); display: inline-block;"> <p>This document has been approved for public release and sale; its distribution is unlimited.</p> </div>		
17. DISTRIBUTION STATEMENT (of the abstract entered in Block 20, if different from Report)		
18. SUPPLEMENTARY NOTES		
19. KEY WORDS (Continue on reverse side if necessary and identify by block number)		
<b>Turbulence, Jets, Coherent Structures</b>		
20. ABSTRACT (Continue on reverse side if necessary and identify by block number)		
<p>The characteristics of the coherent structures of a plane jet were evaluated experimentally and with a kinematic numerical representation.</p> <p>Distributions of intermittency and interface crossing frequency were measured for <math>10 &lt; x/D &lt; 60</math>. These properties, including the maximum interface crossing frequency, were found to scale as</p>		

self-preserving flow variables.

Spatially coherent patterns within the turbulent velocity field were evaluated utilizing two point velocity correlation measurements. From these, it was found that the instantaneous velocity fluctuation distributions are antisymmetric with respect to the centerline and coherent over the entire width of the flow field. In addition, the patterns are periodic in the streamwise direction.

The two-dimensionality of the large structures was evaluated through the comparison of longitudinal and vertical integral length scales derived from correlations in both the fully turbulent zone and the intermittent region. In the intermittent region, the integral scales were approximately equal while in the fully turbulent zone, the longitudinal scale was approximately double the vertical one.

Utilizing a combination of flow visualization, structural passage frequency measurement and similarity considerations, the convective velocity of the vortex-like structures was estimated to be one half the mean centerline velocity.

From the experimental results, a hypothetical vortex street representation of the plane jet was formulated and evaluated numerically. This kinematic representation was found to be capable of generating realistic distributions of mean longitudinal and lateral velocity as well as the proper spreading and velocity decay rates. Although the correct magnitude of the Reynolds stress was calculated, its sign was in error. The small scales of turbulence were not included in the model and consequently, it was not possible to predict reasonable distributions of the fluctuation intensities, the energy spectra or interface properties.

# PURDUE UNIVERSITY

THE RAY W. HERRICK LABORATORIES  
A GRADUATE STUDENT RESEARCH FACILITY OF  
THE SCHOOL OF MECHANICAL ENGINEERING


July 24, 1980

Defense Technical Information  
Center  
Cameron Station  
Alexandria, VA 22314

Gentlemen:

Enclosed please note 12 microfiche and one hard bound copy of Report HL 80-6 prepared under ONR N0014-75-C-1048. Twelve hard bound copies will follow. They are currently being prepared by the printers.

Sincerely,

  
Victor W. Goldschmidt  
Professor of Mechanical  
Engineering

VWG/clm

Enclosure

cc: S. Doroff



West Lafayette, Indiana 47907  
Message Center: (317) 749-6321  
Telex: 272396 (HERL PU WLAF)

**Note:**

This report is part of a Thesis submitted by Dr. J.W. Oler in partial fulfillment of the requirements for his Ph.D. degree. The research described was completed in February 1980. Professor V.W. Goldschmidt assisted in the work as thesis advisor and major professor.

Accession For	
NTIS GRA&I	<input checked="checked" type="checkbox"/>
DDC TAB	<input type="checkbox"/>
Unannounced	<input type="checkbox"/>
Justification	for FL
182	20 Aug
By	80 on file
Distribution/	
Availability Codes	
Dist	Avail and/or special
A	

# TABLE OF CONTENTS

	Page
LIST OF TABLES . . . . .	vi
LIST OF FIGURES . . . . .	vii
NOMENCLATURE . . . . .	x
ABSTRACT . . . . .	xv
CHAPTER I - INTRODUCTION . . . . .	1
CHAPTER II - GENERAL BACKGROUND . . . . .	3
A. The Turbulent Plane Jet . . . . .	3
1. Initial Region . . . . .	3
2. Transition Region . . . . .	5
3. Similarity Region . . . . .	5
4. Intermittent Region . . . . .	9
B. Large Scales Structures in Turbulent Free Shear Flows . . . . .	9
1. Turbulent Mixing Layers . . . . .	10
2. Wake Flows . . . . .	13
3. Jet Flows . . . . .	14
CHAPTER III - EXPERIMENTAL TECHNIQUES . . . . .	20
A. Flow Field Apparatus . . . . .	20
B. Turbulence Detection and Inter- mittency Measurement . . . . .	22
1. The Indicator Signal, $S(\vec{r}, t)$ . . . . .	23
2. The Threshold, $C$ . . . . .	25
3. The Hold Time, $\tau_h$ . . . . .	27
4. The Analysis Technique . . . . .	30
C. Correlation Measurements . . . . .	32
1. Velocity Cross-Correlations . . . . .	32
2. Intermittency Cross-Correlations . . . . .	33



	Page
CHAPTER IV - EXPERIMENTAL RESULTS . . . . .	36
A. Intermittency and Interface Crossing Frequency . . . . .	37
B. Spatial Characteristics of the Large Structures . . . . .	45
1. Velocity Correlation Results . . . . .	46
2. Intermittency Correlation Results . . . . .	46
C. Two-Dimensionality . . . . .	49
1. Length Scales of the Intermittent Region . . . . .	51
2. Length Scales of the Turbulent Velocity Field . . . . .	54
D. Convective Velocities . . . . .	55
E. Summary . . . . .	66
CHAPTER V - A NUMERICAL SIMULATION . . . . .	67
A. Introduction . . . . .	67
B. Formulation of the Model . . . . .	69
1. The Rankine Vortex . . . . .	69
2. Similarity Scaling of the Vortex Street . . . . .	73
3. Specification of the Longitudinal Vortex Coordinates . . . . .	75
4. Calculation of Temporally Averaged Flow Properties . . . . .	78
C. Details of the Numerics . . . . .	81
D. Numerical Calculation Results . . . . .	83
1. Mean Longitudinal Velocities . . . . .	83
2. Mean Lateral Velocities . . . . .	87
3. Reynolds Stress Distributions . . . . .	92
4. Velocity Fluctuation Intensities . . . . .	95
5. Limitations of the Model . . . . .	98
E. The Mechanisms of Entrainment and Reynolds Stress Production . . . . .	99
F. Summary . . . . .	113

	Page
CHAPTER VI - CONCLUSIONS AND RECOMMENDATIONS . .	115
A. Conclusions Based on Experimental Results . . . . .	115
B. Conclusions Based on the Numerical Simulation . . . . .	117
LIST OF REFERENCES . . . . .	119
APPENDICES	
APPENDIX A - LITERATURE REVIEW - TURBULENCE DETECTION . . . . .	126
APPENDIX B - THE DIGITAL INTERMITTENCY MEASUREMENT TECHNIQUE . . . . .	133
APPENDIX C - THE HYBRID INTERMITTENCY INSTRUMENT . . . . .	141
APPENDIX D - NUMERICAL SENSITIVITY STUDY . .	160
VITA . . . . .	176

## LIST OF TABLES

Table		Page
4-1	Summary of Reported Structural Frequencies . . . . .	43
4-2	Summary of Structural Related Convection Velocities . . . . .	58
5-1	Summary of Numerical Simulation Parameters . . . . .	82

Appendix  
Tables

A-1	Turbulence Detection Techniques . . . . .	132
B-1	Program TDAP . . . . .	136
B-2	Program $\Delta$ TECTR . . . . .	139
C-1	Register Assignments . . . . .	146
C-2	Signal Analysis Timing Parameters . . . . .	148
C-3	Turbulence Analysis Routines . . . . .	151
C-4	Delay Line Routine . . . . .	158

## LIST OF FIGURES

Figure		Page
2-1	The Two-Dimensional Jet . . . . .	4
2-2	$\bar{U}/U_m$ vs. $y/b$ . . . . .	6
2-3	$U_m/U_o$ vs. $x/D$ . . . . .	7
2-4	$b/D$ vs. $x/D$ . . . . .	8
2-5	Organized Structures in Two-Dimensional Free Shear Flows . . . . .	17
3-1	Schematic of Plane Jet Apparatus . . . . .	21
3-2	Oscilloscope Trace of $S(\vec{r}, t)$ . . . . .	24
3-3	Formulation of $I(\vec{r}, t)$ . . . . .	26
3-4	Sensitivity of $f_Y/f_{Ym}$ to $\tau_h$ . . . . .	29
3-5	Sensitivity of $f_Y/f_{Ym}$ to Local Time Scales . . . . .	31
4-1	$\gamma$ vs. $(y-y_m)/b$ . . . . .	38
4-2	$f_Y/f_{Ym}$ vs. $(y-y_m)/b$ . . . . .	39
4-3	$f_{Ym}D/U_o$ vs. $x/D$ . . . . .	41
4-4	$R_U(0; 0, \delta_Y, 0)$ . . . . .	47
4-5	$R_U(0; \delta_X, \delta_Y, 0)$ . . . . .	48
4-6	$R_I(\tau; 0, 0, 0)$ . . . . .	50
4-7	$R_I(0; \delta_X, 0, 0)$ and $R_I(0; 0, 0, \delta_Z)$ . . . . .	52
4-8	$\Lambda_X^I/D$ and $\Lambda_Z^I/D$ vs. $x/D$ . . . . .	53
4-9	$R_U(0; \delta_X, 0, 0)$ and $R_U(0; 0, 0, \delta_Z)$ . . . . .	55
4-10	$R_I(\tau; \delta_X, 0, 0)$ . . . . .	60
4-11	$\tau_{peak}$ vs. $\Delta x$ . . . . .	61
4-12	$U_{CI}$ vs. $x/D$ . . . . .	62
4-13	$C_L$ vs. $x/D$ . . . . .	65
5-1	Tangential Velocity Field of a Rankine Vortex . . . . .	70
5-2	Induced Longitudinal and Lateral Velocities . . . . .	72

Figure		Page
5-3	Descriptive Parameters of a Vortex Street . . . . .	74
5-4	$\bar{U}(X,Y/B)/\bar{U}_m(X)$ vs. $Y/B$ . . . . .	84
5-5	$\bar{U}_m(X)$ vs. $X$ . . . . .	86
5-6	$\bar{U}(X,Y/B)/\bar{U}_m(X)$ vs. $Y/B$ for various $X_{max}$ . . . . .	88
5-7	Enlargement of Figure 5-6 . . . . .	89
5-8	$\bar{V}(X,Y/B)/\bar{U}_m(X)$ vs. $Y/B$ . . . . .	91
5-9	$ \bar{UV}(X,Y/B)/\bar{U}_m(X)^2 $ vs. $Y/B$ . . . . .	93
5-10	$U'(X,Y/B)/\bar{U}_m(X)$ vs. $Y/B$ . . . . .	96
5-11	$V'(X,Y/B)/\bar{U}_m(X)$ vs. $Y/B$ . . . . .	97
5-12	$U(X,Y/B;t)/\bar{U}_m(X)$ vs. $Y/B$ ; A spreading jet . . . . .	101
5-13	$U(X,Y/B;t)/\bar{U}_m(X)$ vs. $Y/B$ ; A parallel flow jet . . . . .	102
5-14	Temporal relationships between $U$ , $V$ and $UV$ . . . . .	104
5-15	Effect of $\beta$ on $\bar{U}(X,Y/B)/\bar{U}_m(X)$ vs. $Y/B$ . . . . .	107
5-16	Effect of $\beta$ on $\bar{V}(X,Y/B)/\bar{U}_m(X)$ vs. $Y/B$ . . . . .	108
5-17	Effect of $\beta$ on $ \bar{UV}(X,Y/B)/\bar{U}_m(X) $ vs. $Y/B$ . . . . .	109
5-18	$\delta\phi$ vs. $\beta$ . . . . .	110
5-19	Effect of $\beta$ on $U'(X,Y/B)/\bar{U}_m(X)$ vs. $Y/B$ . . . . .	111
5-20	Effect of $\beta$ on $V'(X,Y/B)/\bar{U}_m(X)$ vs. $Y/B$ . . . . .	112

#### Appendix Figure

B-1	The Digital Intermittency Detection Procedure . . . . .	134
C-1	The Hybrid Intermittency Detection Procedure . . . . .	142
C-2	A Circular Data Buffer . . . . .	144
C-3	Comparison of Hybrid and Digital Analysis Results . . . . .	150
D-1	Sensitivity of $\bar{U}(X,Y/B)/\bar{U}_m(X)$ to $C_R$ . . . . .	162
D-2	Sensitivity of $\bar{V}(X,Y/B)/\bar{U}_m(X)$ to $C_R$ . . . . .	163
D-3	Sensitivity of $ \bar{UV}(X,Y/B)/\bar{U}_m(X)^2 $ to $C_R$ . . . . .	164

Figure		Page
D-4	Sensitivity of $U'(X,Y/B)$ and $V'(X,Y/B)$ to $C_R$ . . . . .	165
D-5	Sensitivity of $\bar{U}(X,Y/B)/\bar{U}_m(X)$ to $C_H$ . . . . .	166
D-6	Sensitivity of $\bar{V}(X,Y/B)/\bar{U}_m(X)$ to $C_H$ . . . . .	167
D-7	Sensitivity of $ \bar{UV}(X,Y/B)/\bar{U}_m(X)^2 $ to $C_H$ . . . . .	168
D-8	Sensitivity of $U'(X,Y/B)$ and $V'(X,Y/B)$ to $C_H$ . . . . .	169
D-9	Alternate Vortex Velocity Distribution . . . . .	170
D-10	Sensitivity of $\bar{U}(X,Y/B)/\bar{U}_m(X)$ to Vortex Model Choice . . . . .	172
D-11	Sensitivity of $\bar{V}(X,Y/B)/\bar{U}_m(X)$ to Vortex Model Choice . . . . .	173
D-12	Sensitivity of $ \bar{UV}(X,Y/B)/\bar{U}_m(X)^2 $ to Vortex Model Choice . . . . .	174
D-13	Sensitivity of $U'(X,Y/B)$ and $V'(X,Y/B)$ to Vortex Model Choice . . . . .	175

## NOMENCLATURE

$A(X, t)$	Integrated vortex flux defined in Eq. 5.33 (dimensionless)
$b$	Velocity halfwidth (m)
$B$	$b/D$
$C$	Threshold applied to $S(\vec{r}, t)$
$C_F$	Frequency coefficient in Eq. 4.6b
$C_T$	Circulation strength coefficient in Eq. 5.17
$C_H$	Offset distance coefficient in Eq. 5.15
$C_L$	Wavelength coefficient in Eq. 4.23b
$C_R$	Core radius coefficient in Eq. 5.16
$C_U$	Vortex center velocity coefficient in Eq. 4.6a
$D$	Jet exit slotwidth (m)
$f(\eta)$	Self-preserving longitudinal velocity distribution (dimensionless)
$f_1$	Flapping frequency determined by $\tau$ for first correlation peak ( $s^{-1}$ )
$f_2$	Flapping frequency determined from average of peak to peak delay intervals ( $s^{-1}$ )
$F_{ch}$	Characteristic frequency of $S(\vec{r}, t)$ ( $s^{-1}$ )
$f_f$	Flapping frequency ( $s^{-1}$ )
$f_y$	Interface crossing frequency ( $s^{-1}$ )
$f_{ym}$	Maximum interface crossing frequency ( $s^{-1}$ )
$f_s$	Structural passage frequency ( $s^{-1}$ )
$F_s$	$f_s D/U_o$
$g(\eta)$	Self-preserving lateral velocity distribution (dimensionless)
$G(\vec{r}, t)$	Partially formulated intermittency function
$h$	Vortex center offset distance (m)
$H$	$h/D$
$I(\vec{r}, t)$	Intermittency function

$u'$	$u'/U_o$ , longitudinal velocity fluctuation intensity
$U_c$	Convective velocity (m/s)
$U_{cI}$	Convective velocity deduced from interface motion (m/s)
$u_s$	Convective velocity of vortex centers (m/s)
$U_s$	$u_s/U_o$
$u_A, u_B$	Longitudinal velocity fluctuation (m/s)
$u'_B, u'_B$	Longitudinal velocity fluctuation intensity (m/s)
$U_m$	Mean centerline velocity (m/s)
$U_m$	$U_m/U_o$
$U_o$	Jet exit velocity (m/s)
$U^o$	Longitudinal velocity induced by the reference vortex (scaled by $U_o$ )
$U_i^d$	Longitudinal velocity induced by the $i$ th downstream vortex (scaled by $U_o$ )
$U_i^u$	Longitudinal velocity induced by the $i$ th upstream vortex (scaled by $U_o$ )
$v$	Lateral velocity (m/s or scaled by $U_o$ in Chapter V)
$\bar{v}$	Mean lateral velocity (m/s or scaled by $U_o$ in Chapter V)
$v'$	Lateral velocity fluctuation intensity (scaled by $U_o$ )
$v^o$	Lateral velocity induced by the reference vortex (scaled by $U_o$ )
$v_i^d$	Lateral velocity induced by the $i$ th downstream vortex (scaled by $U_o$ )
$v_i^u$	Lateral velocity induced by the $i$ th upstream vortex (scaled by $U_o$ )
$v_e$	Entrainment velocity (scaled by $U_o$ )
$x$	Longitudinal or streamwise jet coordinate (m)
$X$	$x/D$
$X_o$	Longitudinal coordinate of the reference vortex (scaled by $D$ )
$x_i^d$	Longitudinal coordinate of the $i$ th downstream vortex from $X_o$ (scaled by $D$ )
$x_i^u$	Longitudinal coordinate of the $i$ th upstream vortex from $X_o$ (scaled by $D$ )



$y$	Lateral or transverse jet coordinate (m)
$Y$	$y/D$
$y_o$	Lateral coordinate of the reference vortex (scaled by $D$ )
$y_i^d$	Lateral coordinate of the $i$ th downstream vortex from $X_o$ (scaled by $D$ )
$y_i^u$	Lateral coordinate of the $i$ th upstream vortex from $X_o$ (scaled by $D$ )
$z$	Vertical or spanwise jet coordinate (m)

$I_p$	Anemometer probe current (mA)
$l_K$	Kolmogoroff length (m)
$l_{min}$	Minimum interface length scale (m)
$l_s$	Structural pattern wavelength (m)
$L_s$	$l_s/D$
$M(X_o, X)$	Integrated vortex count defined in Eq. 5.24 (dimensionless)
$n$	Vortex density per unit longitudinal length
$N$	$nD$
$q(n)$	Self-preserving Reynolds stress distribution (dimensionless)
$\dot{q}_n$	Vortex production rate ( $m^{-1}s^{-1}$ )
$\dot{Q}_N$	$\dot{q}_n D^2/U_o$
$\vec{r}$	Position vector (m)
$r$	Radial distance from vortex center (m)
$r_c$	Vortex core radius (m)
$R_U(\tau; \delta \vec{r})$	Normalized correlation coefficient based on velocity
$R_I(\tau; \delta \vec{r})$	Normalized correlation coefficient based on intermittency
$R_D$	Jet Reynolds number based upon the slotwidth
$Re$	Reynolds number based upon the cylinder diameter for two-dimensional wakes or streamwise distance for mixing layers
$S(\vec{r}, t)$	Turbulence indicator signal
$\dot{S}(\vec{r}, t)$	$dS(\vec{r}, t)/dt$
$S_f$	Dimensionless flapping frequency constant, $f_f b/U_m$
$S_s$	Dimensionless structural passing frequency constant, $f_s b/U_m$
$t$	Time (s)
$\tilde{t}$	$tU_o/D$ (dimensionless)
$T$	Period of structural pattern (s)
$\tilde{T}$	$TU_o/D$ (dimensionless)
$U$	Longitudinal velocity (M or scaled by $U_o$ in Chapter V)
$\bar{U}$	Mean longitudinal velocity (M or scaled by $U_o$ in Chapter V)

## Greek Symbols

$\beta$	Jet widening rate
$\gamma$	Intermittency fraction
$\Gamma$	Vortex circulation strength ( $\text{m}^2/\text{s}$ )
$\tilde{\Gamma}$	$\Gamma/U_0 D$
$\Delta \vec{r}$	Relative orientation vector between $\vec{r}_1$ and $\vec{r}_2$ (m)
$\Delta \theta$	Mean temperature excess of turbulent flow relative to surrounding ambient temperature ( $^{\circ}\text{C}$ )
$\Delta \theta_0$	Temperature excess at jet exit ( $^{\circ}\text{C}$ )
$\delta_x$	Longitudinal separation distance (m)
$\delta_y$	Lateral separation distance (m)
$\delta_z$	Vertical separation distance (m)
$\delta \phi$	Phase change induced by jet widening rate (radians)
$\delta_2$	Momentum thickness (m)
$\nu$	Kinematic viscosity ( $\text{m}^2/\text{s}$ )
$\eta$	y/b or lateral coordinate of a vortex centered coordinate system in Figure 5-2
$\tau$	Time delay (s)
$\tau_h$	Hold time applied to $G(\vec{r}, t)$ (s)
$\tau_{\text{peak}}$	Time delay yielding the maximum space-time correlation (s)
$\xi$	Longitudinal coordinate of the vortex centered coordinate system of Figure 5-2
$\Lambda_x^I$	Longitudinal integral length scale based upon correlations of the intermittency function (m)
$\Lambda_z^I$	Vertical integral length scale based upon correlations of the intermittency function (m)
$\Lambda_x^u$	Longitudinal integral length scale based upon correlations of velocity fluctuations (m)
$\Lambda_z^u$	Vertical integral length scale based upon correlations of velocity fluctuations (m)

## ABSTRACT

Oler, James Walter, Ph.D., Purdue University, May 1980.  
Coherent Structures in the Similarity Region of a Two-dimensional Turbulent Jet : A Vortex Street. Major Professor: V. W. Goldschmidt.

The characteristics of the coherent structures of a plane jet were evaluated experimentally and with a kinematic numerical representation.

Distributions of intermittency and interface crossing frequency were measured for  $10 \leq x/D \leq 60$ . These properties, including the maximum interface crossing frequency, were found to scale as self-preserving flow variables.

Spatially coherent patterns within the turbulent velocity field were evaluated utilizing two point velocity correlation measurements. From these, it was found that the instantaneous velocity fluctuation distributions are antisymmetric with respect to the centerline and coherent over the entire width of the flow field. In addition, the patterns are periodic in the streamwise direction.

The two-dimensionality of the large structures was evaluated through the comparison of longitudinal and vertical integral length scales derived from correlations in both the fully turbulent zone and the intermittent region. In the intermittent region, the integral scales

were approximately equal while in the fully turbulent zone, the longitudinal scale was approximately double the vertical one.

Utilizing a combination of flow visualization, structural passage frequency measurement and similarity considerations, the convective velocity of the vortex-like structures was estimated to be one half the mean centerline velocity.

From the experimental results, a hypothetical vortex street representation of the plane jet was formulated and evaluated numerically. This kinematic representation was found to be capable of generating realistic distributions of mean longitudinal and lateral velocity as well as the proper spreading and velocity decay rates. Although the correct magnitude of the Reynolds stress was calculated, its sign was in error. The small scales of turbulence were not included in the model and consequently, it was not possible to predict reasonable distributions of the fluctuation intensities, the energy spectra or interface properties.

## CHAPTER I

### INTRODUCTION

In recent years, there has been a gradual shift in the approach to turbulent fluid mechanics research. It is becoming increasingly clear that much of what has been traditionally considered random phenomena has much more deterministic aspects than previously thought. In particular, a growing body of experimental evidence is accumulating which demonstrates that much of the physics of turbulent shear flow may be controlled by a finite set of coherent large scale eddying motions. The relative importance of these large scales has been emphasized in several recent review articles (Kovaszny (1977), Roshko (1976), Davies and Yule (1975), Laufer (1975) and Mollo-Christensen (1971)). While the acceptance of the nonrandom aspects of turbulence is common, it is by no means universal. (See for instance Pui and Gartshore (1979), Chandrsuda, et al. (1978) and Bradshaw (1976)). However, the presence of the large scale structures and to some extent, their importance, have become experimentally established facts.

The goal of the research described herein has been to examine the fully developed two-dimensional plane turbulent jet for evidence of the effects of the large scale eddies characteristic of that flow field. One of the original incentives was to investigate the transport characteristics within the jet conditioned on the instantaneous position of the turbulent-nonturbulent interface. During the course of these measurements, the presence of an apparent antisymmetric

and periodic vortical pattern was noted, suggesting a two-dimensional and ordered pattern similar to that found in two-dimensional mixing layers (Brown & Roshko (1971)) and wakes (Papailiou and Lykoudis (1974)). Consequently, the majority of the experiments and modeling effort was devoted to evaluating the degree to which these features are present in the plane turbulent jet.

## CHAPTER II

### GENERAL BACKGROUND

The purpose of this chapter is to first introduce the reader to the classical characteristics and descriptive terms for turbulent plane jets. Following that, a survey of the literature pertaining to large scale structures in other free turbulent shear flows will be given. Finally, the concept of a von Kármán 'vortex street' type pattern will be developed for a two-dimensional plane turbulent jet.

#### A. The Turbulent Plane Jet

##### 1. Initial Region

Turbulent plane jets result from the flow of a two-dimensional nozzle emanating into an infinite environment. The most general case is that resulting from an initially uniform velocity profile (except for two boundary layers) flowing into an otherwise quiescent environment. This is the case now treated.

A plan view of the flow field is given in Figure 2-1. Three distinct regions of flow development may be defined, the first of which is the initial region beginning at the jet exit. The initial region is characterized by a potential cone of uniform velocity,  $U_0$ , bounded on either side by plane turbulent shear layers.

For properly designed nozzles, the shear layers originate from initially laminar boundary layers, then transition to turbulence and develop linearly with respect to downstream distance. The growing mixing layers eventually meet at the centerline which marks the end of the potential



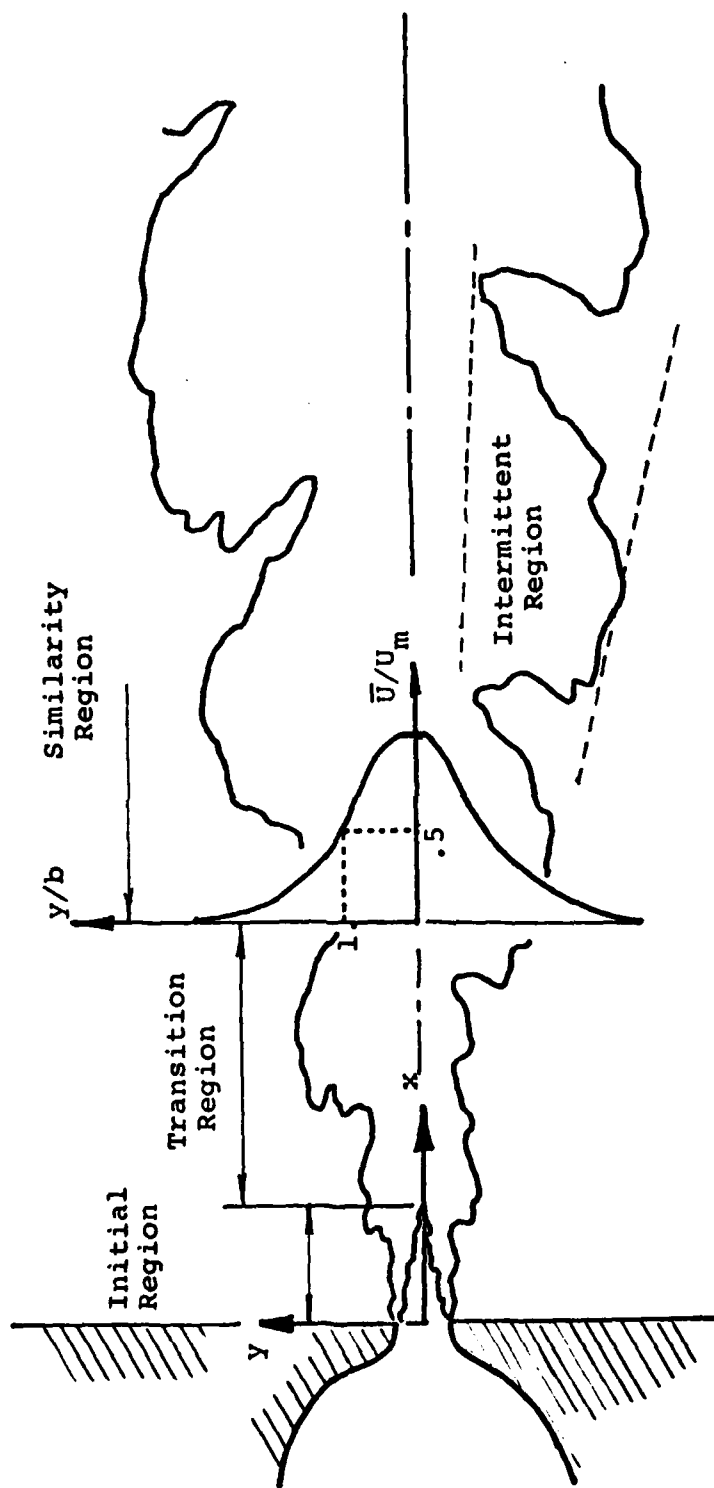


Figure 2-1 The Two-Dimensional Jet

cone and initial region. This usually occurs four to six slotwidths,  $D$ , from the jet exit. Prior to this point, the shear layers interact through the mutually induced pressure field only.

## 2. Transition Region

From the point of contact at the end of the potential cone, the shear layers go through a period of interaction or transition until a state of dynamic equilibrium is reached across the entire width of the flow field. This is generally accomplished within the first 30 slot widths of flow travel.

## 3. Similarity Region

Similarity exists for a developing flow field when one velocity scale and one length scale are sufficient to make distributions of reduced velocities in terms of reduced coordinates identical. The two-dimensional plane jet is characterized by this property as demonstrated for distributions of the mean longitudinal velocity,  $\bar{U}$ , in Figure 2-2. The velocity and length scales utilized are the mean centerline velocity,  $U_m$ , and the velocity halfwidth,  $b$  (the distance from the jet centerline to the lateral location at which  $\bar{U} = .5U_m$ ). From derivations based on similarity arguments (See, for instance, Townsend (1956) or Hinze (1975)), it may be shown that the velocity and length scales must themselves be functions of the downstream distance,  $x$ . In particular, one expects  $U_m \propto (x/D)^{-1/2}$  and  $b \propto (x/D)$  which is verified by the data illustrated in Figures 2-3 and 2-4. The variation of these scales is independent of the jet Reynolds number,  $R_D = U_0 D/\nu$ .\*

---

\* In a strict sense, perfect similarity requires an independence of the initial conditions which is only approximately true in real flows. This is evidenced by a lack of coincidence of the kinematic and dynamic virtual origins.

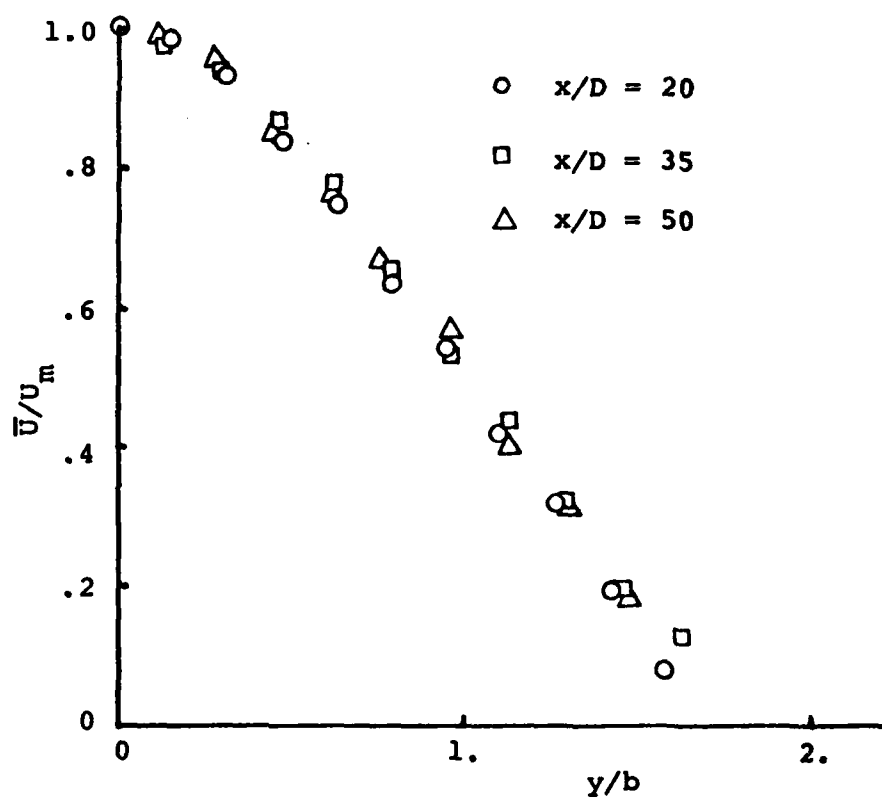


Figure 2-2  $\bar{U}/U_m$  vs.  $y/b$

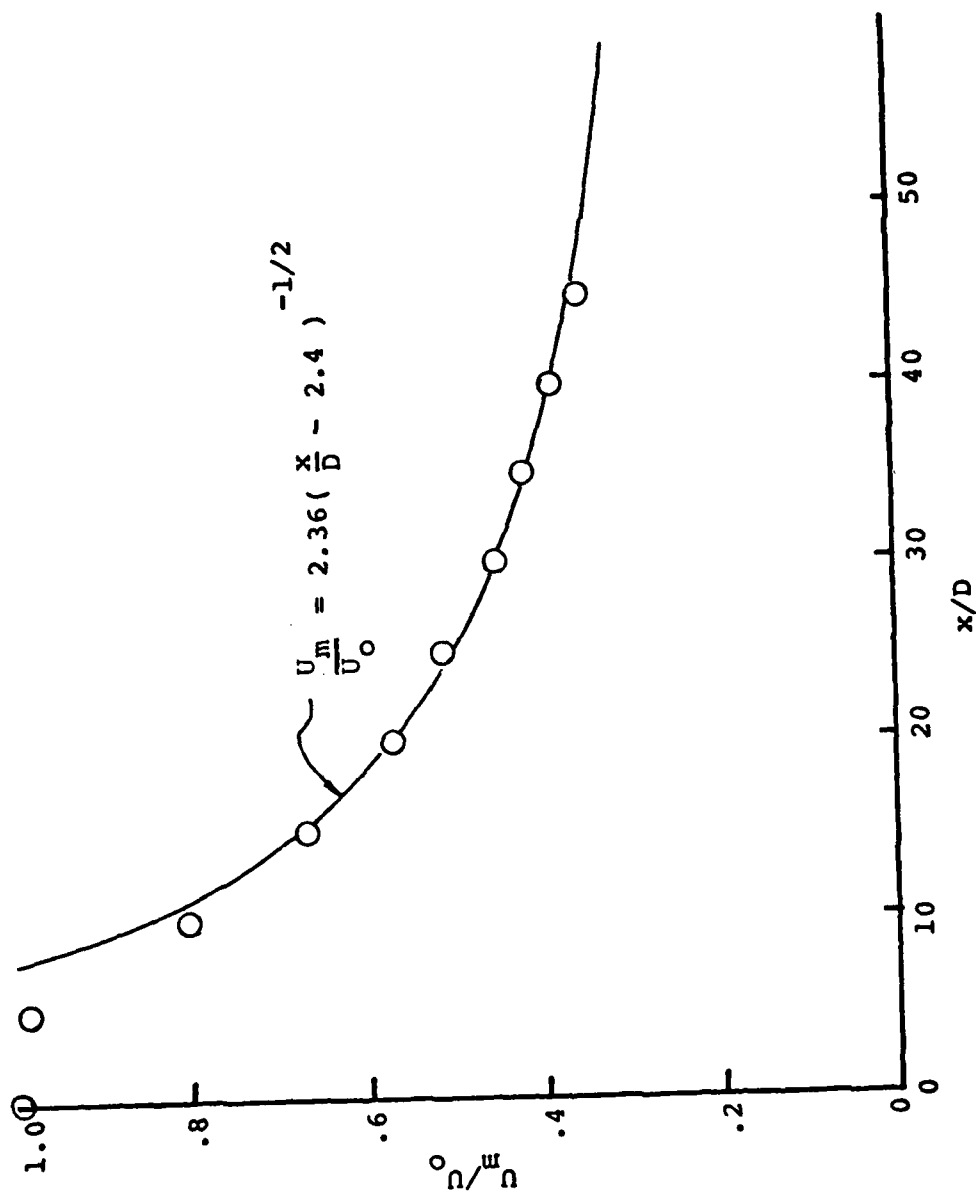
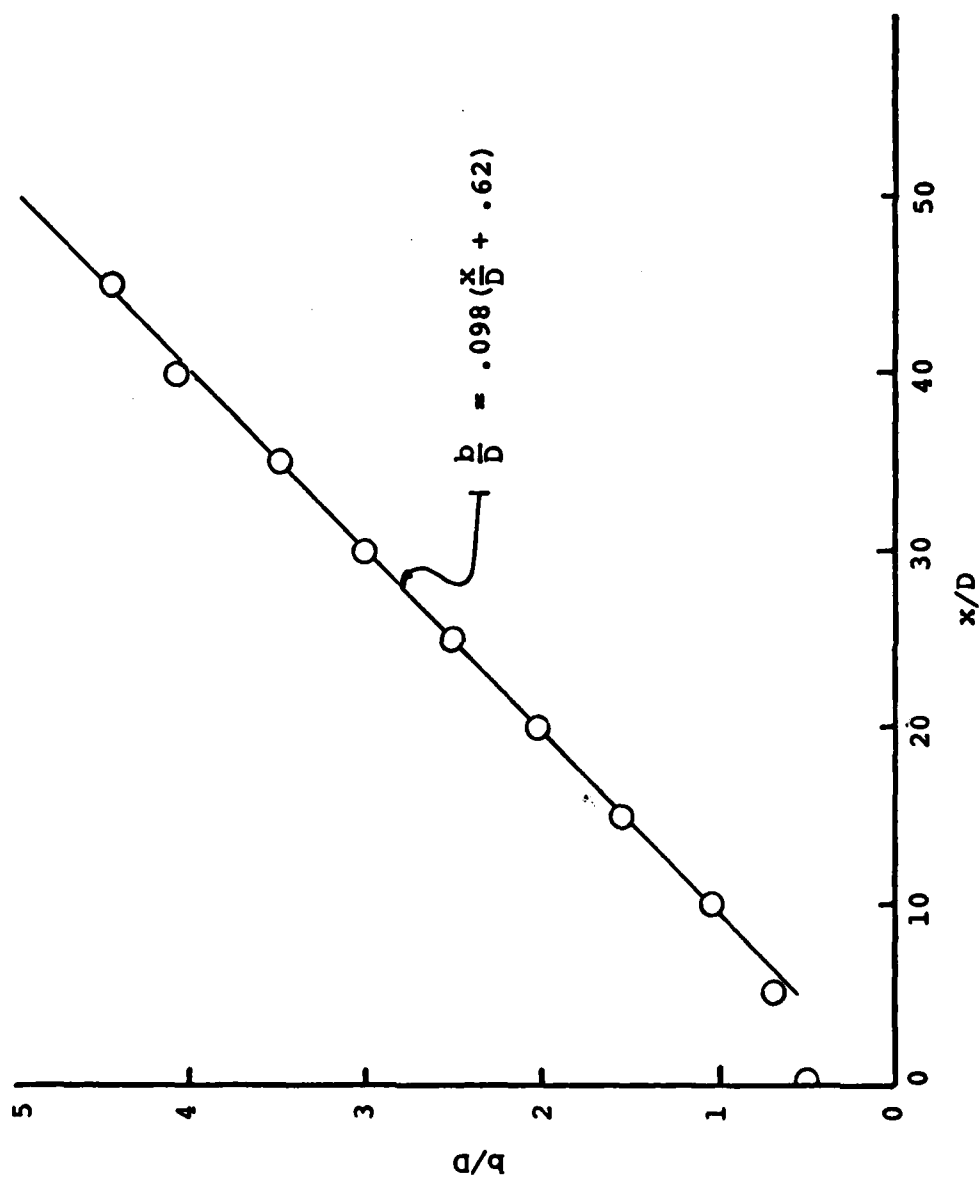


Figure 2-3  $U_m/U_o$  vs.  $x/D$

Figure 2-4  $b/D$  vs.  $x/D$

#### 4. Intermittent Region

One of the most distinctive characteristics of turbulent shear flows with at least one free boundary is the existence of a sharply defined interface separating the vortical, or turbulent flow, from the nonvortical, or nonturbulent, ambient fluid. Driven by the large scales of the turbulent motion (Corrsin & Kistler (1954)), the interface is characterized by large bulges whose maximum and minimum extensions define the width of the intermittent region. For an observer at a fixed point in the intermittent region, the flow may be described as intermittently turbulent as the deformations in the turbulent-nonturbulent interface are convected past. Following the convention of Townsend (1949), an intermittency function,  $I(\vec{r}, t)$ , may be defined as taking on the values of one or zero when the flow is turbulent or nonturbulent, respectively, at a fixed point,  $\vec{r}$ , in the flow field. A temporal average of  $I(\vec{r}, t)$  is the intermittency,  $\gamma(\vec{r})$ , or fraction of time that the flow is turbulent at  $\vec{r}$ . The interface crossing frequency,  $f_\gamma$ , is defined as the rate at which the bulges in the interface cross a fixed point.

#### B. Large Scale Structures in Turbulent Free Shear Flows

Recognition of the importance of the large scale structures in turbulent shear flows dates back at least as far as Townsend (1956) and Grant (1958). Townsend's concept of a double structured nature of turbulence and hypothesis for the "dynamic equilibrium of the large structures" remain quite useful in the interpretation of recent data concerning the large structures. He postulated that the large scale motion plays a central role in the dynamics of flow development and energy exchange between the mean flow and small scales. A state of equilibrium exists between the rate at which energy is extracted from the mean flow by the large scale structures and the rate at which these structures lose

energy to the small scales of turbulence.

Coherent turbulent structures have since been identified in both bounded and free shear flows although the boundary conditions and instability mechanisms are different.

Recent revelations concerning the coherent motions near the wall of a boundary layer have somewhat confused the concept of a "cascade" of energy from the large to small scales since the relationship appears to be reversed for that flow. However, in free shear flows, the energy cascade and dynamic equilibrium hypothesis appear to be valid. The following discussion will deal only with large scale structures as they relate to free shear flows, such as the plane turbulent jet.

1. Turbulent Mixing Layers

Much of the current emphasis on the large eddies of turbulence is a result of the flow visualization experiments of Brown & Roshko (1971, 1974) in a turbulent mixing layer. Their shadowgraphs of the mixing layer between two parallel streams of unequal velocity and density clearly illustrate the existence of large, essentially two-dimensional roller vortices with axis perpendicular to the plane of mean shear. Photographs indicate that the large structures scale on the dimensions of the mean flow as they are convected downstream at a velocity approximately equal to the average of the two stream velocities. In fact, it is apparent that the growth of the mixing layer is controlled by the large eddies as they undergo discontinuous development through a mechanism of eddy coalescence.\*

---

\* The coalescence event has been alternately described as merger, pairing and agglomeration. The term "coalescence" will be used throughout this work.

Visualization experiments were repeated over a wide range of Reynolds numbers with no apparent effect on the growth rate or eddy coalescence. The only difference in the flows was the increasingly high small scale turbulent energy for higher Reynolds numbers. This is explained by Townsend's dynamic equilibrium hypothesis in that as more energy is extracted by the large scales from the mean flow for the higher Reynolds numbers, an equally greater amount of energy is transferred from the large eddies to the smaller ones. This, in turn, requires increasingly smaller scales for the viscous dissipation of energy as described by the Kolmogoroff hypothesis. Hence, the large eddies are independent of viscosity and dependent only on the mean flow characteristics. The small scales, on the other hand, are dependent on viscosity due to the overall energy dissipation requirements.

Brown & Roshko emphasized that their mixing layer fit the classical characteristics of fully developed turbulent mixing layers in every way, including mean and fluctuating velocities and stress distributions. The large eddies are believed to be characteristic of the flow rather than the result of some artificial experimental forcing.

Winant & Browand (1974) and Browand & Weidman (1976) made similar observations for a mixing layer in water at low Reynolds numbers. In the latter investigation, a combination of flow visualization and conditional sampling was used to examine the details of the vortex coalescence process. By ensemble averaging the velocity signals resulting from the passage of pairs of vortices in various transitional states of coalescence, the instantaneous characteristics of the process were deduced. It was found that the vorticity of an isolated noninteracting vortex is concentrated near its center and that the same vorticity distribution is recovered following the coalescence of two such isolated vortices. In



addition, the rate of Reynolds stress production during the active coalescence of vortices was found to be almost double that for a passive vortex.

An interesting argument was developed by Browand & Weidman to emphasize the importance of the large eddies to Reynolds stress production. They noted that their distribution of measured dimensionless Reynolds stress is essentially identical to that of Liepmann & Laufer (1947) in spite of the large difference of Reynolds number. This is not true for the distributions of the r.m.s. velocity fluctuations. Based on these observations, they suggested that it must be the large scale eddies which are responsible for the bulk of the Reynolds stress production since it is only those which are unaffected by the Reynolds number.

In response to skepticism concerning the universality of the two-dimensional structure in mixing layers with Reynolds numbers (see for instance, Bradshaw(1976)), Dimotakis & Brown (1976) performed an investigation of this effect. While Brown & Roshko utilized a mixing layer at  $Re = 10^5$  and Winant & Browand used  $Re = 300$ , the mixing layer of Dimotakis & Brown was investigated at  $Re = 3 \times 10^6$ . The two-dimensional structure and vortex coalescence mechanism were noted to still be apparent.

Dimotakis & Brown also investigated the entrainment mechanism by observing the paths of dye streaks injected into the free streams. They found that entrainment is accomplished in two distinct stages:

- 1) Dye is drawn into the mixing layer symmetrically from both sides through an engulfment process induced by the large structures.
- 2) Once drawn into the large eddies, little molecular mixing is evident since the entwined dye streaks remain identifiable. This situation perseveres until the identity of the eddy is lost through coalescence or a secondary mechanism they described as vortex tearing. At that point

complete diffusion of the dye is almost instantaneous.

The concept of an essentially two-dimensional structure in a fully developed turbulent flow has not met with universal acceptance. Chandrsuda, et al. (1978) and Pui & Gartshore (1979) reported experiments in mixing layers where the large scale two-dimensional eddies either were not evident at all or transitioned to a fully three-dimensional turbulent field a short distance from the splitter plate. Degradation of the two-dimensional structure appeared to be caused by comparatively low level turbulence in the free streams or in the initial shear layer. The proponents of "organized" turbulence were undaunted, however, and Wygnanski, et al. (1979) reported an equally well documented experiment in which the two-dimensional structure survived severe background turbulence in the free streams and in the initial shear layer.

## 2. Wake Flows

The existence of a well organized vortex street in the near wake of a cylinder has long been known, but until recently, this structure was thought to degenerate quickly with downstream distance (see Roshko (1954)). Experiments by Taneda (1959), Bevilacqua & Lykoudis (1971), Papailiou & Lykoudis (1974) and Townsend (1979) have indicated that the large eddies of the turbulent motion may be characterized by the von Kármán vortex street at much greater downstream distances and Reynolds number than previously thought possible.

Although the vortex street in a plane wake is a natural intuitive extension of the roller vortices in a mixing layer, there appear to be fundamental differences. First, in none of the experiments listed above has there been any indication of eddy coalescence. Papailiou & Lykoudis noted that the breakdown of the large eddies is accomplished through the separation of the eddies into smaller rotating

parts. These parts initially remained within the vortex but eventually separated, forming yet smaller lumps of rotating fluid. Taneda observed that this breakdown is often followed by a regeneration of the two-dimensional structure at a point farther downstream. The concept of generation, growth and decay cycles for the large structures has been put forward by Townsend. His recent investigation provides some evidence of the phenomena and he has illustrated the degradation to correlation measurements that results from averaging over eddies in different stages of their life cycle.

Bevilaqua & Lykoudis and Papailiou & Lykoudis have observed that entrainment in plane wakes occurs in a manner similar to that observed by Dimotakis & Brown in the mixing layer. In the first stage, ambient fluid is entwined into the large rotating eddies by turbulent shearing. The second stage of complete assimilation of the recently entrained fluid is accomplished at the point of eddy breakdown as described above.

As in the plane mixing layer, there is some question as to the degree of two-dimensionality of the large eddies. Barsoum, Kawall & Keffer (1978) have made measurements of the space-time correlations derived from the intermittency function for a plane wake. They found that the bulges in the turbulent-nonturbulent interface have a characteristic streamwise dimension approximately double the spanwise dimension. In addition, there was no evidence of periodicity of the intermittency function with respect to downstream distance. Both of these features are incompatible with the concept of an ordered vortex street structure.

### 3. Jet Flows

The majority of the reported research into the large scale structures of jet flow has dealt with the initial region. This is the result of the importance of these

structures to noise production in that zone. The following investigations are representative of this type: Bradshaw, et al. (1964), Becker & Massaro (1968), Wooldridge & Wooten (1971), Ko & Davies (1971), Crow & Champagne (1971), Lau, et al. (1972), Fuchs (1972), Liu (1974), Merkin & Liu (1975), Lau & Fisher (1975), Bruun (1977), Ffowcs Williams & Kempton (1978). In the initial region, the flow field is essentially that of a plane mixing layer wrapped around the lip of the nozzle. Ring vortices are shed from the lip more or less periodically and go through a process of growth through repeated eddy coalescence as they are convected downstream. Due to the inherent instabilities of a vortex ring, the structures become increasingly three-dimensional so that by the end of the potential cone, an apparently fully turbulent flow is established. Noise production in the initial region appears to be controlled by the initially highly coherent ring vortices and the intense first few eddy coalescence events.

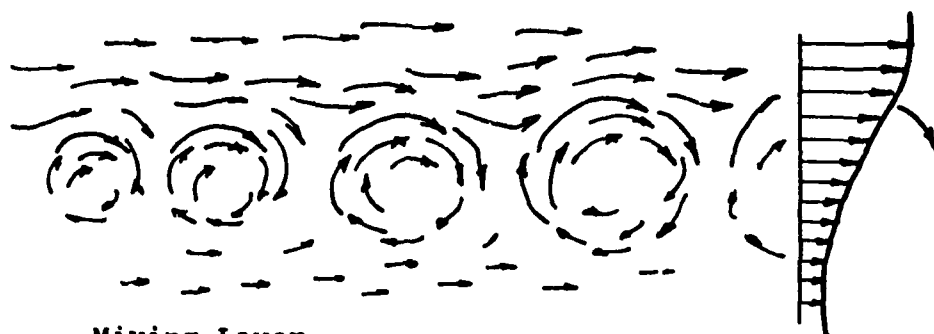
Comparatively fewer experiments have been undertaken in the similarity region of turbulent jets. The strongest indication of an ordered structure is the well documented apparent "flapping" behavior of turbulent two-dimensional jets. This characteristic is easily detected by measuring the correlation between the fluctuating longitudinal velocities from opposite sides of the jet centerline. For a zero time delay the result is a negative correlation coefficient indicating a lateral motion of the instantaneous velocity profile. In the past, this behavior has been compared to the flapping of a flag in which the centerline of the mean profile is periodically displaced about its average location. It was thought that the flapping was essentially a traveling wave instability rather than an indication of organized large scale structure. Flapping two-dimensional jets have been reported by Bradbury (1965),

Goldschmidt & Bradshaw (1973), Weir & Bradshaw (1975), Gutmark & Wygnanski (1976), Everitt & Robins (1978) and Cervantes (1978).

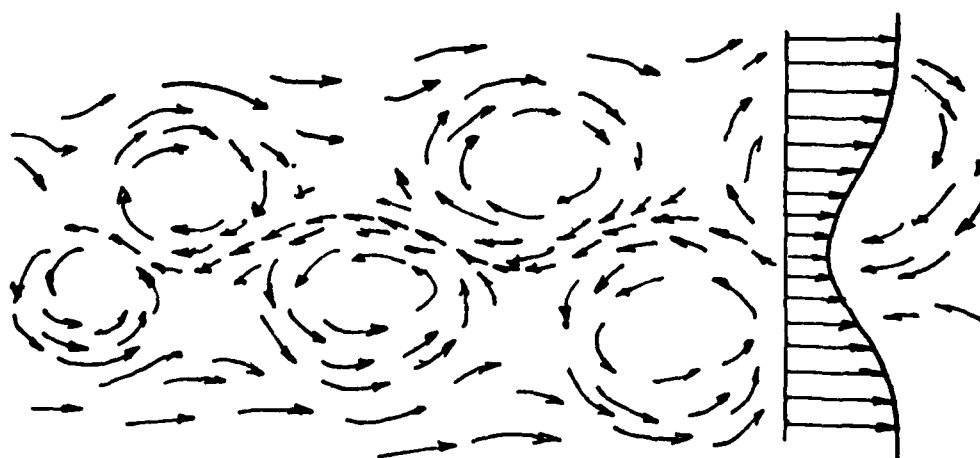
In the detailed investigation by Cervantes, the frequency of the flapping was inferred from the oscillating correlation function that resulted from introducing a time delay to one of the signals. The frequency thus determined was found to be independent of the centerline to probe distances, thereby indicating a structure which spanned the entire flow. A similar measurement of the autocorrelation function for the fluctuating transverse velocity component at the centerline led to the same flapping frequency.

Cervantes also found that the variation of the flapping frequency with respect to downstream distance is compatible with the similarity scaling relationships for the plane jet. Consequently, the flapping frequency, when nondimensionalized by the local mean velocity and length scales, is equal to a constant,  $S_f = f_f b / U_m = 0.1$ . Approximate agreement with this value may be inferred from the investigations of Bradbury, Everitt & Robins, Goldschmidt & Bradshaw and Weir & Bradshaw. The similarity scaling and agreement between the various investigators on the dimensionless flapping frequency,  $S_f$ , implies a Reynolds number independence that was verified by Cervantes.

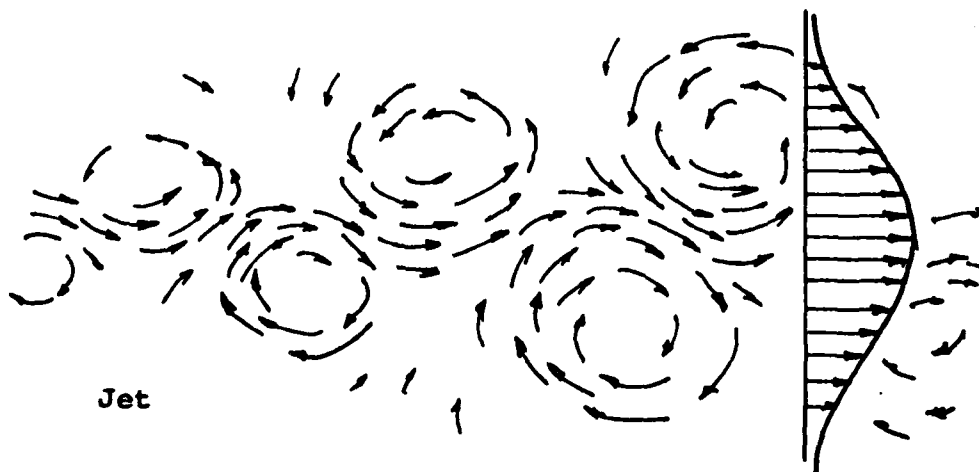
While the traveling wave phenomena is a plausible explanation for the flapping jet behavior, an alternate possibility is the presence of large scale eddies of a von Kármán vortex street type. Although more order is implied by this structure than traditionally expected for a turbulent plane jet, the similarity between the characteristics of the jet, wake and mixing layer make it a plausible hypothesis (see Figure 2-5). In particular, the weaving flow evident in the flapping jet is strongly suggestive of the trailing wake vortex street. The similarity scaling



Mixing Layer



Wake



Jet

Figure 2-5 Organized Structures in Two-dimensional  
Free Shear Flows

and Reynolds number independence of the jet structural frequency are also two of the most distinctive features of the large eddies in the plane mixing layer.

Recent flow visualization experiments by Moallemi (1980) strongly suggest a vortex street type pattern of the large structures in a plane jet. By stretching oil coated smoke wires parallel to and on either side of the jet centerline in the ambient fluid, the silhouette of apparently two-dimensional large eddies could be discerned as the smoke was carried into the turbulent-nonturbulent interface. Stretching a single wire normal to the centerline revealed that the entrainment velocity vector has a negative longitudinal component that is approximately 15% of the lateral component.

Mattingly & Criminale (1971) have made a spatial stability analysis of the two-dimensional plane jet. They found that the most unstable and rapidly amplified mode led to the generation of a vortex street type of structure. It was also illustrated that this structure would be the most effective in the transfer of energy from the mean flow to the turbulent field.

In summary, a simplified hypothetical model of the overall structural development of the plane jet may be described in terms of the three regions.

1. In the initial region, small perturbations of the initially laminar boundary layers are amplified into the characteristic two-dimensional vortices of a turbulent mixing layer. The characteristic scales in this region are the centerline velocity,  $U_0$ , and momentum thickness,  $\delta_2$ . The mixing layers grow until at a downstream distance which scales on the slotwidth, they contact each other and a fundamental change in the structure takes place.
2. Within the transition region, an overall pattern of the large eddies evolves which produces instantaneous and

periodically repeatable antisymmetric velocity profiles. The length and velocity scales within this region include the halfwidth and mean centerline velocity.

3. Further downstream, the jet has adjusted itself to the new eddy patterns and a state of dynamic equilibrium and structural similarity is established. In the work that follows, the similarity region will be the focus of attention.



## CHAPTER III

### EXPERIMENTAL TECHNIQUES

#### A. Flow Field Apparatus

All results presented herein were obtained from measurements in the two-dimensional plane jet depicted in Figure 3-1. The flow was generated by a 3/4 hp blower discharging to a 56 x 51 cm plenum chamber. A gradual contraction led to a 15.2 x 30.4 cm channel where the flow passed through straighteners and screens before the final contraction to a 1.27 x 30.4 cm slot and discharging normal to a 91.4 x 30.4 cm wall. The developing jet was bounded above and below by 91.4 x 120.0 cm parallel walls. Heating for the jet was accomplished with a 4 kW mesh wire heating element in the plenum chamber.

The jet was operated at a constant Reynolds number ( $Re_D = 1.74 \times 10^4$ ,  $U_o = 21 \text{ msec}^{-1}$ ) and overheat ( $\Delta\theta_o = 12^\circ\text{C}$ ) above the ambient temperature.

Mean flow measurements were made with a pitot tube while fluctuating velocity and temperature signals were derived from the output of a TSI 1050 series anemometer. The flow temperature was equal to the ambient while velocity measurements were made so that there was no temperature contamination of the signal. An overheat of 1.8 in the constant temperature mode was used for those measurements. Fluctuating temperature measurements were made using a constant current probe with  $I_p = 1.5 \text{ mA}$ . An analysis by Jenkins (1974) with the same apparatus revealed that the maximum contamination error of the temperature signal due

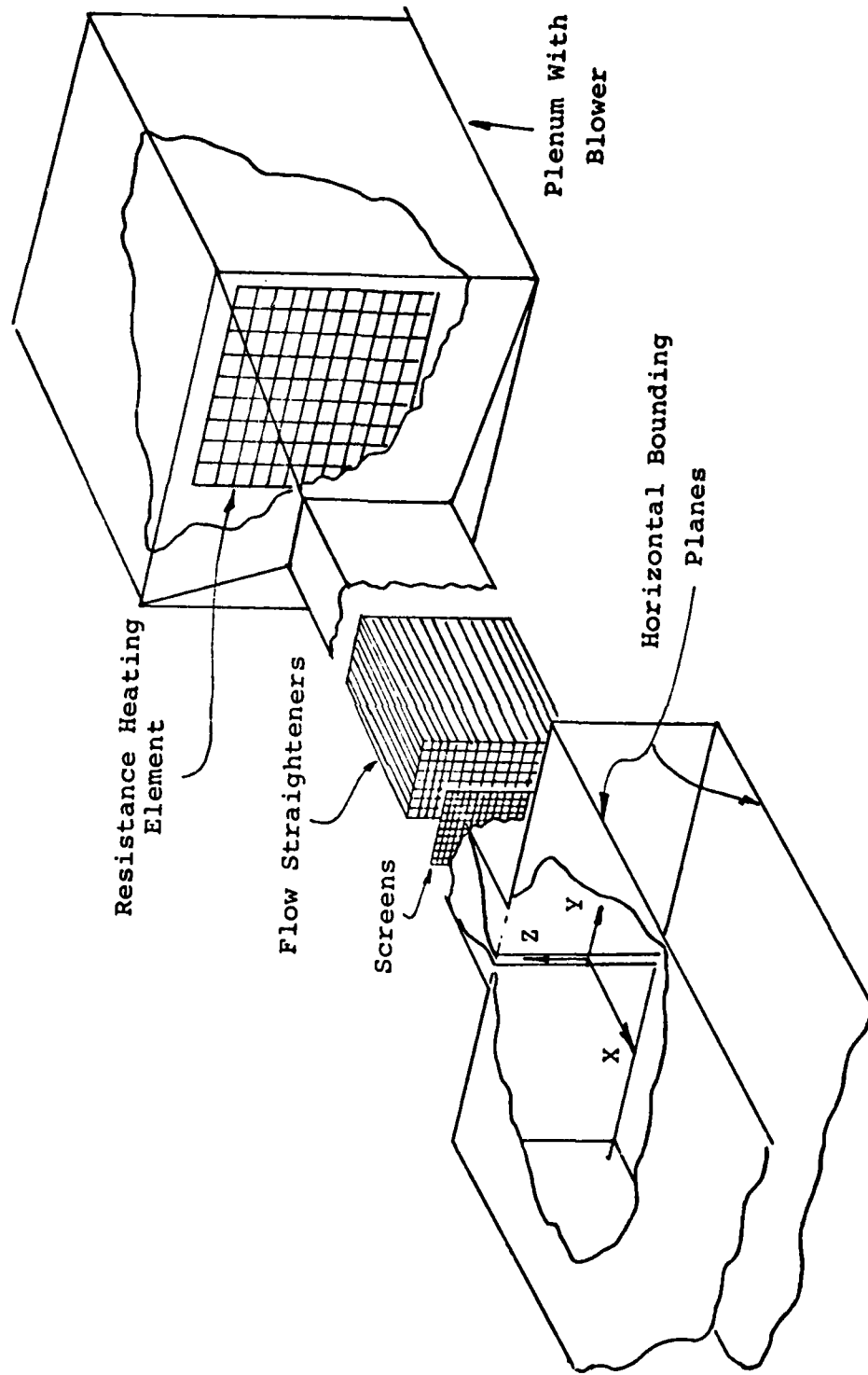


Figure 3-1 Schematic of Plane Jet Apparatus

to the velocity fluctuations is less than 4%.

#### B. Turbulence Detection and Intermittency Measurement

The existence of a sharply defined interface separating the turbulent and nonturbulent flow near the free stream boundary of a turbulent shear flow was first reported by Corrsin (1943) for an axisymmetric circular jet. The intermittent or burst-like behavior of a hot wire anemometer signal resulting from the alternate convection of turbulent and nonturbulent flow past the probe was quantified by Townsend (1949). He defined the intermittency function  $I(\vec{r}, t)$  as a square wave which takes on the value of unity or zero corresponding to periods of turbulence (vortical flow) or nonturbulence (nonvortical flow), respectively, at a fixed point in the flow field. The intermittency  $\gamma(\vec{r})$ , may be found by taking the time average of  $I(\vec{r}, t)$  and is interpreted as the fraction of time that the flow is turbulent at a particular position. The time derivative of  $I(\vec{r}, t)$  yields a train of alternating positive and negative unit impulses that correspond to the unique events of leading and trailing edge interface crossings. The frequency of occurrence of the positive (or negative) impulses is defined as the interface crossing frequency,  $f_\gamma(\vec{r})$ .

Townsend also developed an intermittency detection instrument that became the predecessor to many similar devices that have followed. The primary features of these circuits are:

- 1) Definition of a turbulence indicator signal,  $S(\vec{r}, t)$ , that is derived from some measurable flow property which exhibits a strong contrast between nonturbulent low level portions of the signal and turbulent, higher level segments.
- 2) Application of a gate or threshold level to  $S(\vec{r}, t)$  which defines an intermediate square wave,  $G(\vec{r}, t)$ , taking on the values of one or zero corresponding to intervals for which  $S(\vec{r}, t)$  is above or below the threshold  $C$ .

3) Application of a hold time,  $\tau_h$ , to  $G(\vec{r}, t)$  where  $\tau_h$  is the prescribed minimum length of time during which  $I(\vec{r}, t)$  is allowed to make two changes of state. The hold time provides a means of discriminating between the minimum burst (turbulent segment of  $S(\vec{r}, t)$ ) and void (nonturbulent segment of  $S(\vec{r}, t)$ ) time intervals expected from the flow and the apparent shorter ones resulting from high frequency turbulent fluctuations of  $S(\vec{r}, t)$  and scales of interface motion below the range of interest.

4) The analysis technique, typically a choice between an analog circuit or computer analysis of digitized data records.

The choices made for  $S(\vec{r}, t)$ ,  $C$ ,  $\tau_h$  and the analysis technique are described below. A representative review of the literature relating to turbulence detection and intermittency measurement is given in Appendix A.

1. The Indicator Signal,  $S(\vec{r}, t)$

The indicator signal used for the present investigation is the instantaneous temperature. Turbulence detection is based on the discrimination between slightly heated turbulent fluid and relatively uniform temperature ambient fluid. This type of technique has been utilized by several previous investigators (Barsoum, et al. (1977), Freymuth & Uberoi (1973), Hedley & Keffer (1974), and Kohan (1969)) and a systematic evaluation of the technique is given by LaRue (1974).

The primary advantage of temperature measurement as a criterion for  $S(\vec{r}, t)$  is that the signal provides a strong contrast between turbulent bursts and nonturbulent voids without encountering the zero crossing problem. This is illustrated in Figure 3-2 which is a photograph of an oscilloscope trace of  $S(\vec{r}, t)$ . Since only positive deviations from the ambient temperature level occur, rectification is unnecessary and the number of extraneous threshold crossings

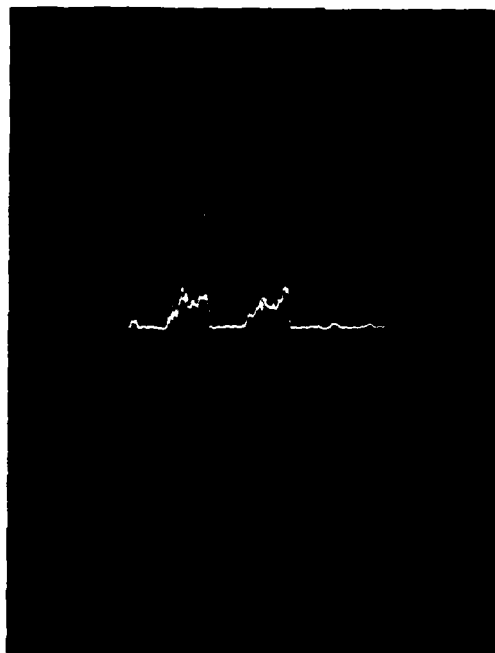


Figure 3-2 Oscilloscope Trace of  $S(\bar{r}, t)$

is much less than for  $S(\vec{r}, t)$  based on velocity fluctuations or their derivatives. This characteristic allows a good degree of confidence in the choice of  $C$  and  $\tau_h$  since the dependence of the measured intermittencies, crossing frequencies and conditional averages on these parameters is diminished.

All measurements described in this document were made with a jet overheat of  $12^\circ\text{C}$  at the exit. This allowed a centerline mean temperature excess of 3 to  $8^\circ\text{C}$  over the measurement range which is comparable with the  $4.5^\circ\text{C}$  used by Barsoum, et al. (1978), and considerably less than the  $15^\circ$  to  $22^\circ\text{C}$  range used by Jenkins and Goldschmidt (1974). Mean velocity and temperature measurements were taken to verify that they were consistent with the similarity principles for a plane jet. Repetition of the measurements at various spanwise locations did not reveal any appreciable deviations of the mean flow from two dimensionality over the region of interest due to buoyancy effects.

## 2. The Threshold, $C$

The role of the threshold in the turbulence detection procedure is illustrated in Figure 3-3. In choosing the optimum  $C$ , it is desirable to set it as close as possible to the ambient level without encroaching into the noise band surrounding the ambient signal. The noise referred to here is believed to be the result of small amplitude temperature fluctuations in the room air. If the threshold is chosen below the maximum level of the noise fluctuations, false indications of interface crossings will result.

There are two consequences of being unable to use the ideal threshold, that is,  $C$  infinitesimally above the ambient level. The first of these is that the intermittency function will be systematically underestimated due to the finite slope of the leading and trailing edge temperature profiles as shown in Figure 3-3. The second is that the probability of mistaking a short period, low temperature dip

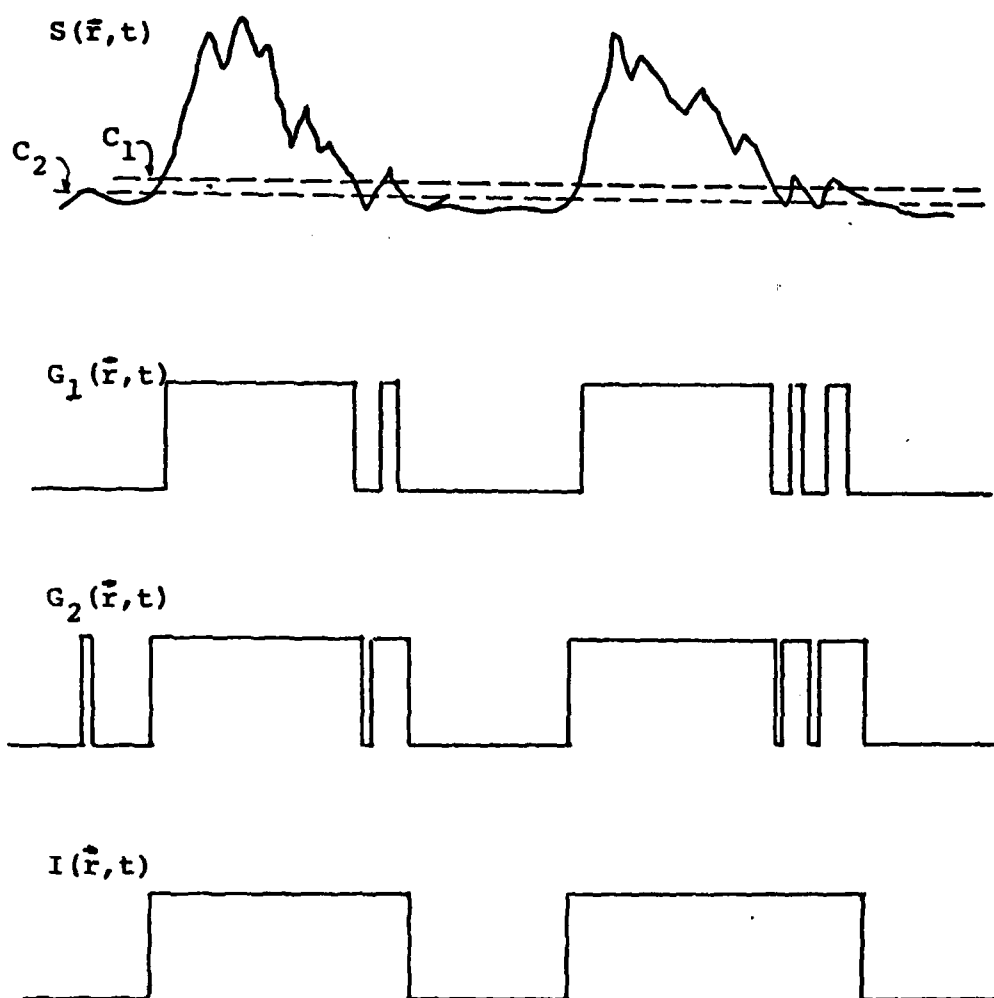


Figure 3-3 Formulation of  $I(\vec{r}, t)$

within a turbulent burst as a true separation between bursts increases with increasing  $C$ . This is also due to the finite rise and fall time of the temperature level since the dips are of increasingly longer duration for higher thresholds. Since it is the function of the hold time to compensate for the short period dips below  $C$ , a higher threshold increases the uncertainty in the choice of  $\tau_h$ . This problem has also been discussed by LaRue (1974).

The choice of threshold for the present investigation was made from subjective inspections of  $S(\vec{r}, t)$  for various intermittencies. From these, the width of the noise band around the ambient level could be estimated and the threshold set accordingly. Visual observations suggested that the amplitude of the noise band did not vary significantly with longitudinal or transverse position. Since the primary consideration in choosing  $C$  was the width of the noise band, no advantage would be gained from varying  $C$  at different locations. To have varied  $C$  would have in fact introduced additional uncertainty into the measurement of  $\gamma$  and  $f_\gamma$  due to their systematic dependence on  $C$  as described in the previous paragraph. The dependence of  $\gamma$  and  $f_\gamma$  on the threshold is illustrated in Oler & Goldschmidt(1978).

### 3. The Hold Time, $\tau_h$

The function of the hold time is to eliminate short period "apparent" voids within bursts or inversely, bursts during voids as illustrated in Figure 3-3. As pointed out by Kibens and Kovasznay (1970), an investigation of the intermittency characteristics of a particular flow field should be predicated on a definition of the degree of detail desired concerning the interface geometry. For the present investigation, the large scale eddies are of principal interest.

The nominal value of  $\tau_h$  at  $x/D = 30$  was determined (using the preselected threshold) by arbitrarily choosing the value which would give agreement between the measured



crossing frequency and the frequency as determined from visual inspection of strip chart recordings of  $S(\vec{r}, t)$  (at the position of maximum crossing frequency). The value determined in this way at  $x/D = 30$  was  $\tau_h = 4$  msec. It was held constant for all measurements in the transverse plane at that  $x/D$ .

For  $x/D \neq 30$ , the hold time was varied in direct proportion with a global time scale derived from the variation of the centerline velocity and velocity halfwidth. For a self-preserving plane jet, the halfwidth,  $b$ , is expected to vary linearly with  $x/D$  and the centerline velocity,  $U_m$ , should vary as  $\left[\frac{x}{D}\right]^{-1/2}$ . This behavior is demonstrated in Figures 2-3 and 2-4. The variation of the ratio  $b/U_m$  is expected to go as  $\left[\frac{x}{D}\right]^{3/2}$  and may be interpreted as a global time scale for the plane jet. The hold time variation was proportional to this scale with the constant of proportionality determined at  $x/D = 30$ . This resulted in  $.7 \text{ msec} \leq \tau_h \leq 11.5 \text{ msec}$  for  $10 \leq x/D \leq 60$  which is consistent with the 3.6 - 7.5 msec range utilized by Jenkins and Goldschmidt (1974), for  $25 \leq x/D \leq 55$  in the same flow field. Their choice of  $\tau_h$  was based on a characteristic frequency derived from  $S(\vec{r}, t)$  as suggested by Kibens and Kovasznay (1970). Ajagu and Goldschmidt (1976) used a constant  $\tau_h = 10$  msec for  $25 \leq x/D \leq 45$  for their measurements in a plane jet. In addition, Kohan (1969) chose  $3.4 \text{ msec} \leq \tau_h \leq 4.1 \text{ msec}$  in a two-dimensional wall jet and Kibens and Kovasznay (1970), used  $\tau_h = 4$  msec for a turbulent boundary layer.

The sensitivity of the interface crossing frequency to  $\tau_h$  is illustrated in Figure 3-4. Variation of the hold time produces a large change in the measured frequencies and a distortion of the normalized distribution of  $f_y/f_{ym}$ . These effects are the result of varying the degree of interface detail included in the formulation of the intermittency function.

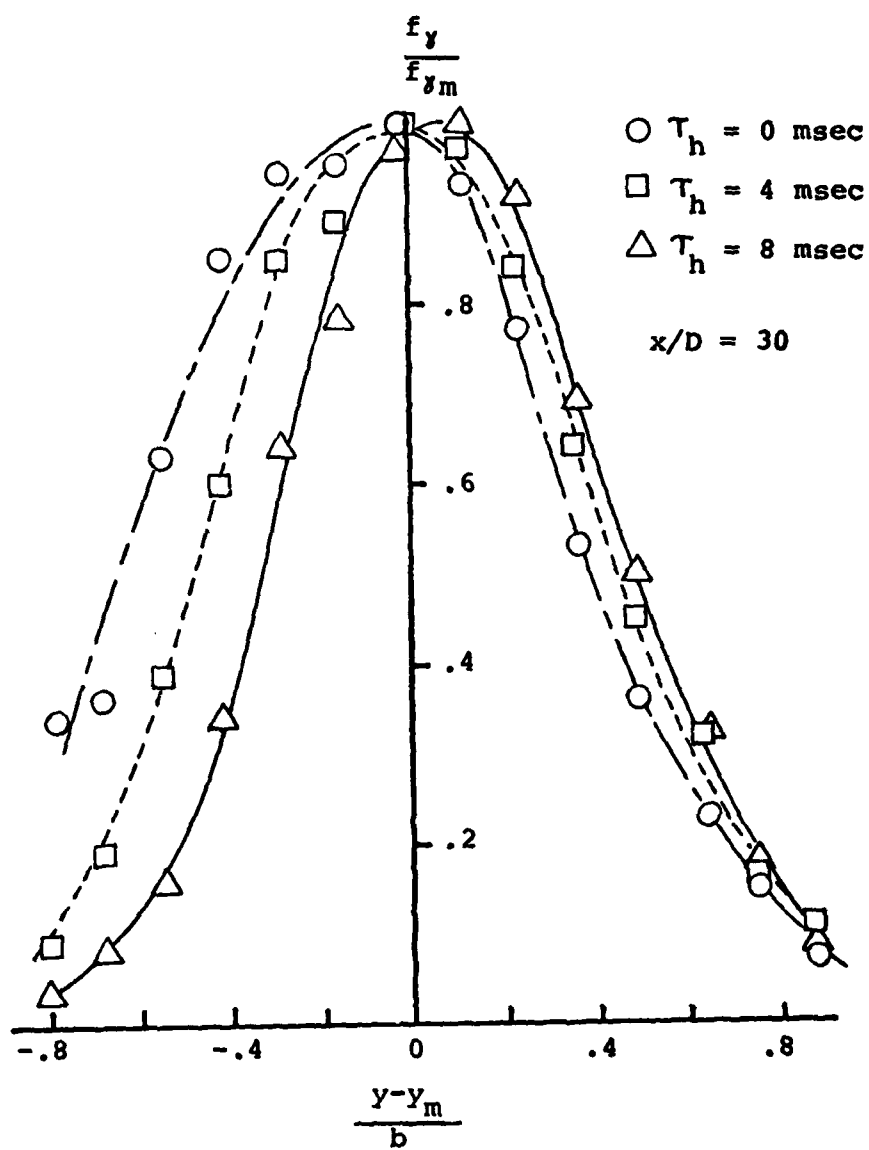


Figure 3-4 Sensitivity of  $f_y/f_{ym}$  to  $\tau_h$

The analogous case, in which  $\tau_h$  is held constant and the time scales of the interface motion change for increasing  $x$  is illustrated in Figure 3-5. Distributions of  $f_y/f_{ym}$  measured at  $x/D = 30, 40$ , and  $50$  exhibit approximately the same discrepancies as in Figure 3-4. Clearly, if a meaningful comparison of interface motion is to be made over a wide range of streamwise positions, the hold time must be varied appropriately. Failure to do so results in an inconsistent discrimination between the various scales of interface motion in the formulation of the intermittency function.

#### 4. The Analysis Technique

Although the exact manner in which  $S$ ,  $C$  and  $\tau_h$  have been incorporated varies widely in the literature, the basic analysis techniques may be classified as either analog or digital. Analog intermittency detection instruments typically offer low set-up and operating costs. In addition, there is a certain amount of convenience that results from having a continuous, real time intermittency signal available for analysis. These features are obtained at the expense of some precision in the application of  $C$  and  $\tau_h$  to  $S(\vec{r}, t)$  to obtain  $I(\vec{r}, t)$ . Digital intermittency analysis techniques offer a high degree of precision that is limited only by the resolution and speed of the analog-to-digital converter. This precision is, however, obtained with much higher equipment purchase and operating costs than for a similar analog instrument. In addition, digital analysis techniques are typically less conveniently accomplished in the laboratory environment than analog techniques. Any improvement in convenience in digital system usage is usually associated with much higher costs.

Two methods of digital analysis have been utilized in the present research. In the early stages of the program, analog recordings of the indicator signal were made for

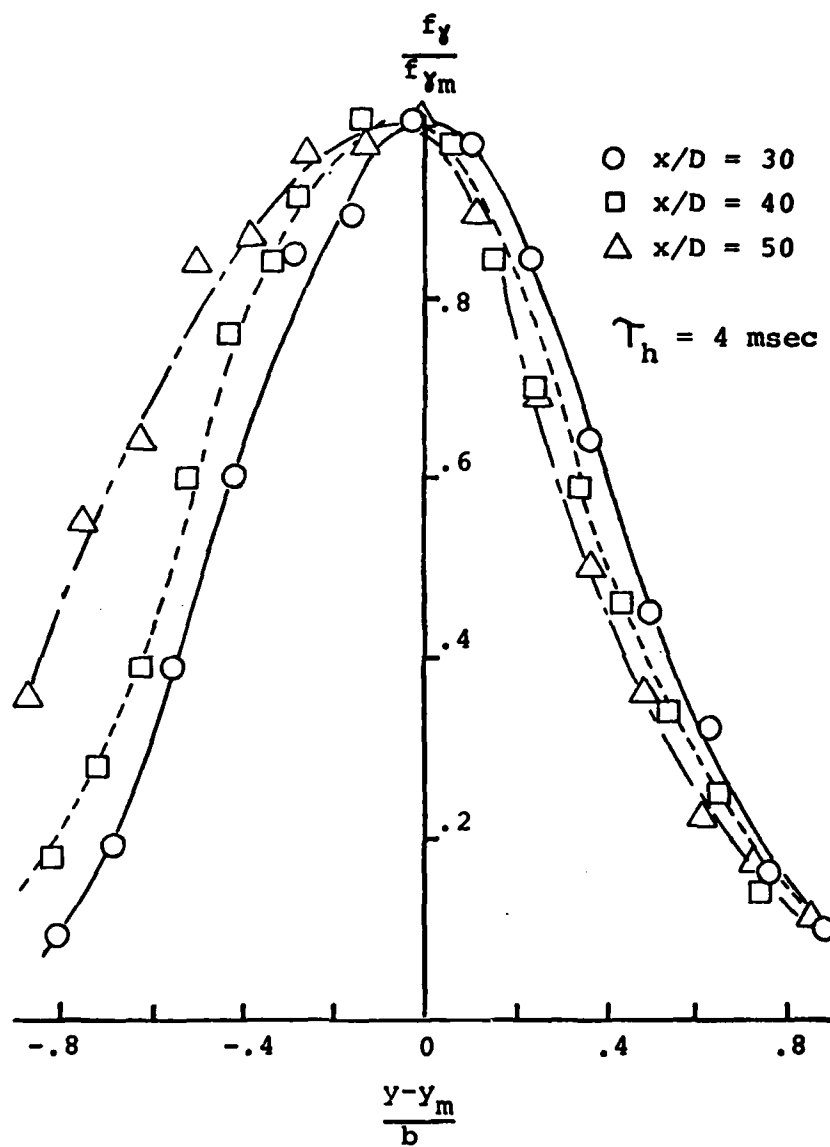


Figure 3-5 Sensitivity of  $f_y/f_{ym}$  to Local Time Scales

playback and analysis using a General Automation mini-computer. The details of the procedure and the fortran programs involved are described in detail by Oler & Goldschmidt (1978) and in Appendix B.

The final analysis procedure which was utilized for the majority of the intermittency measurements utilizes an original hybrid technique. The application of the threshold to the indicator signal was accomplished with an analog comparator circuit. Application of the hold time to this signal was then performed by an online microcomputer whose output was the completely conditioned, real-time intermittency signal. A description of the analog circuitry, microcomputer and machine language code is given by Oler & Goldschmidt (1979) and in Appendix C.

With the intermittency signal available as a continuous real-time analog signal, it was necessary to measure the average value (intermittency) and the pulse rate (interface crossing frequency). The former was accomplished by using the intermittency signal to control the gate of a digital counter whose input was a 10 kHz sine wave. Allowing the counter to run over an interval of 100 sec with gate intervals specified by the intermittency function resulted in a final count which was some fraction of  $1 \times 10^6$ . This fraction is equivalent to the intermittency fraction. The interface crossing frequency was measured by inputting the intermittency function directly to the counter and averaging over 100 sec.

### C. Correlation Measurements

Correlation measurements made during the research program consisted of two types: 1) two point fluctuating longitudinal velocity cross-correlations and 2) two point intermittency function cross-correlations.

#### 1. Velocity Cross-correlations

All fluctuating velocity correlations were measured

utilizing a Thermo-Systems, Inc. analog correlator and true rms voltmeters. Due to the low normalized correlation coefficients which were involved, it was necessary to use the 100 sec time constant settings and allow four time constants for settling.

## 2. Intermittency Cross-correlations

For normalized correlations it is necessary to have signals with zero mean values. To correlate intermittency signals, it was not possible to AC couple or high pass filter the signals prior to input to the analog correlator due to the distortion of the square wave patterns and lack of accuracy that would result. An original alternate method was utilized which took advantage of the logic level pulse train character of the intermittency signals.

The normalized correlation coefficient is defined as:

$$R_I(\Delta \vec{r}, \tau) = \frac{\overline{[I_1(t) - \gamma_1][I_2(t + \tau) - \gamma_2]}}{\{ \overline{[I_1(t) - \gamma_1]^2} \overline{[I_2(t + \tau) - \gamma_2]^2} \}^{1/2}} \quad (3.1)$$

where  $\Delta \vec{r} = \vec{r}_1 - \vec{r}_2$

$$(\overline{\quad}) = \lim_{T \rightarrow \infty} \frac{1}{T} \int_{-T/2}^{T/2} (\quad) dt$$

$$\gamma_1 = \overline{I_1(t)} = \overline{I(\vec{r}_1, t)}$$

$$\gamma_2 = \overline{I_2(t)} = \overline{I(\vec{r}_2, t)}$$

Utilizing the fact that  $\overline{I_i \delta_j} = \delta_i \delta_j$ , Eq. 3.1 may be expanded as

$$R_I(\Delta \vec{r}, \tau) = \frac{\overline{I_1(t)I_2(t + \tau)} - \gamma_1\gamma_2}{\{ \overline{[I_1(t)^2 - \gamma_1^2]} \overline{[I_2(t + \tau)^2 - \gamma_2^2]} \}^{1/2}} \quad (3.2)$$

Eq. 3.2 may be simplified further utilizing the fact that  $I(t)$  only takes on the values (0,1). Therefore,

$$\overline{I(t)^2} = \overline{I(t)} = \gamma$$

so that Eq. 3.2 becomes

$$R_I(\Delta \vec{r}, \tau) = \frac{\overline{I_1(t)I_2(t+\tau)} - \gamma_1\gamma_2}{\{[\gamma_1 - \gamma_1^2][\gamma_2 - \gamma_2^2]\}^{1/2}} \quad (3.3)$$

The intermittencies in Eq. 3.3 were determined using the gated oscillator technique described previously. Noting that the product of two logic level signals is the equivalent of the two signals logically ANDed together, the same technique was utilized to measure the time average of  $\overline{I_1(t)I_2(t+\tau)}$  after performing the logical AND operation electronically.

An additional complication in measuring the cross-correlation between two intermittency signals resulted from the on-line microcomputer being capable of applying the hold time to only one signal at a time. This problem was remedied by applying the hold time to one signal and recording the output simultaneously with the other signal. The hold time could be applied to the second signal on playback resulting in the availability of both intermittency signals for the zero time delay correlations. This procedure, utilizing the recorder, has the additional feature of allowing the time averages  $\overline{I_1(t)}$ ,  $\overline{I_2(t+\tau)}$  and  $\overline{I_1(t)I_2(t+\tau)}$  to be taken over simultaneous data records.

Time delays were introduced using a second on-line microcomputer. It was programmed to sample the fully formulated intermittency functions at 5 kHz, store the result in a data buffer and simultaneously output the saved status of the

intermittency signals with a prescribed delay. The machine language code required for this function is given in Appendix C.



## CHAPTER IV

### EXPERIMENTAL RESULTS

The primary goal of the research program, as noted in Chapter I, was to investigate the coherent structures of a fully developed plane jet. Early in the research, the presence of a vortex street type structure was suspected and hence hypothesized for the remainder of the work. The task then became to test the compatibility of the vortex street model with respect to measurable jet properties.

A vortex street type structure would have to exhibit:

- 1) Periodicity
- 2) Organization over large distances
- 3) Some degree of two-dimensionality
- 4) Compatibility with similarity considerations.

The requirement for two-dimensionality should not be interpreted too rigorously. Conceivably, a vortex structure could consist of a complex, yet organized and periodic structure such as that observed by Perry & Lim (1978) and Pao & Kao (1977). Although their investigations were in axisymmetric fields, the possibility of a slanted or looped structure in a two-dimensional field (especially one confined by horizontal planes) should not be discarded.

Compatibility with similarity considerations is a requirement if the structure is to play a consistent role in the transport dynamics of a self-preserving flow. However, if the structure were simply propagated or convected through by the mean field, similarity would not be necessary for its existence. As it turns out, every indication has been that the primary source of energy transfer from the mean flow to

the fine scale turbulence is the large scale structures. From that point of view, structural similarity would be required by the concept of local dynamic equilibrium in a developing and self-preserving flow. In Chapter V, the inducing nature of the vortex-like structure will be discussed, showing that it is not simply a wave-type motion impressed on the mean flow.

The major objective of the experimental program has been to evaluate the extent of compliance of the real jet flow with the vortex street characteristics described above. The properties measured were the intermittency, interface crossing frequency and space-time correlations. These and inferences from them are now presented.

#### A. Intermittency and Interface Crossing Frequency

A vortex-like structure should dominate the characteristics of the flow field and dictate the instantaneous position of the turbulent-nonturbulent interface. If the geometry of the interface is controlled by the underlying turbulent structure, then properties of that structure may be inferred from intermittency measurements.

The lateral distributions of the intermittency,  $\gamma$ , and normalized interface crossing frequency,  $f_\gamma/f_{\gamma m}$ , are given in Figures 4-1 and 4-2. The lateral coordinate used for these plots has been centered at the position of maximum crossing frequency ( $y_m/b = 1.6 \pm .05$ ) and scaled by the local velocity halfwidth,  $b$ . For this jet (see Figure 2-4),

$$b/D = .098 (x/D + .619) \quad (4.1)$$

when  $x/D > 10$

The plots exhibit similarity in that the curves from various longitudinal positions collapse on the  $y/b$  coordinate.

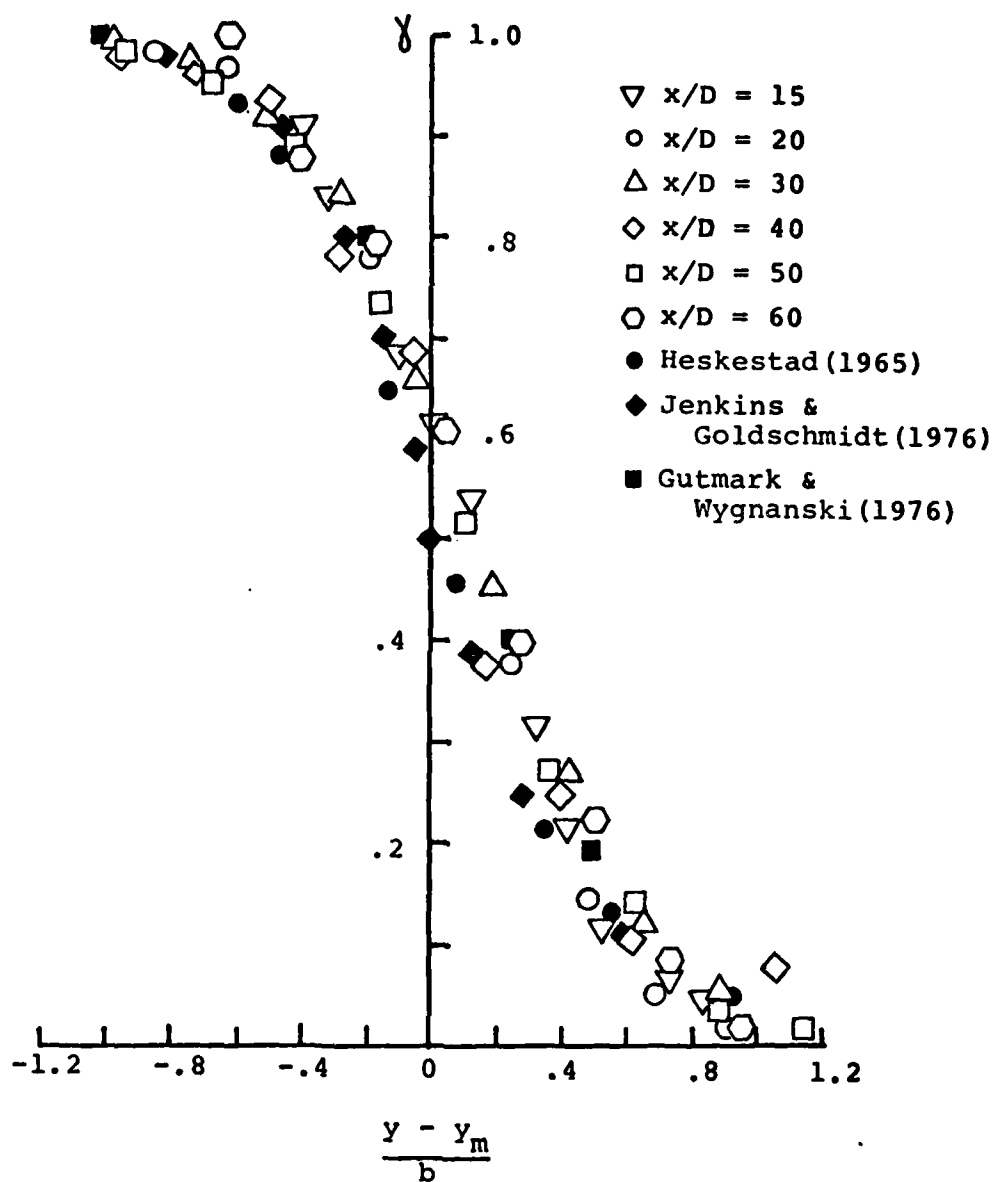


Figure 4-1  $\gamma$  vs.  $(y - y_m)/b$

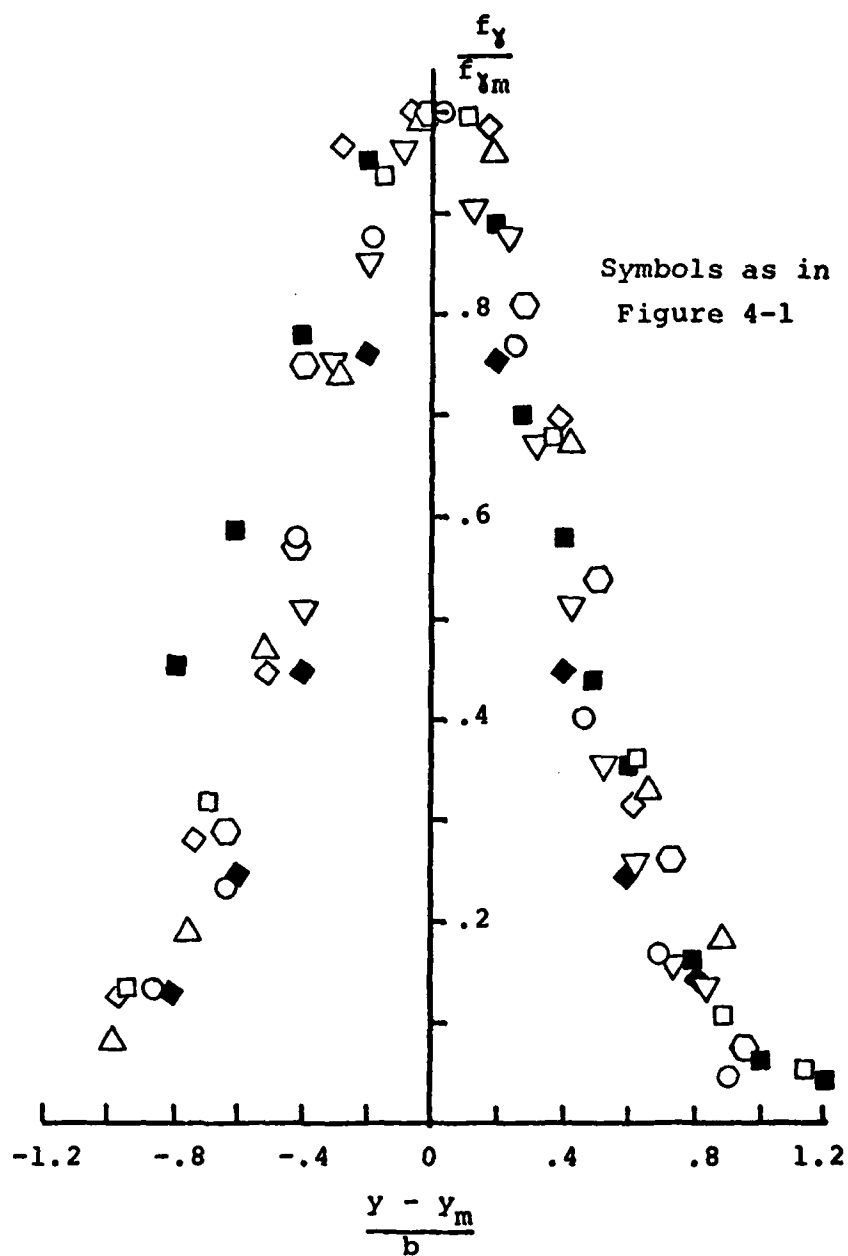
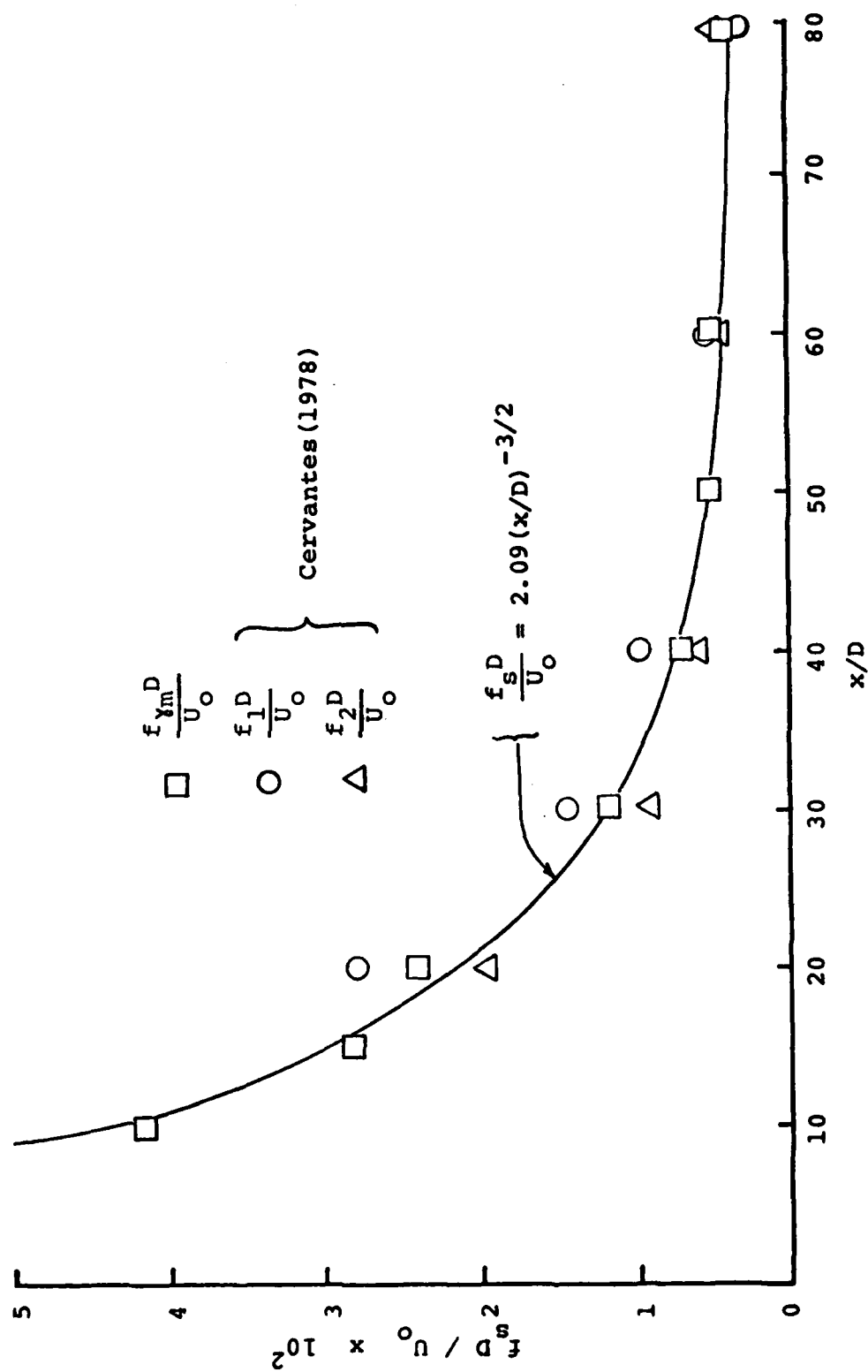


Figure 4-2  $f_y/f_{ym}$  vs.  $(y - y_m)/b$

The mean interface position is given by the point of maximum crossing frequency. At that location, as noted from Figure 4-1, the corresponding intermittency is approximately 0.6, not 0.5 as would be demanded by a symmetric distribution function. The same feature ( $\gamma > 0.5$  at  $f_\gamma = f_{\gamma m}$ ) has been noted by Gutmark & Wygnanski (1976), Moum, et al. (1979) and Everitt & Robins (1978). The explanation is that the interface is more sharply folded in its troughs than on its crests. In the present investigation, this feature indicates that the interface maintains a qualitatively similar shape at all streamwise positions since the  $\gamma = 0.6$  value is maintained.

The fact that the curves collapse on a  $y/b$  plot also implies similarity for the underlying lateral turbulent length scales and geometries. Similarity scaling or simply structural similarity is critical to proving the validity of the vortex street model since the large eddies are expected to play a consistent role in the downstream development of the jet. Additional indications of structural similarity will be noted throughout the rest of this chapter and the concept will provide the key to formulation of the interpretive model given in the next chapter.

The downstream variation of  $f_{\gamma m}$  is given in Figure 4-3 along with the apparent "flapping" frequency of Cervantes (1978). Cervantes measured the frequencies with the cross-correlation function of longitudinal velocity fluctuations from opposite sides of the jet.  $f_1$  corresponds to the frequency inferred from the time delay for the first peak of the oscillating correlation function while  $f_2$  represents that derived from the average of the peak to peak delay intervals. Rather than "flapping" frequency, the term structural passage frequency (or simply structural frequency) will be used throughout the remainder of this report.

Figure 4-3  $f_s D / U_o$  vs.  $x/D$

Strong support for the assumption of relatedness between the interface geometry and underlying structure is given by Figure 4-3. Although both experiments were made at the R. W. Herrick Laboratories, they were completely independent of each other and were made on totally separate jet apparatus.

From similarity arguments for the plane jet, global length scales are expected to vary in proportion with  $x/D$  while velocity scales should go as  $(x/D)^{-1/2}$ . Therefore, a global frequency scale should vary as  $(x/D)^{-3/2}$ . This behavior is verified by the crossing frequency data of Figure 4-3. If a dimensionless frequency is formed from the structural frequency,  $f_s$ , velocity halfwidth and mean centerline velocity, a flow constant,  $S_s$ , results. Values of this constant for the present research and reported measurements of "flapping" frequency are given in Table 4.1. The relatively close agreement suggests a universal instability mechanism similar to that analyzed by Mattingly & Criminale (1971) (see Section II.B.4).

From the streamwise variation of  $f_{ym}$ , it may be shown that the net number of large scale structures per unit length decreases as the flow develops. If  $u_s(x/D)$  is the convective velocity of the structures, then the average wavelength of the pattern is given by

$$\ell_s(x/D) = u_s(x/D)/f_s(x/D) . \quad (4.2)$$

Since the pattern represented by Figure 2-5 consists of two vortices per wavelength, the density of vortices in a cross-stream section of unit thickness is

$$n(x/D) = 2/\ell_s(x/D) . \quad (4.3)$$

Combining Eqs. 4.2 and 4.3 yields

Table 4-1. Summary of Reported Structural Frequencies

$\frac{f_s b}{U_m}$	$x/D$	$R_D$	Investigator
0.1 - 0.2 <sup>++</sup>	44-71	-	Bradbury (1965)
0.06*	45	$2.6 \times 10^4$	Goldschmidt & Bradshaw (1973)
0.12 <sup>‡</sup>	12	$10^5$	Weir & Bradshaw (1975)
0.08 - 0.14 <sup>+</sup>	20-100	$7.9 \times 10^3$ - $1.5 \times 10^4$	Cervantes (1976)
0.1 - 0.15 <sup>++</sup>	100	$3 \times 10^4$	Everitt & Robins (1978)
.09 <sup>++</sup>	10-60	$1.7 \times 10^4$	present

\* Determined from average peak to peak intervals of the correlation function between velocity fluctuations

<sup>+</sup> Determined by interval to the first peak of the correlation function between velocity fluctuations

<sup>‡</sup> Determined by peak in cross-spectral density distribution of velocity fluctuations

<sup>++</sup> Determined from interface crossing frequencies



$$n(x/D) = 2f_s(x/D)/u_s(x/D) . \quad (4.4)$$

Treating the structural density as a transferable flow quantity, a measure of the net local "production" rate of the vortices is

$$\dot{q}_n(x/D) = u_s(x/D) \frac{dn(x/D)}{d(x/D)} \quad (4.5)$$

The variation of  $u_s$ ,  $f_s$  and  $n$  may be described by the similarity scaling relationships given in Eqs. 4.6

$$\frac{u_s(x/D)}{U_o} = C_U(x/D)^{-1/2} ; U_s = C_U X^{-1/2} \quad (4.6a)$$

$$\frac{f_s(x/D)D}{U_o} = C_F(x/D)^{-3/2} ; F_s = C_F X^{-3/2} \quad (4.6b)$$

$$n(x/D)D = 2 \frac{C_F}{C_U} (x/D)^{-1} ; N = 2 \frac{C_F}{C_U} X^{-1} \quad (4.6c)$$

Substituting Eqs. 4.6 into Eq. 4.5 yields

$$\begin{aligned} \dot{Q}_N &= \dot{q}_n D^2 / U_o \\ &= U_s dN/dX \\ &= -2 C_F X^{-5/2} \end{aligned} \quad (4.7)$$

From Figure 4-3,  $C_F = 2.09$  and Eq. 4.7 becomes

$$\dot{Q}_N = -4.18 x^{-5/2} \quad (4.8)$$

Although a net reduction in the number of large structures is indicated by the minus sign in Eq. 4.8, no conclusions may be drawn concerning the mechanism which accounts for that loss. Either eddy coalescence or a net unbalance of the natural generation and decay of the large eddies are viable possibilities.

#### B. Spatial Characteristics of the Large Structures

A vortex street structure in a fully developed jet flow would have to exhibit specific spatial relationships for the instantaneous velocity field and turbulent-nonturbulent interface geometry. In particular, the counter rotating vortices positioned on opposite sides of the centerline would produce antisymmetric transverse distributions of longitudinal velocity and intermittency. Additionally, there would be a periodically repeated pattern of the velocity field and interface geometry with respect to downstream distance.

The existence of the spatial relationships described above may be tested experimentally by measurements of space-time correlations of velocity fluctuations and the intermittency function. The correlation coefficients of the longitudinal velocity fluctuations and intermittency functions at points A and B with separations  $\delta_x$ ,  $\delta_y$  and  $\delta_z$  and relative time delay,  $\tau$ , are given by Eqs. 4.9 and 4.10.

$$R_u(\tau; \delta_x, \delta_y, \delta_z) = \frac{\overline{u_A(t)u_B(t+\tau)}}{\overline{u_A'} \overline{u_B'}} \quad (4.9)$$

$$R_I(\tau; \delta_x, \delta_y, \delta_z) = \frac{(I_A(t) - \gamma_A)(I_B(t+\tau) - \gamma_B)}{[(I_A - \gamma_A)^2 (I_B - \gamma_B)^2]^{1/2}} \quad (4.10)$$

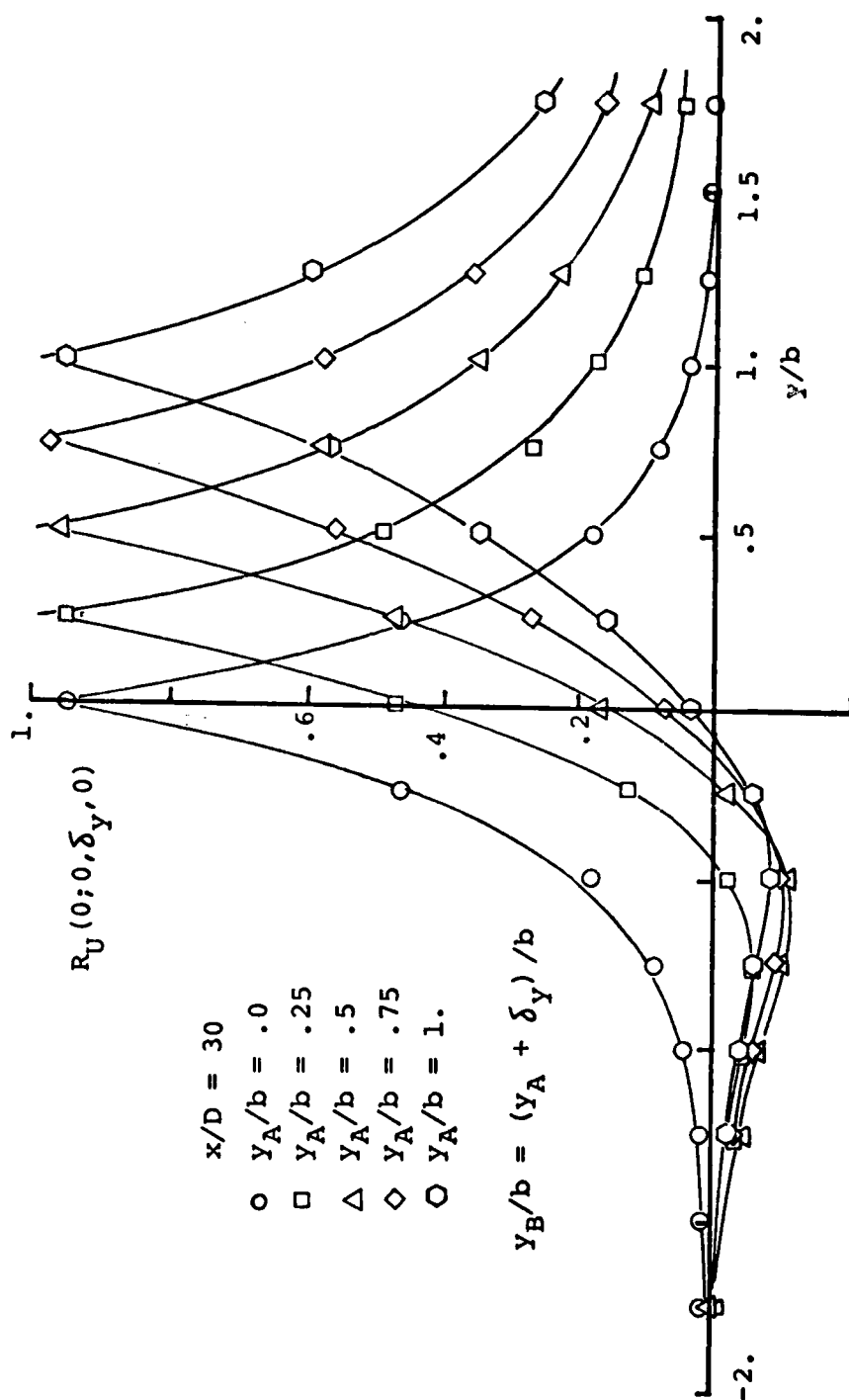
### 1. Velocity Correlation Results

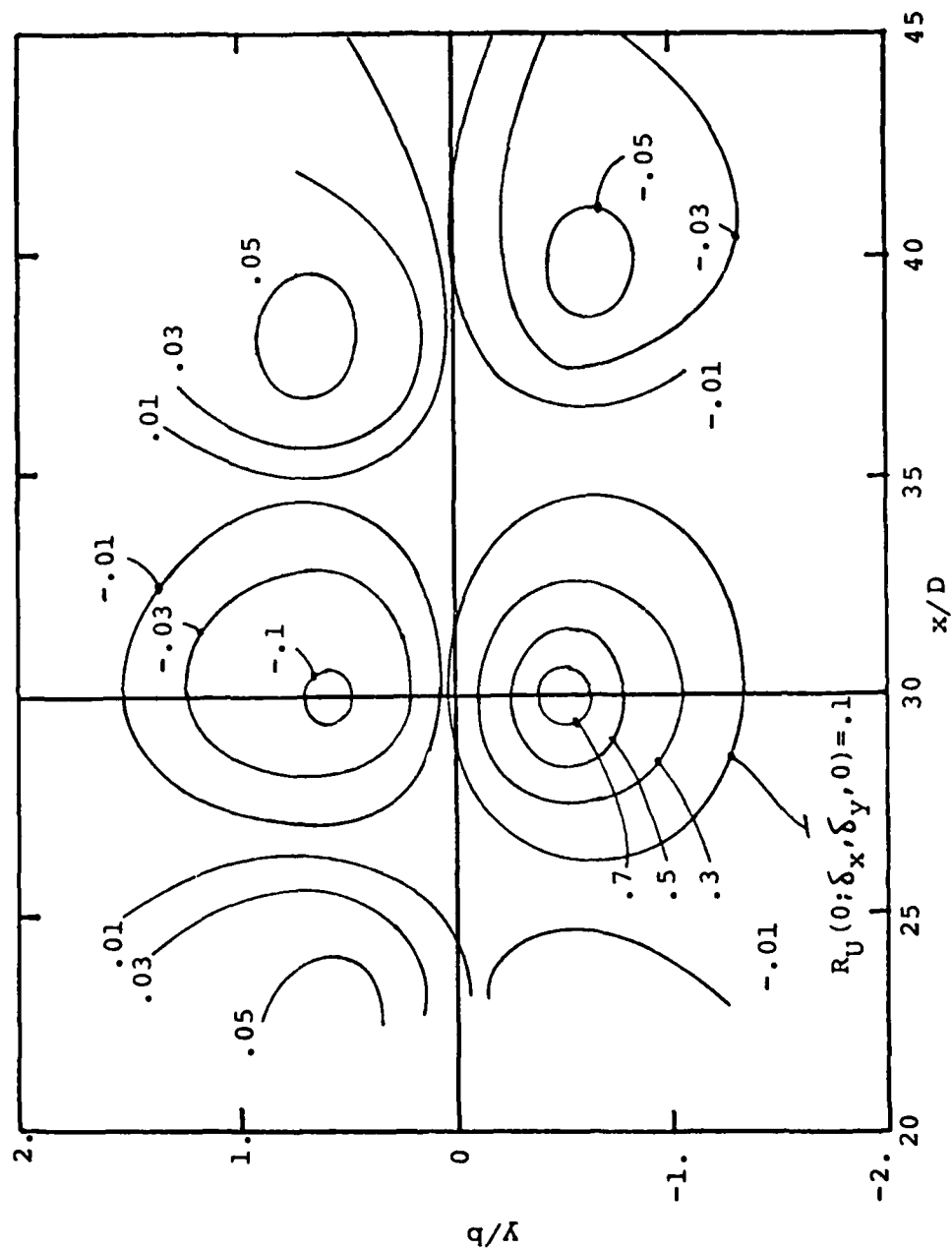
The instantaneous asymmetry of the longitudinal velocity distribution is evidenced by the distributions of  $R_u(0; 0, \delta_y, 0)$  given in Figure 4-4. The most obvious feature of the distributions are the strong negative correlations between the velocity fluctuations on opposite sides of the centerline and extending well into the intermittent regions. Similar results have been found by Goldschmidt & Bradshaw (1973), Gutmark & Wygnanski (1976), Cervantes (1978) and Everitt & Robins (1978).

The correlation measurements which result from both longitudinal and lateral separation of the velocity probes are presented in Figure 4-5 in the form of an isocorrelation contour map. The map provides a graphic illustration of the instantaneously antisymmetric velocity field and periodically repeatable structural pattern. The actual distance over which the measurable flow organization exists ( $x/D \approx 20$  to 45) is quite remarkable and strongly supports the possibility of a vortex street eddy pattern.

### 2. Intermittency Correlation Results

The correlation,  $R_I(0; 0, \delta_y, 0)$ , was measured for the intermittency signals at points symmetrically placed on either side of the centerline such that  $\gamma_A = \gamma_B = 0.5$ . A vortex street structure should force an antisymmetric displacement of the interfaces such that the resulting correlation is negative. The measurements revealed, however, a zero correlation, indicating that the motions of the interfaces were independent of one another. The same conclusion was found by Wygnanski & Gutmark (1971) and Moum, et al. (1979).

Figure 4-4  $R_U(0; 0, \delta_y, 0)$



$(x_A/D, y_A/b) = (30, .5)$ ,  $x_B/D = (x_A + \delta_x)/D$ ,  $y_B/b = (y_A + \delta_y)/b$

Figure 4-5  $R_U(0; \delta_x, \delta_y, 0)$

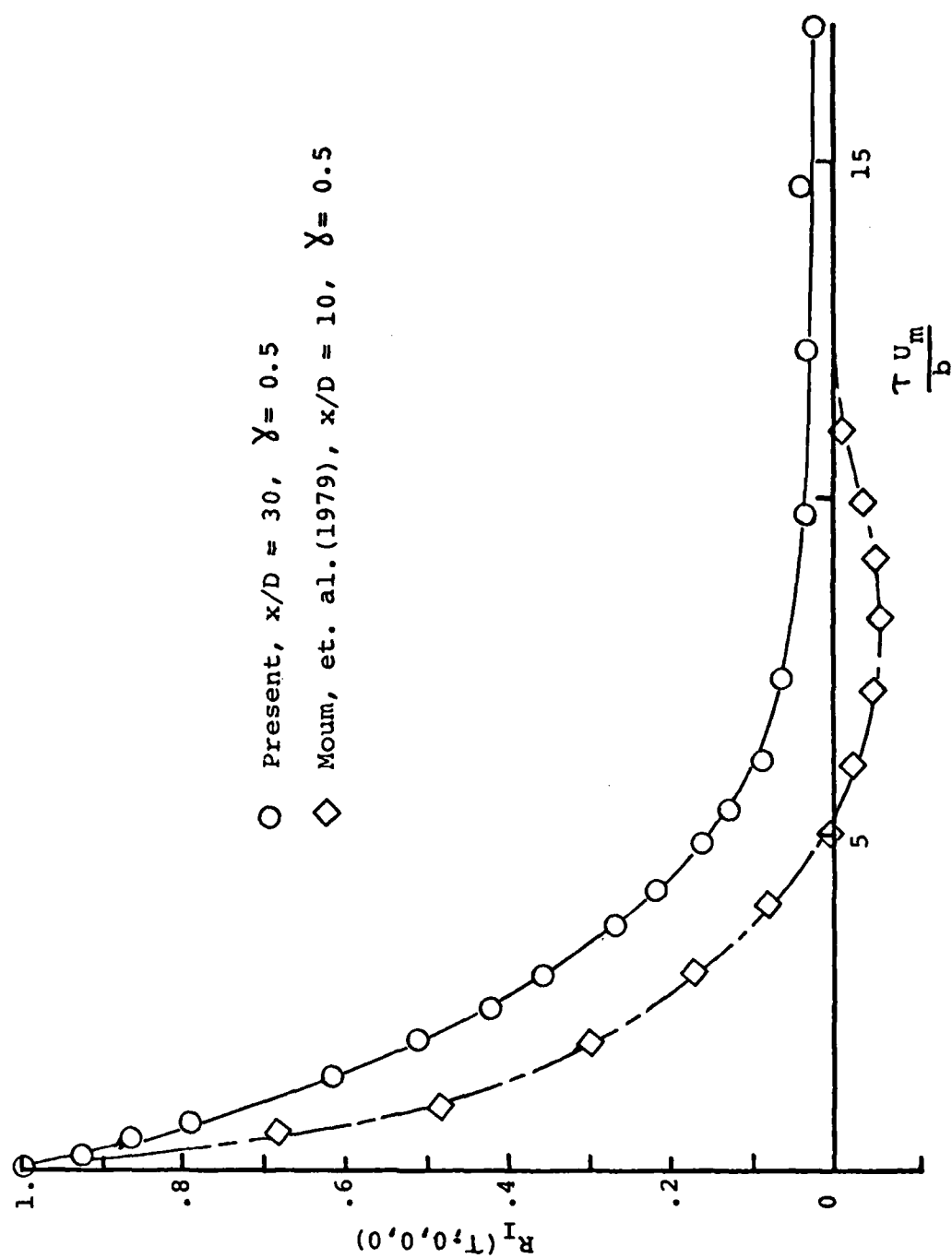
The periodicity of a vortex street-type structure should produce periodic interface geometries. An indication of this should be present in autocorrelations of the intermittency functions. Results of measurements of this type are given in Figure 4-6 ( $x/D = 30$ ,  $\gamma = 0.5$ ). For comparison, similar experimental results by Moum, et al. are included ( $x/D = 10$ ,  $\gamma = 0.5$ ). For a meaningful comparison of the experiments, the time delay,  $\tau$ , has been made dimensionless by the local length and velocity scales,  $b$  and  $U_m$ , respectively.

Although there is no indication of periodicity in the present investigation, the results of Moum, et al., do contain a weak negative lobe. They ascribe the negative correlations to statistical instabilities that result from applying Fourier transforms to finite length data records. If instead, the time interval for the negative peak were interpreted as a half-period of the interface motion, a dimensionless structural frequency of  $S_s = 0.06$  would be indicated. This interpretation of the Moum, et al. data compares favorably with the values of Table 4.1, supporting further the hypothesis of a vortex street structure. Unfortunately, the present data do not exhibit the expected negative lobe. This may be attributed to either the different techniques used in the determination of  $I(\vec{r}, t)$  and  $R_I(\tau)$ , to the difference in measurement positions ( $x/D = 30$  vs.  $x/D = 10$ ) or to violation of the hypothesis.

### C. Two-Dimensionality

The vortex street structure of a fully developed plane jet flow should exhibit a certain degree of two-dimensionality, subject to the qualifications given at the beginning of this chapter. This two-dimensionality should be reflected in the internal turbulent velocity field as well as in the interface geometry.

Quantification of the degree of two-dimensionality is accomplished experimentally by comparing characteristic



longitudinal and vertical length scales. These length scales are derived from the correlations of velocity and intermittency (see Eqs. 4.9 and 4.10) and are defined as:

$$\Lambda_x^g = \int_0^\infty R_g(0; \delta_x, 0, \delta_z) d\delta_x \quad (4.11)$$

$$\Lambda_z^g = \int_0^\infty R_g(0; \delta_x, 0, \delta_z) d\delta_z \quad (4.12)$$

with  $g = u$  or  $I$ .

1. Length Scales of the Intermittent Region

Figure 4-7 illustrates correlations of the intermittency function at  $x/D = 30$  and  $\gamma = 0.5$ . Similar measurements were taken for  $10 \leq x/D \leq 60$ . It should be noted that the space correlations,  $R_I(0; \delta_x, 0, 0)$ , like the autocorrelations,  $R_I(\tau; 0, 0, 0)$ , of the previous section, do not exhibit a negative lobe.\* (A negative lobe would have further confirmed the hypothesized periodicity of the interface geometry).

The integral length scales were derived from  $R_I(0; \delta_x, 0, 0)$  and  $R_I(0; 0, 0, \delta_z)$  curves such as Figure 4-7 using Eqs. 4.11 and 4.12.

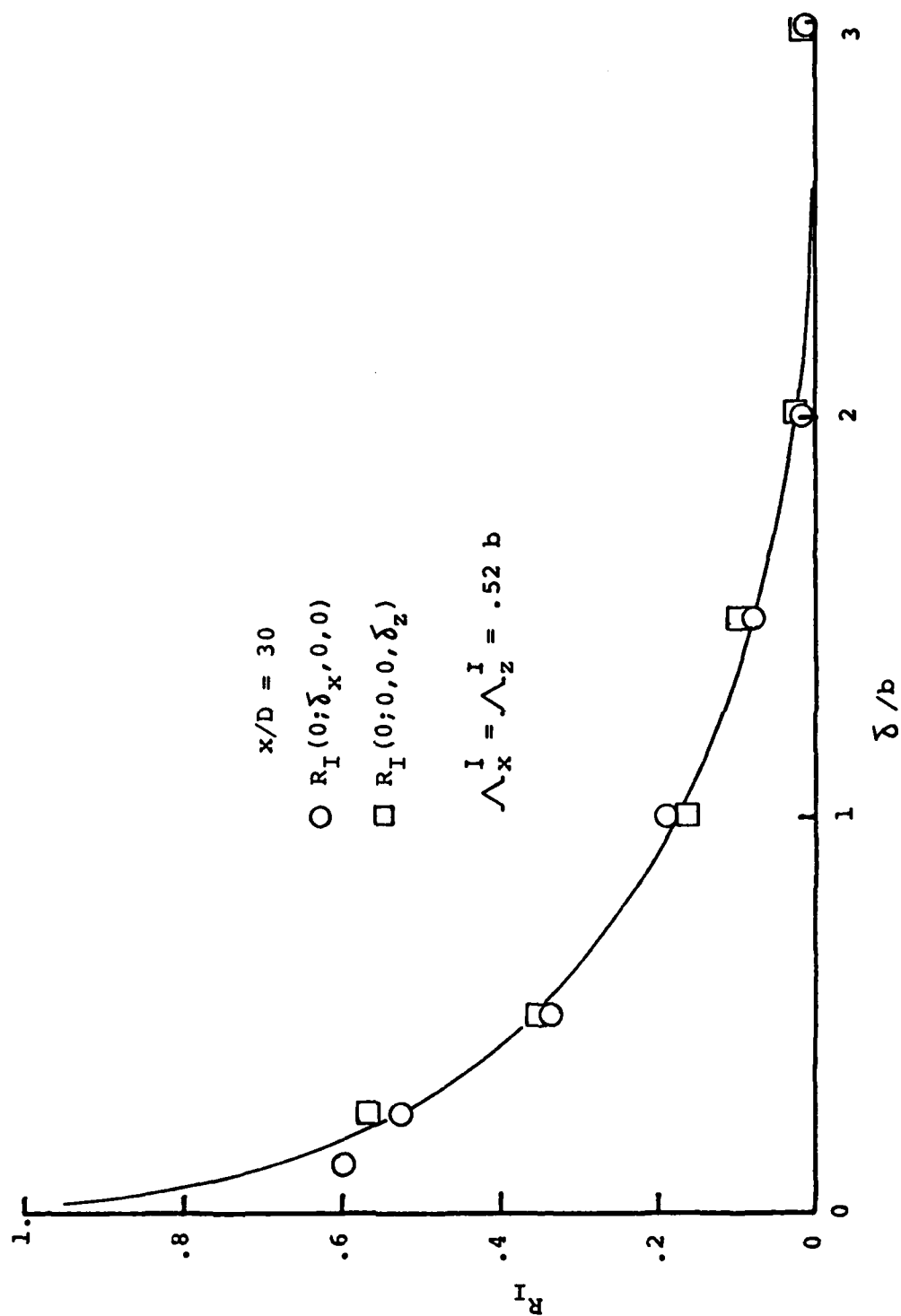
The resulting streamwise distributions of  $\Lambda_x^I$  and  $\Lambda_z^I$  are given in Figure 4-8. Once again, the self-preserving variation of all intermittency length scales is evident. From Figure 4-8, it is apparent that the longitudinal and vertical length scales are approximately equal.

$$\Lambda^I = \Lambda_x^I = \Lambda_z^I$$

---

\* Auto and space correlations in the mean flow direction may be related by invoking Taylor's hypothesis, i.e.,  $R(0; \delta_x, 0, 0) = R(-u_s \tau; 0, 0, 0)$ .



Figure 4-7  $R_I(0; \delta_x, 0, 0)$  and  $R_I(0; 0, 0, \delta_z)$

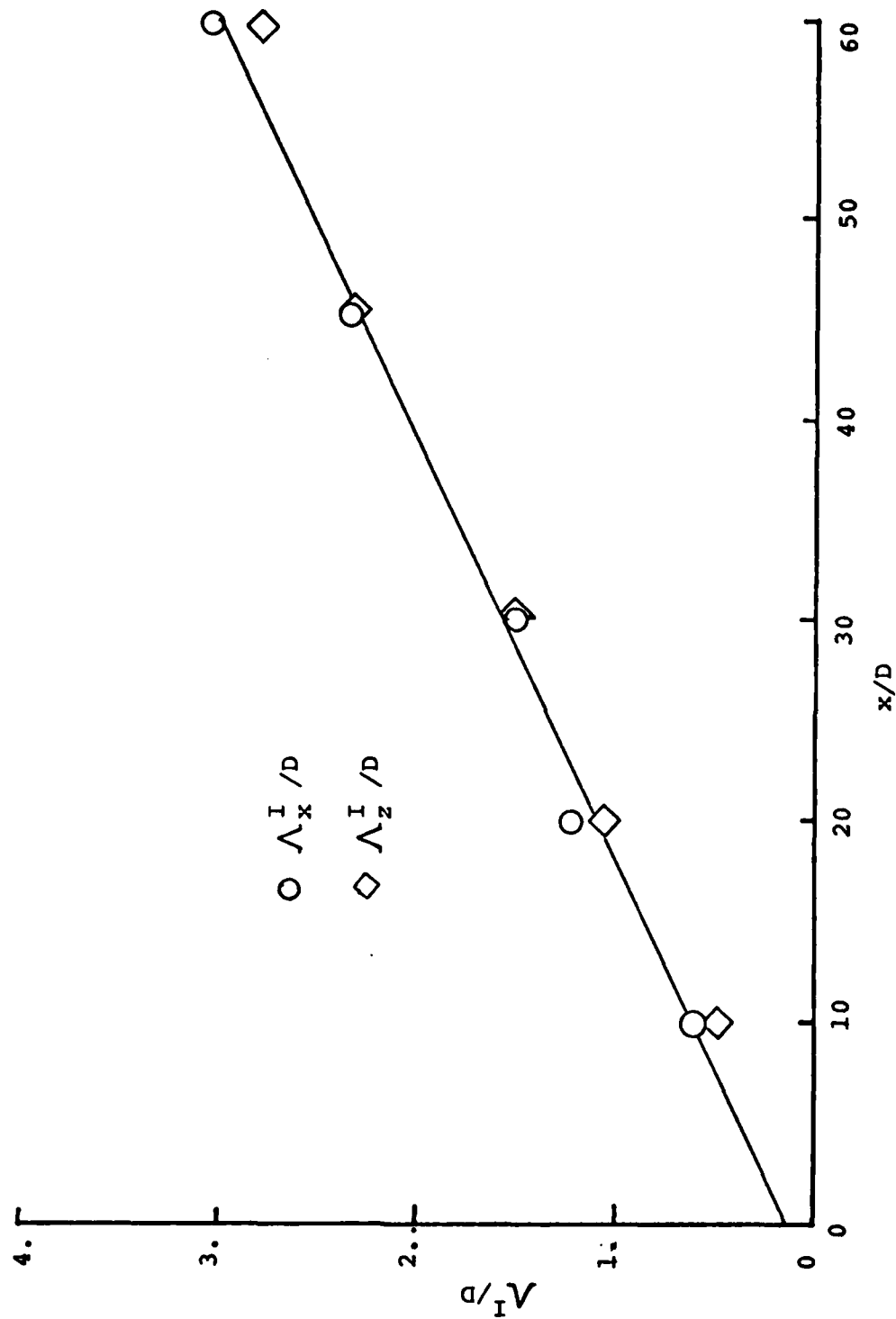


Figure 4-8  $\Lambda_x^I/D$  and  $\Lambda_z^I/D$  vs.  $x/D$

$$\text{or } \Lambda^I/D = .047 (x/D + 2.5) \quad (4.13)$$

$$\Lambda^I/b = .480 \quad (4.14)$$

Moum, et al. have also reported the near equivalency of  $\Lambda_x^I$  and  $\Lambda_z^I$ . At  $x/D = 10$ , they report  $\Lambda_x^I \approx \Lambda_z^I = .47b$ .

## 2. Length Scales of the Turbulent Velocity Field

Determination of the integral length scales at  $x/D = 30$  and  $y/b = 0.0, 0.25, 0.5$  was accomplished utilizing correlations of the longitudinal velocity fluctuations. In this case, the integration with respect to the separation distances was limited to the intervals over which the correlations were positive.

A typical result is plotted in Figure 4-9. The average length scales determined from the correlation curves are

$$\Lambda_x^u/b = .65 \pm .03 \quad (4.15)$$

$$\Lambda_z^u/b = .28 \pm .02 \quad (4.16)$$

The indication here is that

$$\Lambda_x^u/\Lambda_z^u \approx 2, \quad (4.17)$$

which is surprising considering the measurements in the intermittent region. However, the results are consistent with those reported by Everitt & Robins (1978), i.e.,

$$\Lambda_x^u/b = .47 \pm .02 \quad (4.18)$$

$$\Lambda_z^u/b = .23 \pm .02 \quad (4.19)$$

indicating

$$\Lambda_x^u/\Lambda_z^u \approx 2. \quad (4.20)$$

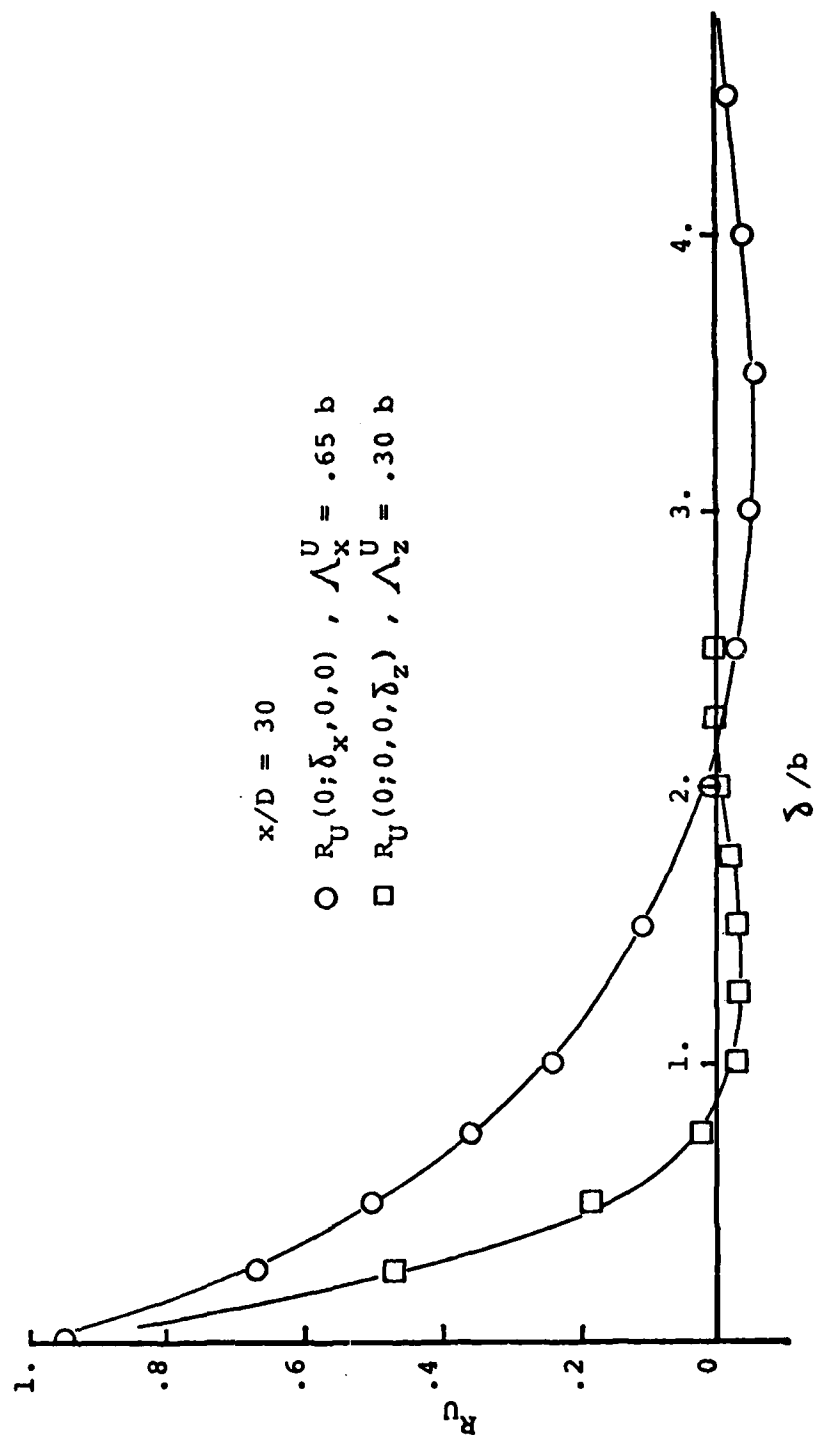


Figure 4-9  $R_U(0; \delta_x, 0, 0)$  and  $R_U(0; 0, 0, \delta_z)$

Another unexpected feature of Figure 4-10 is the negative lobe in the  $R(0;0,0,\delta_z)$  correlation. There are three possible explanations:

- 1) A combination of streamwise tilting of the large vortices and the streamwise periodicity of the velocity field (see Figure 4-5) results in the negative  $R_u(0;0,0,\delta_z)$  correlations.
- 2) The vortices undulate periodically along their length and the negative lobe in the correlation is an indication of the first wavelength.
- 3) There is a lack of coherence of the vortices in the vertical direction so that the correlation is dominated by the near isotropic small scales. The negative lobe is then the result of continuity requirements in isotropic turbulence correlations.

Based on the comparison of integral scales alone, the degree of two-dimensionality characteristic of the large structures is quite limited. However, two points must be noted:

- 1) The flow visualization experiments of Moallemi (1980) have indicated an apparently two-dimensional structure.
- 2) A similar contradiction between visualization and inferences from integral scales concerning two-dimensionality is also present in the plane mixing layer. (See Wygnanski & Fiedler (1970), Chandrsuda, et al. (1979), Pui & Gartshore (1979) and Wygnanski, et al. (1979)).

#### D. Convective Velocities

In this section, four different experimental approaches to the determination of the convective velocity of the vortex-like structure are presented.

The classical technique for the determination of convective velocities is to determine the space-time correlation function for velocity probes separated in the mean flow direction. By noting the separation distance and the

time delay which yields the peak correlation coefficient, the convective velocity may be determined from their ratio. Measurements of this type have been made by Ott (1972) and the results are tabulated in Table 4.2. A variation on this approach is to band-pass filter the velocity signals prior to forming the correlation function. Young (1973) made measurements utilizing this technique and those are also given in Table 4.2.

Between the measurements of Young and Ott, those by Young based on the lowest frequencies should be most closely tied to the velocity of the underlying large scale structure. However, the difficulty with the results of both experiments is that the convective velocities decrease monotonically away from the centerline (but not as a fixed ratio of the local mean velocity). There is no clear choice for a single velocity that could be associated with the underlying pattern.

Cervantes (1978) measured a convective velocity of the "flapping" motion which, based on the comparisons of Section IV.A, should correspond to the convective velocity of the vortex-like large structures. In addition to the symmetric spacing of the probes on opposite sides of the centerline, Cervantes also introduced a streamwise separation. By observing the shift of the negative peak correlation, the convective velocity was estimated in a manner analogous to that of Young and Ott.

The experiment was repeated for two values of the lateral spacing and the results are given in Table 4.2. Again, the convective velocities are noted to be nonconstant and their relationship to a unique structural velocity is not clear.

In the presently reported research program, a convective velocity was determined two ways.

First, it was obtained from space-time correlations of the intermittency function. Examples of these measurements

Table 4-2. Summary of Structural Related Convective Velocities

$u_c/u_m$ ***	$y/b$	Investigator
1.0	.0	† Ott (1972)
.95	.5	
.82	.75	
.68	1.0	
.57	1.5	
.425	0	* Young (1973)
.39	.5	
.39	.75	
.38	1.0	
.30	1.5	
.75	.65	‡ Cervantes
.61	1.0	
.27	1.6	++ present
.50	-	** present

+ Measured from broad band space-time correlations

\* Measured from lowest frequency narrow band correlations

‡ Measured by extension of flapping frequency correlations

++ Measured from space-time correlations of the intermittency function

\*\* Measured utilizing flow visualization technique

\*\*\* The symbol ' $u_c$ ' is used to represent all of 'convective' velocities described IV.D

for various probe separations are given in Figures 4.10 and 4.11. The results are given in Figure 4-12 and were tabulated in Table 4.2. The indicated convective velocities of the interface bulges are  $U_{CI}/U_m \approx 0.27 \pm .02$ .

Secondly, in collaboration with Moallemi (1980), the convective velocity of the structural pattern was obtained from the instantaneous positions of the vortices using flow visualization and consideration of the self-preserving nature of plane jets.

At a given longitudinal position, the structural frequency, pattern wavelength and structural velocity are related by Eq. 4.2, or

$$u_s = \ell_s * f_s \quad (4.21)$$

Since the jet is a self-preserving flow, Eq. 4.21 may be expressed in terms of the similarity variables:

$$U_s = L_s * F_s \quad (4.22)$$

where , following Eqs. 4.6

$$F_s = C_F X^{-3/2} \quad (4.23a)$$

$$L_s = C_L X \quad (4.23b)$$

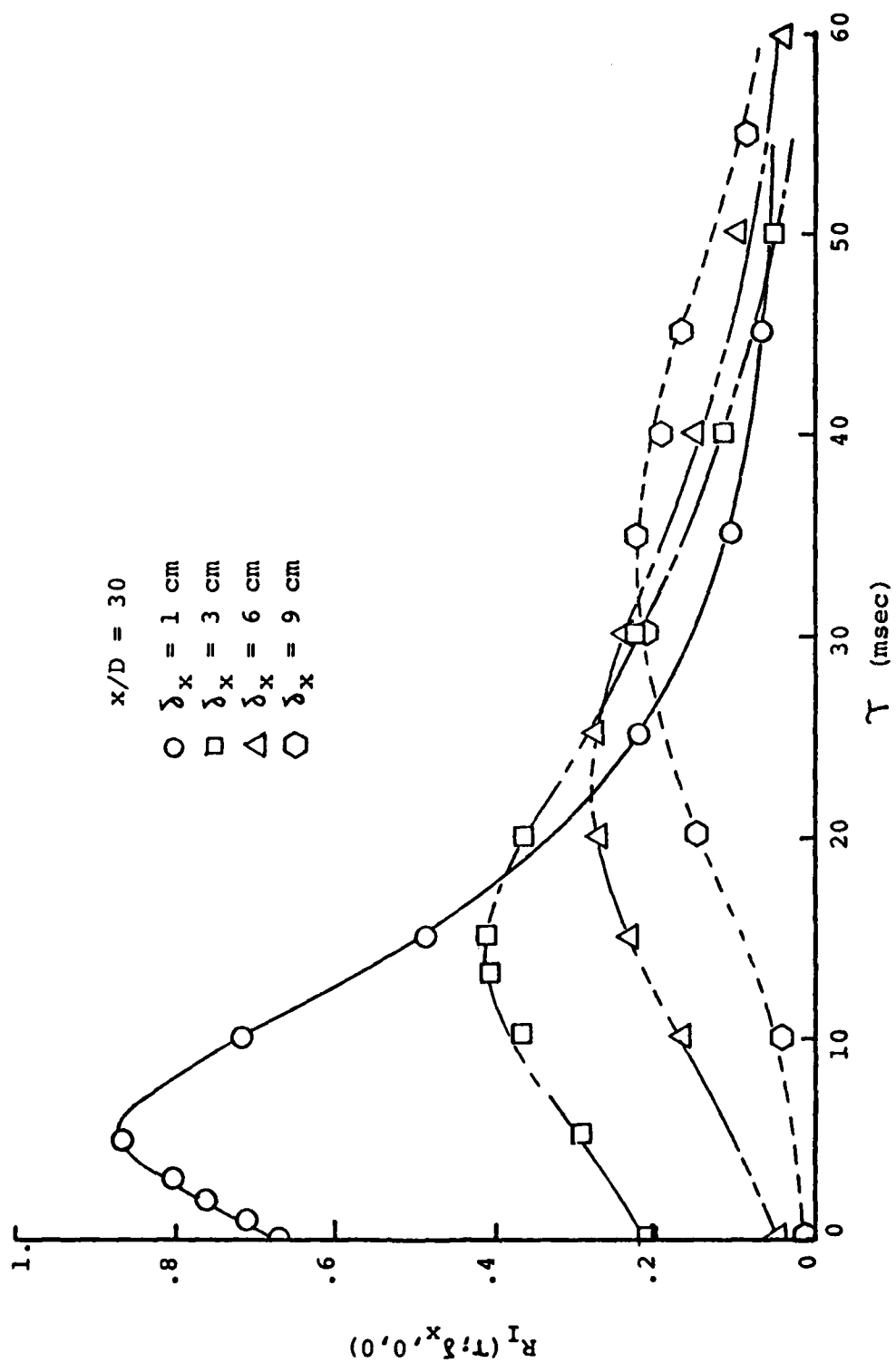
$$U_s = C_U X^{-1/2} . \quad (4.23c)$$

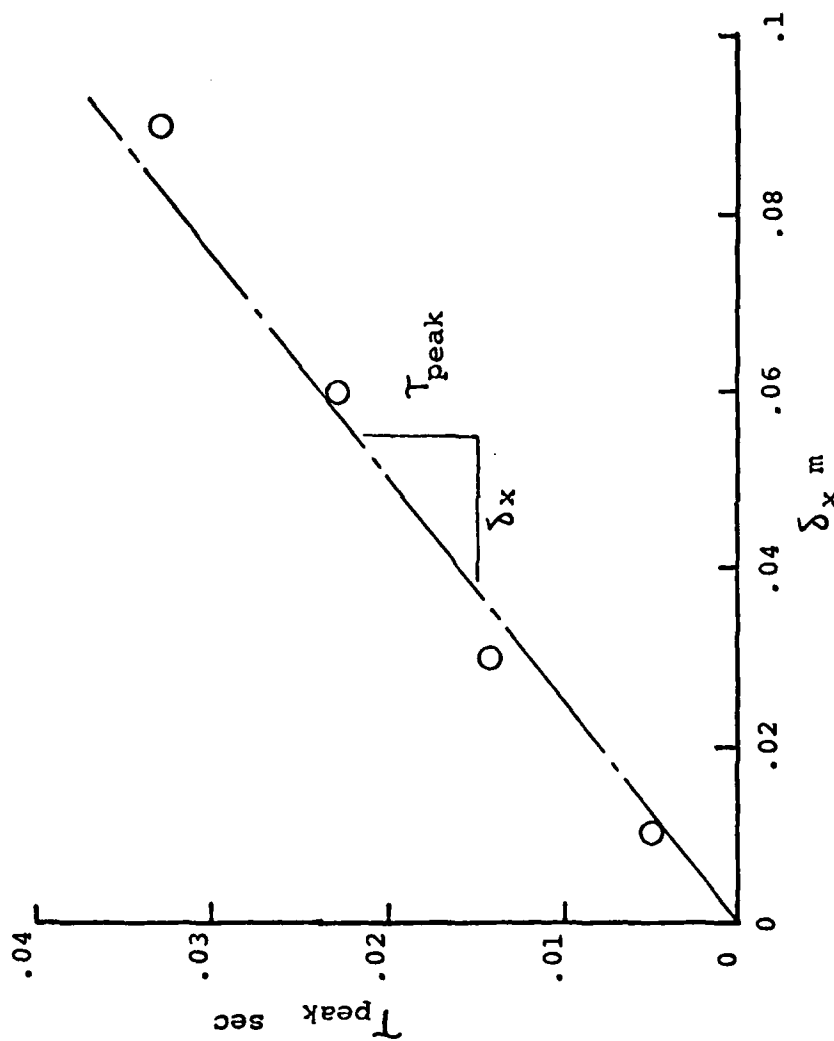
Substitution of Eqs. 4.23 into Eq. 4.22 yields

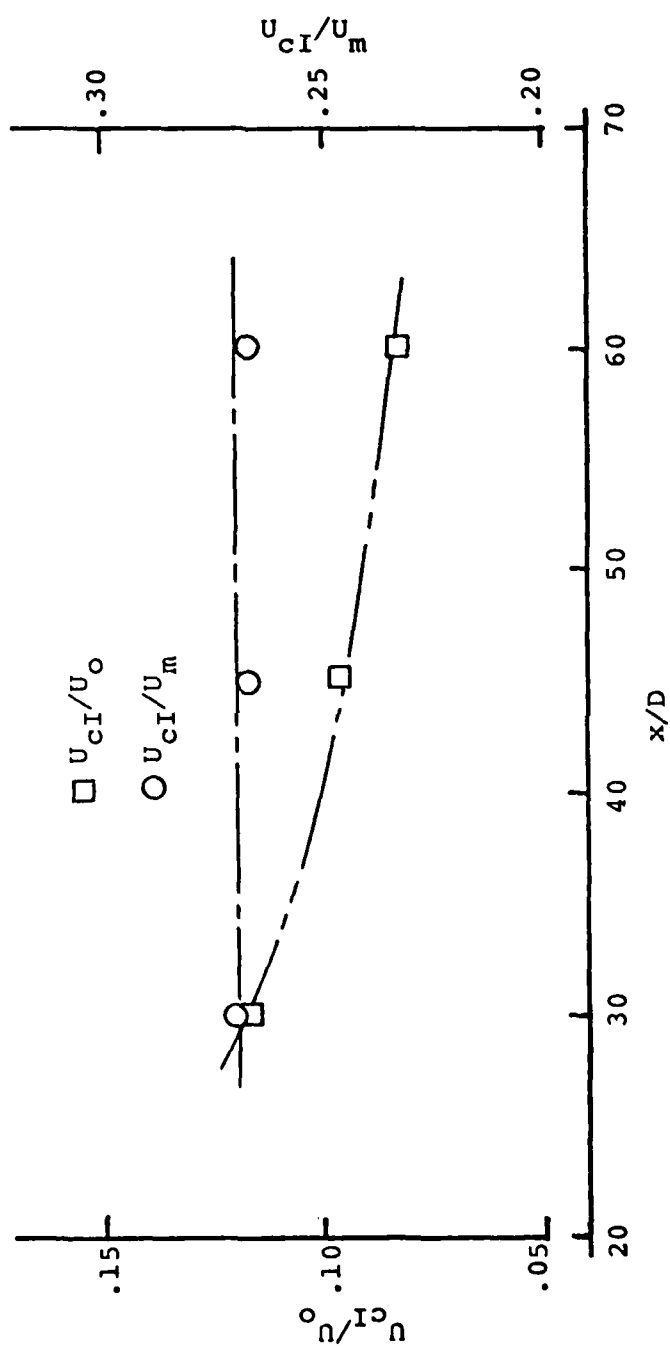
$$C_U = C_L * C_F \quad (4.24)$$

If  $C_L$  and  $C_F$  are determined experimentally, then the  $C_U$  will be given by Eq. 4.24 and the structural velocity by Eq. 4.23c.



Figure 4-10  $R_I(T; \delta_x, 0, 0)$

Figure 4-11  $T_{\text{peak}}$  vs.  $\delta_x$

Figure 4-12  $U_{cI}$  vs.  $x/D$

From Section IV.A (Table 4.1), the structural frequency constant was defined as

$$S_s = \frac{f_s b}{U_m} = 0.1. \quad (4.25)$$

For the plane turbulent jet (see Figures 2-3 and 2-4)

$$b/D \approx 0.1 (x/D) \quad (4.26)$$

$$U_m/U_o \approx 2.36 (x/D)^{-1/2} \quad (4.27)$$

Combining Eqs. 4.26 and 4.27 with Eq. 4.25 yields

$$\begin{aligned} F_s &= \frac{f_s D}{U_o} \\ &= S_s \frac{D}{b} \frac{U_m}{U_o} \\ &= 2.36 x^{-3/2} \end{aligned} \quad (4.28)$$

Therefore, from Eq. 4.23a,

$$C_F = 2.36 \quad (4.29)$$

In the following chapter, it will be shown that the longitudinal positions of the vortices in a vortex street which obeys the similarity laws for a plane jet, are uniquely defined. In particular, if a vortex is instantaneously at  $x_0$  and the position of the  $n^{\text{th}}$  downstream vortex is  $x_n^d$ , then (see Eq. 5.27)

$$C_L = \frac{2 \ln(x_n/x_0)}{n} \quad (4.30)$$

As a consequence of a Eq. 4.30, if the positions of  $n+1$  vortices are indicated from a photograph, then  $n$  estimates of  $C_L$  may be determined.

The above procedure was followed using the flow visualization results of Moallemi. It was found that due to the finite downstream length required for self-preservation to be established,  $C_L$  is a function of  $X$  that approaches its similarity value asymptotically. Therefore, the value of  $C_L$  defined by  $(X_o, X_n)$  using Eq. 4.30 was assigned to an intermediate position,  $\bar{X}$ , representing the equi-distant point in time between  $X_o$  and  $X_n$  and given by (see Chapt. V)

$$\bar{X} = X_o e^{\frac{-C_L n}{4}} \quad (4.31)$$

The results of this experiment are presented in Figure 4-13. The asymptotic value found is

$$C_L = 0.5 \quad (4.32)$$

Substitution of this value for  $C_L$  and  $C_F$  from Eq. 4.29 into Eq. 4.24 yields

$$C_U = 1.18 \quad (4.33)$$

From Eq. 4.23c,

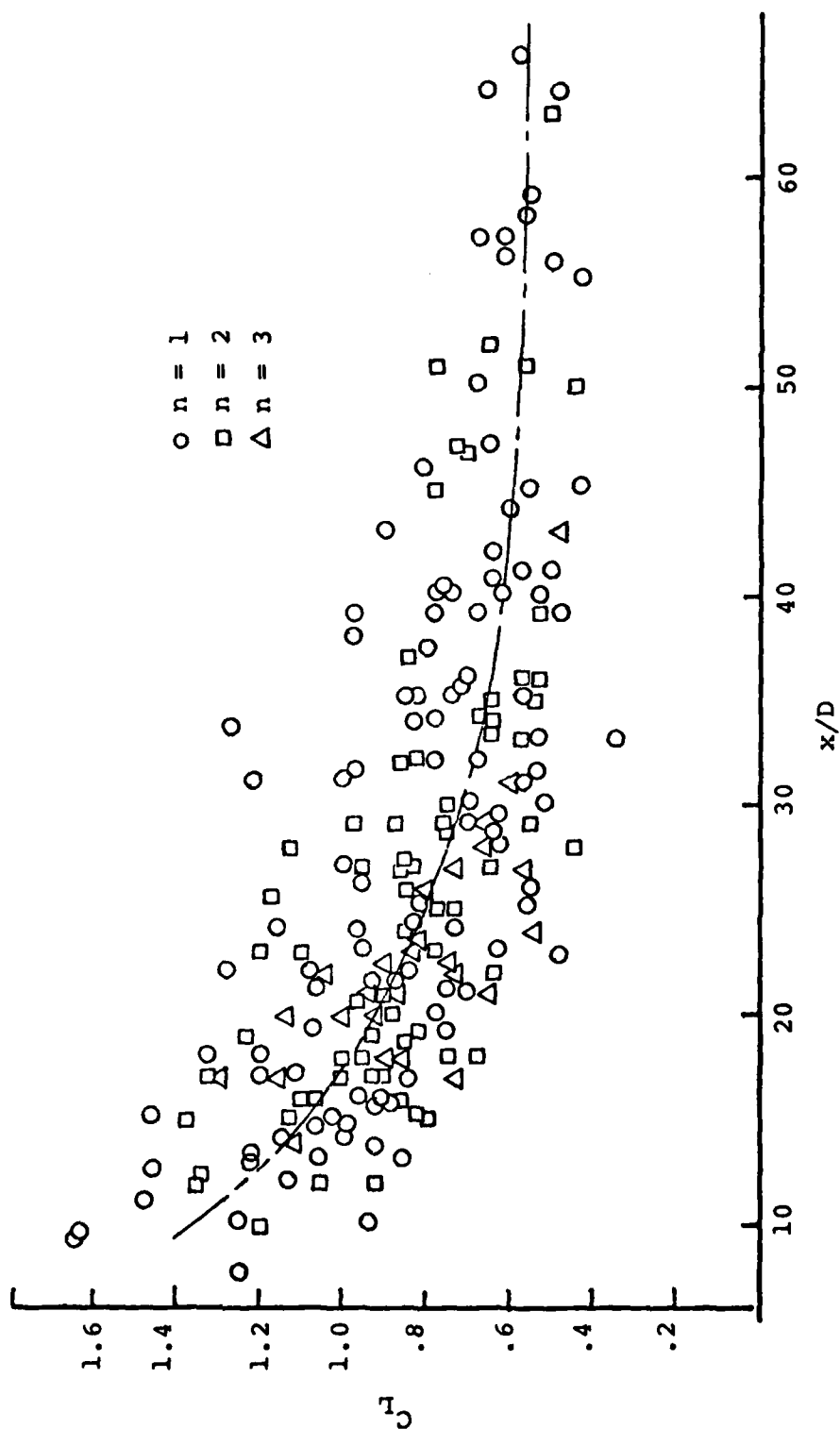
$$U_s = 1.18 X^{-1/2} \quad (4.34)$$

The ratio of the structural velocity and mean centerline velocity comes from Eqs. 4.27 and 4.34, giving

$$u_s/U_m = 0.5 \quad (4.35)$$

This result was also tabulated in Table 4.2.

A review of Table 4.2 shows a substantial difference between the broadband  $U_c$  and the other values. This is

Figure 4-13  $C_L$  vs.  $x/D$

understandable since it includes the high frequency components not characteristic of the large scales. The extrapolated values of Young, those now measured from intermittency correlations and those inferred from photographs are not too different from one another. Those from Cervantes "flapping" measurements are also in agreement although somewhat larger in magnitude. All of these are based on different global characteristics, each of which is attributed to the vortex-like structure. The differences noted could possibly be explained by the inherent differences in the measurement processes.

The highest confidence is placed upon the visualization data as a representation of the actual velocity of the vortex cores. The corresponding value of  $u_s/U_m = 0.5$  will be used in the model derivation in the following chapter.

#### E. Summary

From the experimental tests of the validity of a vortex street model for the large scale structure of turbulent plane jets, the following conclusions are found:

- 1) The global variation of all length, velocity and frequency scales are compatible with similarity requirements.
- 2) The large vortex-like motion is periodic.
- 3) The coherent vortex-like motion extends across the entire width of the flow and for considerable up and downstream distances.
- 4) The structural organization inferred from the measurements has the instantaneously antisymmetric characteristic expected of a vortex street structure.
- 5) Only a limited degree of two-dimensionality may be inferred from the measurements.
- 6) The structural pattern is convected at a velocity near one-half the mean centerline velocity.

## CHAPTER V

### A NUMERICAL SIMULATION

#### A. Introduction

As an alternate means of testing the compatibility of a vortex street model with the known characteristics of plane jet flows, a numerical simulation has been performed. The term simulation is chosen to distinguish this approach from one which makes predictions of turbulent properties based upon the solution of a set of modeling equations. Instead, the simulation provides an investigative tool with which a kinematic representation of the structure may be evaluated. The validity of the hypothesized structure is judged by the extent of agreement between the calculated flow properties and experimental and theoretically based expectations.

The approach taken to a representation of the hypothesized vortex street structure is that of a linear superposition of Rankine vortices.\* The velocity at any point in the flow field is then determined by the additive effects of all vortices making up the pattern. Although a reasonable approximation might have been to superpose the vortex street structure onto an otherwise homogeneous mean flow, that approach was not utilized in the presently reported research. It was assumed instead that the vortices, themselves, are totally responsible for the flow

---

\* The results of identical calculations using a slightly different model for the individual vortices are given in Appendix D.



field. The validity of this assumption will be discussed in the final section of this chapter.

The key consideration in the formulation of the model is the strict application of similarity scaling requirements. Experimental results given in the preceding chapter repeatedly indicated the characteristic of structural similarity in plane jet flows. That property is utilized to prescribe the streamwise variation of all the geometric and dynamic parameters which define the hypothesized structure.

Another feature of the simulated structure which is notable for its absence, is the effect of the small scale turbulence. In the current research program, the large scale structures have been of principal interest and consequently, only those effects have been modeled. The question of how the large structures interact with the small scales is a difficult problem in itself. Undoubtedly, the small scale turbulence is critically important to some of the calculated flow properties and the consequences of their neglect is evident. However, by isolating the effects of the large scales, it is clearly indicated which of the other flow properties are dominated by those scales.

Similar kinematic representations of the vortex street in a two-dimensional near wake have been reported by Hooker (1936) and Schaefer & Eskinazi (1959). These investigations utilized potential vortices, Rankine vortices or a combination of both to simulate the stable formation region of the wake. The calculations were not extended into the fully developed turbulent field.

Takaki & Kovasznay (1978) have utilized a physical representation of the large vortices in a temporally developing mixing layer to predict the eddy coalescence rate. Their primary interest was in the prediction of the statistical distribution of vortex spacings and as such,

did not attempt to calculate the velocities induced by the vortices.

To the author's best knowledge, the structural model formulation described herein is the first to fully account for the consequences of global turbulent flow field development on the determination of local mean properties. As will be shown, this is the key to understanding the effects produced by the coherent, large scale structures.

#### B. Formulation of the Model

The basic elements that make up the numerical simulation of the vortex street model are: 1) specification of the velocity induced by an isolated vortex in terms of its characteristic length and velocity scaling parameters, 2) description of the basic vortex street geometry and specification of the variation of its defining parameters with respect to downstream position, 3) development of a rationale for the determination of the longitudinal coordinates of each vortex making up the pattern, and 4) calculation of the flow properties from the net effect of the entire vortex street.

##### 1. The Rankine Vortex

The vortex street structure is modeled with an array of Rankine vortices. These vortices have the classical circumferential velocity field of a diffusing line vortex (see Lamb (1945)) given by

$$v_{\theta} = \frac{\tilde{\Gamma}}{2\pi r} [1 - \exp(-\frac{r^2}{4\nu t})] \quad (5.1)$$

and illustrated in Figure 5-1. Evaluation of  $dv_{\theta}/dr = 0$  reveals that the maximum velocity occurs at

$$\begin{aligned} r_c &= \text{core radius} \\ &= \sqrt{\frac{1.26}{4\nu t}} \end{aligned} \quad (5.2)$$

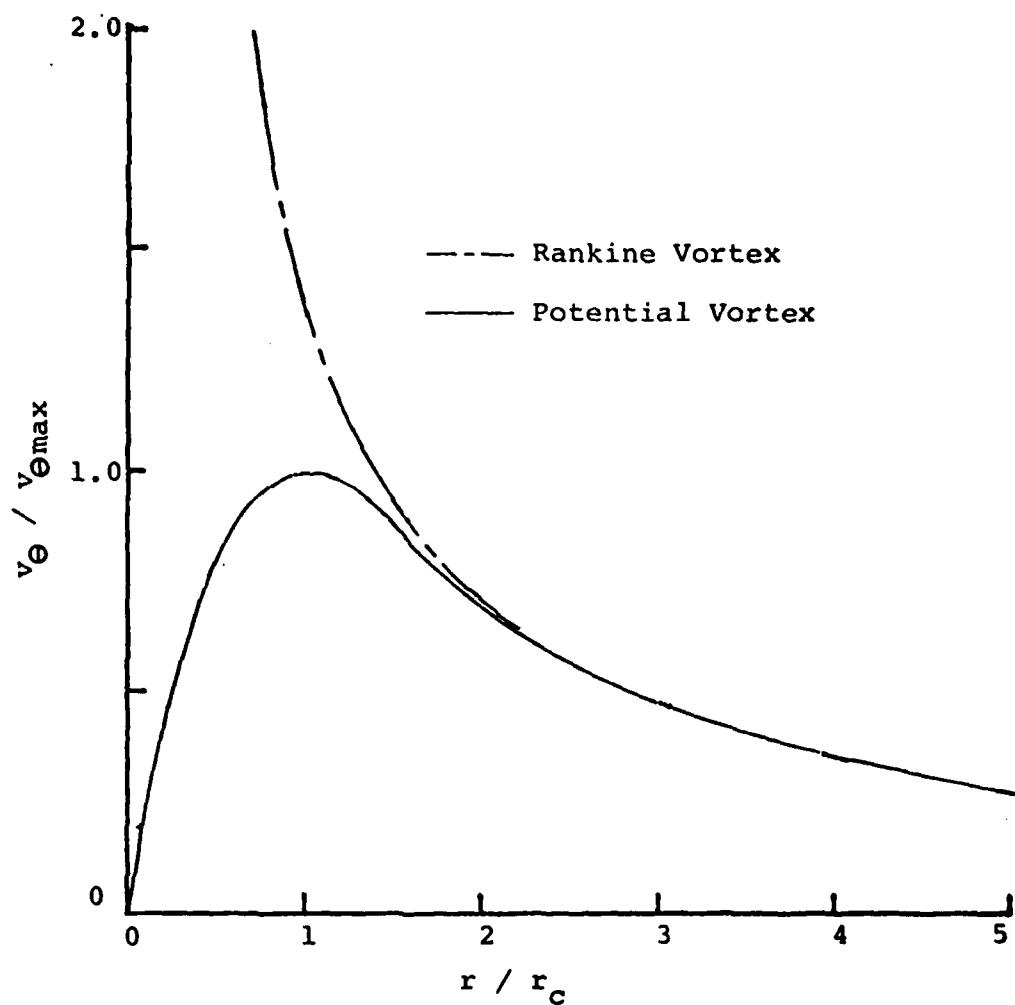


Figure 5-1 Tangential Velocity Field of a Rankine Vortex

Substitution of Eq. 5.2 into Eq. 5.1 yields

$$v_{\theta} = \frac{\tilde{\Gamma}}{2\pi r} \left[ 1 - \exp\left(-1.26 \frac{r^2}{r_c^2}\right) \right] . \quad (5.3)$$

From Eq. 5.3 and Fig. 5-1, it is noted that the velocity field surrounding a Rankine vortex is defined by the parameters  $\tilde{\Gamma}$ , the circulation strength and  $r_c$ , the core radius. For  $r > r_c$ , the induced velocity is essentially that of a potential vortex and for  $r < r_c$ , there is approximately solid body rotation.

If a Rankine vortex is centered at  $(x_i, y_i)$  in the two-dimensional coordinate system shown in Figure 5-2, the velocity components at  $(x, y)$  are given by

$$u_i(x, y) = \frac{-\tilde{\Gamma}_i \eta_i}{2\pi r_i^2} \left\{ 1 - \exp\left[-1.26 \left(\frac{r_i}{r_{ci}}\right)^2\right] \right\} \quad (5.4)$$

$$v_i(x, y) = \frac{\tilde{\Gamma}_i \xi_i}{2\pi r_i^2} \left\{ 1 - \exp\left[-1.26 \left(\frac{r_i}{r_{ci}}\right)^2\right] \right\} \quad (5.5)$$

where

$$r_i^2 = \xi_i^2 + \eta_i^2$$

$$\xi_i = x - x_i$$

$$\eta_i = y - y_i .$$

The parameters which determine the induced velocities at  $(x, y)$  and whose streamwise variation must be specified from similarity scaling relationships are

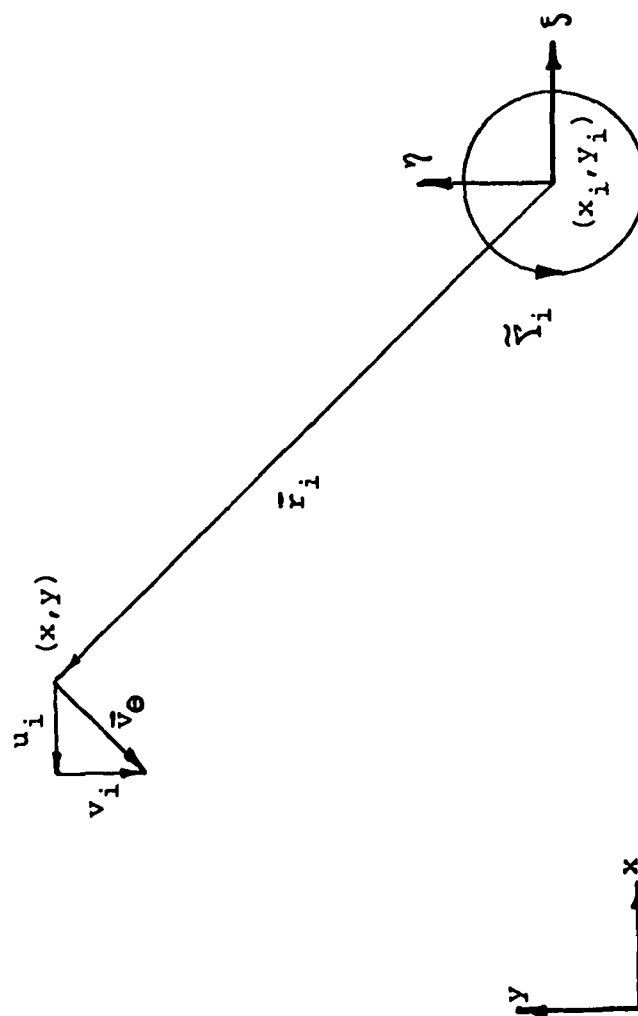


Figure 5-2 Induced Longitudinal and Lateral Velocities

$$y_i = y_i(x_i) \quad (5.6)$$

$$r_{c_i} = r_{c_i}(x_i) \quad (5.7)$$

$$\tilde{\Gamma}_i = \tilde{\Gamma}_i(x_i) \quad (5.8)$$

## 2. Similarity Scaling of the Vortex Street

The hypothesized vortex street representation of a plane jet is illustrated in Figure 5-3. From the figure, it is noted that the defining parameters of the pattern at any longitudinal station are the vortex center offset distance,  $h(x)$ , the core radius,  $r_c(x)$ , and the circulation strength,  $\Gamma(x)$ .

Also indicated in the figure is the indexing system that will be used throughout this chapter. One of the vortices with a negative lateral location is arbitrarily chosen as the reference position and labeled  $(x_0, y_0)$ . Its properties are then given by

$$y_0 = -h(x_0) \quad (5.9)$$

$$r_{c_0} = r_c(x_0) \quad (5.10)$$

$$\tilde{\Gamma}_0 = -\tilde{\Gamma}(x_0) \quad (5.11)$$

The properties of the  $i^{\text{th}}$  up or downstream vortex are given by

$$y_i = (-1)^{i+1} h(x_i) \quad (5.12)$$

$$r_{c_i} = r_c(x_i) \quad (5.13)$$

$$\tilde{\Gamma}_i = (-1)^{i+1} \tilde{\Gamma}(x_i) \quad (5.14)$$



where

$$x_i = x_i^d \text{ or } x_i^u .$$

Since the plane jet is a self-preserving flow and structural similarity is expected for the vortex street, the variation of  $h$ ,  $r_c$  and  $\Gamma$  are defined by the global length and velocity scales. In particular,

$$\frac{h(x/D)}{D} = C_H * \left(\frac{x}{D}\right) ; H(X) = C_H X \quad (5.15)$$

$$\frac{r_c(x/D)}{D} = C_r * \left(\frac{x}{D}\right) ; R_c(X) = C_R X \quad (5.16)$$

$$\frac{\tilde{\Gamma}(x/D)}{U_o D} = C_\Gamma * \left(\frac{x}{D}\right)^{1/2} ; \Gamma(X) = C_\Gamma X^{1/2} \quad (5.17)$$

Substituting Eqs. 5.15 - 5.17 into Eqs. 5.12 - 5.14 yields

$$y_i = (-1)^{i+1} H(X_i) \quad (5.18)$$

$$R_{c_i} = R_c(X_i) \quad (5.19)$$

$$\Gamma_i = (-1)^{i+1} \Gamma(X_i) \quad (5.20)$$

where

$$X_i = x_i^u \text{ or } x_i^d .$$

### 3. Specification of the Longitudinal Vortex Coordinates

The key feature remaining undefined is the instantaneous longitudinal coordinate,  $x_i^u$  or  $x_i^d$ , of each vortex. As the vortices move downstream, the pattern wavelength increases, the convective velocity decreases and the number of vortices per unit length diminishes. All of these



features must be accounted for in the determination of vortex positions utilizing a rationale that is compatible with similarity scaling requirements. This has been accomplished in the presently reported formulation by utilizing the concept of vortex density introduced in Sections IV.A and IV.B. Vortex density is useful in that it allows the description of a delta function (the vortex locations) in terms of a continuous function.

At a longitudinal station,  $X$ , the vortex pattern wavelength (see Eq. 4.22) is given by

$$L_s = U_s / F_s \quad (5.21)$$

$$L_s = C_L X \quad (5.22)$$

It should be noted that the wavelength  $L_s(X)$  is a point property since length scales change continuously up and downstream. For an observer fixed at  $X$ , it is the wavelength that he/she would calculate from knowledge of the pattern velocity and period at that point.

A similar point property is the local vortex density (see Eq. 4.3) defined by

$$N = \frac{2}{L_s}$$

$$N = \frac{2}{C_L X} \quad (5.23)$$

The constant is a consequence of there being two vortices in each wavelength of the pattern.

Consider a vortex instantaneously located at  $(X_0, Y_0)$  which is arbitrarily chosen as the reference vortex as described in the previous section and depicted in Figure 5-3. The number of vortices between  $X_0$  and some downstream

AD-A088 750

PURDUE UNIV LAFAYETTE IND RAY W HERRICK LABS  
COHERENT STRUCTURES IN THE SIMILARITY REGION OF A TWO-DIMENSION--ETC(U)  
MAR 80 J W OLER, V W GOLDSCHMIDT  
HL-80-6

F/G 20/4

N00014-75-C-1048

NL

UNCLASSIFIED

2-3

2-3

2-3

2-3

2-3

2-3

2-3

2-3

2-3

2-3

2-3

2-3

2-3

2-3

2-3

2-3

2-3

2-3

2-3

2-3

2-3

2-3

2-3

2-3

2-3

2-3

2-3

2-3

2-3

2-3

2-3

2-3

2-3

2-3

2-3

2-3

2-3

2-3

2-3

2-3

2-3

2-3

2-3

2-3

2-3

2-3

2-3

2-3

2-3

2-3

2-3

2-3

2-3

2-3

2-3

2-3

2-3

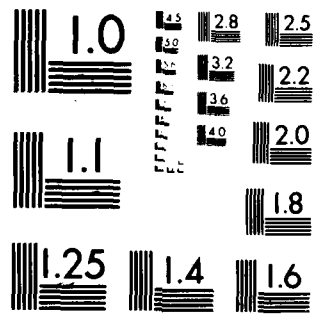
2-3

2-3

2-3

2-3

2-3



MICROCOPY RESOLUTION TEST CHART  
NATIONAL BUREAU OF STANDARDS 1963 A

position  $x^d$  may be found by integrating the vortex density with respect to  $x$ . This quantity is defined as the integrated vortex count,  $M(x_0, x^d)$ , and is given by

$$\begin{aligned} M(x_0, x^d) &= \int_{x_0}^{x^d} N \, dx \\ &= \int_{x_0}^{x^d} \frac{2}{C_L x} \, dx . \end{aligned} \quad (5.24)$$

Similarly, the integrated vortex count between  $x_0$  and an upstream position  $x^u$  is given by

$$M(x_0, x^u) = - \int_{x_0}^{x^u} \frac{2}{C_L x} \, dx . \quad (5.25)$$

Given the reference vortex position,  $x_0$ , the position of the next downstream vortex,  $x_1^d$ , is such that  $M(x_0, x_1^d) = 1$ . Utilizing Eq. 5.24 yields

$$\begin{aligned} M(x_0^d, x_1^d) &= 1 \\ &= \int_{x_0}^{x_1^d} \frac{2}{C_L x} \, dx \end{aligned}$$

therefore

$$\begin{aligned} \frac{C_L}{2} &= \ln \left( \frac{x_1^d}{x_0} \right) \\ x_1^d &= x_0 \exp \left[ \frac{C_L}{2} \right] \end{aligned} \quad (5.26)$$

The position of the  $n^{\text{th}}$  downstream vortex is found in an analogous manner:

$$M(X_0, x_n^d) = n$$

$$= x_0 \int_{x_0}^{x_n^d} \frac{2}{C_L x} dx$$

$$x_n^d = x_0 \exp\left[\frac{nC_L}{2}\right] \quad (5.27)$$

The same procedure is used to determine the position of the first upstream vortex from  $x_0$ ,

$$x_1^u = x_0 \exp\left[-\frac{C_L}{2}\right] \quad (5.28)$$

The position of the  $n^{\text{th}}$  upstream vortex is given by

$$x_n^u = x_0 \exp\left[-\frac{nC_L}{2}\right] \quad (5.29)$$

To summarize, at a given instant, the arbitrary selection of any reference vortex  $(x_0, y_0)$  (with the restriction that  $y_0 = -H(x_0)$ ) is sufficient to completely determine the longitudinal positions of all other up and downstream vortices using Eqs. 5.27 and 5.29, respectively. The corresponding lateral coordinates, core radii and circulation strengths may then be found from Eqs. 5.18 - 5.20.

#### 4. Calculation of Temporally Averaged Flow Properties

The net velocity at a point  $(X, Y)$  resulting from the linear superposition of Rankine vortices making up a vortex street is found by a simple summation of the effects of the individual vortices. Given that the reference vortex is instantaneously at  $(x_0, y_0)$ , the resulting instantaneous velocity components are given by (see Eqs. 5.4 and 5.5)

$$U(X,Y) = U^O + \lim_{n \rightarrow \infty} \sum_{i=1}^n U_i^u(X,Y) + \lim_{n \rightarrow \infty} \sum_{i=1}^n U_i^d(X,Y) \quad (5.30)$$

$$V(X,Y) = V^O + \lim_{n \rightarrow \infty} \sum_{i=1}^n V_i^u(X,Y) + \lim_{n \rightarrow \infty} \sum_{i=1}^n V_i^d(X,Y) \quad (5.31)$$

where

$\left. \begin{matrix} U^O \\ V^O \end{matrix} \right\} = \text{Velocities induced by the reference vortex}$   
 at  $(X_O, Y_O)$

$\left. \begin{matrix} U_i^u \\ V_i^u \end{matrix} \right\} = \text{Velocities induced by the upstream vortex}$   
 at  $(X_i^u, Y_i^u)$

$\left. \begin{matrix} U_i^d \\ V_i^d \end{matrix} \right\} = \text{Velocities induced by the downstream vortex}$   
 at  $(X_i^d, Y_i^d)$

The time average of the fluctuating velocity components,  $U(X,Y,\tilde{t})$  and  $V(X,Y,\tilde{t})$ , may be found by integrating with respect to time over one period of the pattern as it passes the transverse plane at  $X$ .<sup>\*</sup> The time dependence of  $U$  and  $V$  will then be determined by the instantaneous positions of the vortices in the street. When performing this operation, provisions must be made for the fact that equal time increments will not result in equal convection distances of the vortices. This is a consequence of the streamwise variation of length and velocity scales.

The problem is again resolved by utilizing the concept of a continuous vortex density. Consider the convection of vortices past the measuring station  $X$ . Over the time interval, 0 to  $\tilde{t}$ , the number of vortices which pass  $X$  may be defined as the integrated vortex flux,  $A(X,\tilde{t})$ . This

<sup>\*</sup>  $\tilde{t}$  represents a dimensionless time ;  $\tilde{t} = tU_0/D$ .

quantity is given by

$$A(X, \tilde{t}) = \int_0^{\tilde{t}} U_s N dt \quad (5.32)$$

Noting that  $U_s$  and  $N$  are functions of  $X$  only and using Eq. 5.23, Eq. 5.32 becomes

$$A(X, \tilde{t}) = \frac{2U_s}{C_L X} \tilde{t} \quad (5.33)$$

Over the interval of one period of the motion past  $X$ ,  $A(X, t)$  will increase linearly by two, indicating the passage of two vortices. This suggests utilizing the integrated vortex flux as a means of determining the time dependent positions of the vortices making up the vortex street.

The shift of the reference coordinate,  $X_0$ , downstream during the integration period is found by relating the integrated vortex flux and integrated vortex count. In particular, if for  $X_0 = X$  at  $\tilde{t} = 0$ , then from Eq. 5.27,

$$A(X, \tilde{t}) = X \int^{X_0} \frac{2}{C_L X} dx$$

or

$$X_0 = X \exp \left[ \frac{A(X, \tilde{t}) C_L}{2} \right] \quad (5.34)$$

With the instantaneous position of the reference vortex given by Eq. 5.34, the longitudinal coordinates of all other up and downstream coordinates are given by Eqs. 5.29 and 5.27, respectively. This is sufficient to determine the instantaneous velocity components at  $(X, Y; \tilde{t})$  so that the temporal averages can be found in a conventional manner.

### C. Details of the Numerics

The vortex street model formulated in the previous section is based upon the variation of four vortex related similarity variables:

$$L = C_L X \quad (5.35)$$

$$\Gamma = C_\Gamma X^{1/2} \quad (5.36)$$

$$H = C_H X \quad (5.37)$$

$$R_C = C_R X \quad (5.38)$$

As a result, there are four proportionality constants that must be determined;  $C_L$ ,  $C_\Gamma$ ,  $C_H$  and  $C_R$ .

The choices for the constants have been based upon experimental estimates or optimization of the calculated results. The length coefficient,  $C_L$ , was determined from the flow visualization experiments (see Section IV.D) and set equal to 0.5. Specification of the circulation coefficient,  $C_\Gamma$ , was accomplished by choosing the value which gave a match between calculated and experimentally determined mean centerline velocities at  $X = x/D = 45$  (i.e.,  $\tilde{U}_m = U_m/U_o = 2.36*(45)^{-1/2}$ ). The result was  $C_\Gamma = 2.597$ .

The values chosen for the offset and radius coefficients optimize the comparison between experimental and calculated results. Moallemi (1980) has estimated  $C_H = .04$  from his visualization experiments while  $C_H = .05$  was chosen for the calculations.  $C_R$  was set equal to .13 or  $.26C_L$ . The primary consideration in the choice of  $C_H$  and  $C_R$  was to match the experimentally determined spreading rate, i.e.,  $b/D = 0.1(x/D)$ .

Table V-1 provides a tabulation of the coefficients which have been utilized, criteria for their choice and a



Table 5-1 Summary of Numerical Simulation Parameters

Vortex Pattern Parameter	Numerical Value Utilized	Criteria For Choice	Visual Estimate
$C_L$	0.5	Flow visualization results	0.5
$C_T$	2.597	Required $U_m(45) = 2.36(45)^{-1/2}$	-
$C_H$	.05	Required match with experimentally determined spreading rate	.04
$C_R$	.13		.16

comparison with their visually estimated counterparts. Of the four, the choices for  $C_H$  and  $C_R$  are the most arbitrary. Illustrations of the sensitivity of the calculated results to these parameters are given in Appendix D.

Additional parameters which were involved in the numerical simulation are the time step and the vortex street truncation length. For all calculations, the time interval corresponding to one wavelength of travel by the pattern was divided into 20 equal time steps. Except for experiments concerning the truncation length specifically, the effects of 20 vortices both up and downstream of the reference vortex were included in the velocity calculations. For a reference vortex at  $x/D = 45$ , this corresponded to a stream-wise range of  $0.64 \leq x/D \leq 5200$  for the 41 vortex positions.

#### D. Numerical Calculation Results

##### 1. Mean Longitudinal Velocities

The mean longitudinal velocity at  $(X,Y)$  has been calculated as

$$\bar{U}(X,Y) = \frac{1}{T} \int_0^T U(X,Y,\bar{t}) d\bar{t} . \quad (5.39)$$

The resulting transverse distributions of  $\bar{U}(X,Y/B)/\bar{U}_m(X)$  are illustrated in Figure 5-4 for  $X = 15, 30, 45, 60$  and  $75$ . Also included in the figure are analogous experimental distributions and the analytical predictions of Görter (1942) and Reichardt (1943).

The transverse scaling length, or halfwidth (see Section II.A.3),  $B$ , for Figure 5-4 as well as all the following illustrations of lateral distributions is defined as

$$b/D = \beta * (x/D)$$

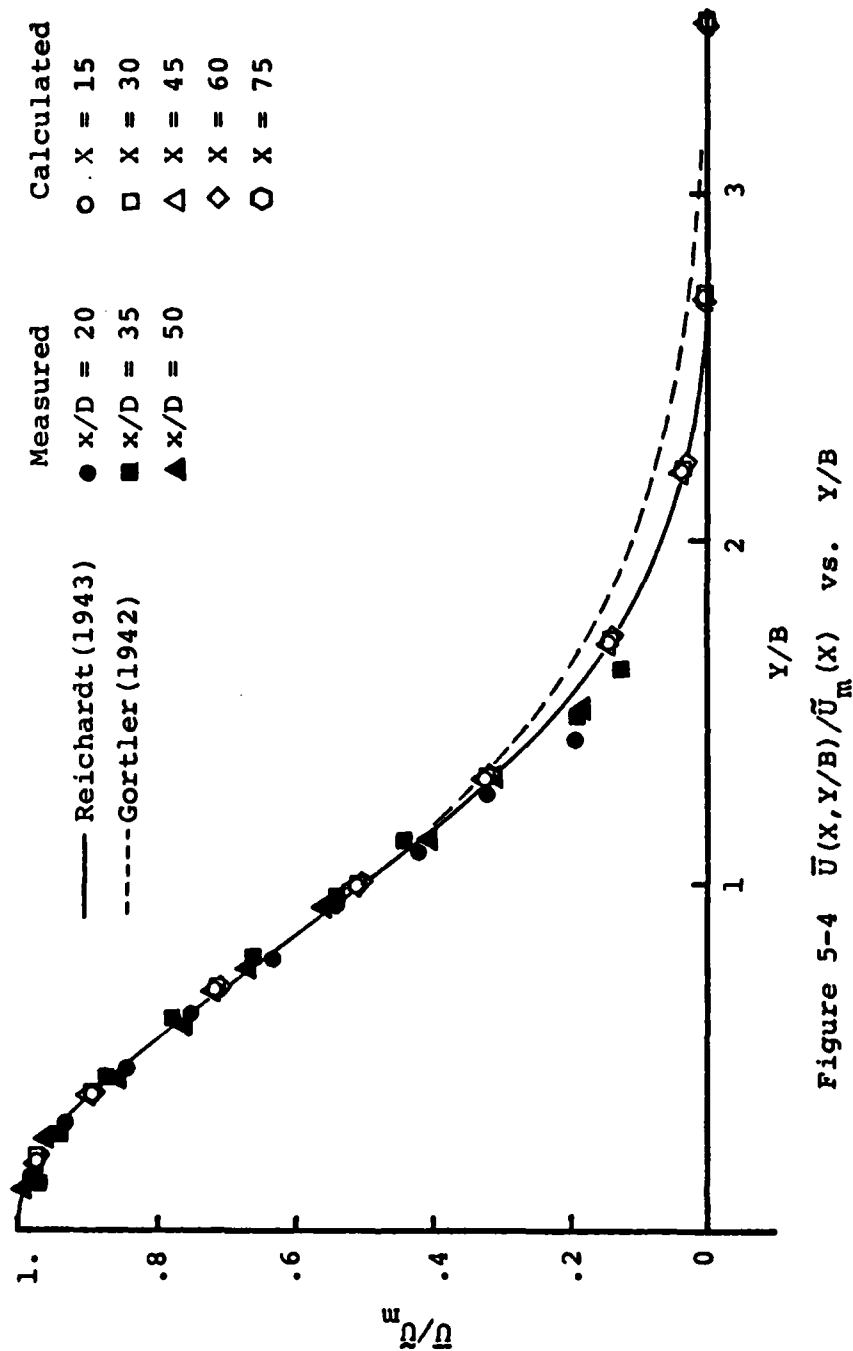


Figure 5-4  $\bar{u}(x, y/B)/\bar{u}_m(x)$  vs.  $y/B$

or

$$B = 0.1 * X . \quad (5.40)$$

The coefficient,  $\beta$ , is defined as the spreading rate and was determined experimentally as shown in Figure 2-4.

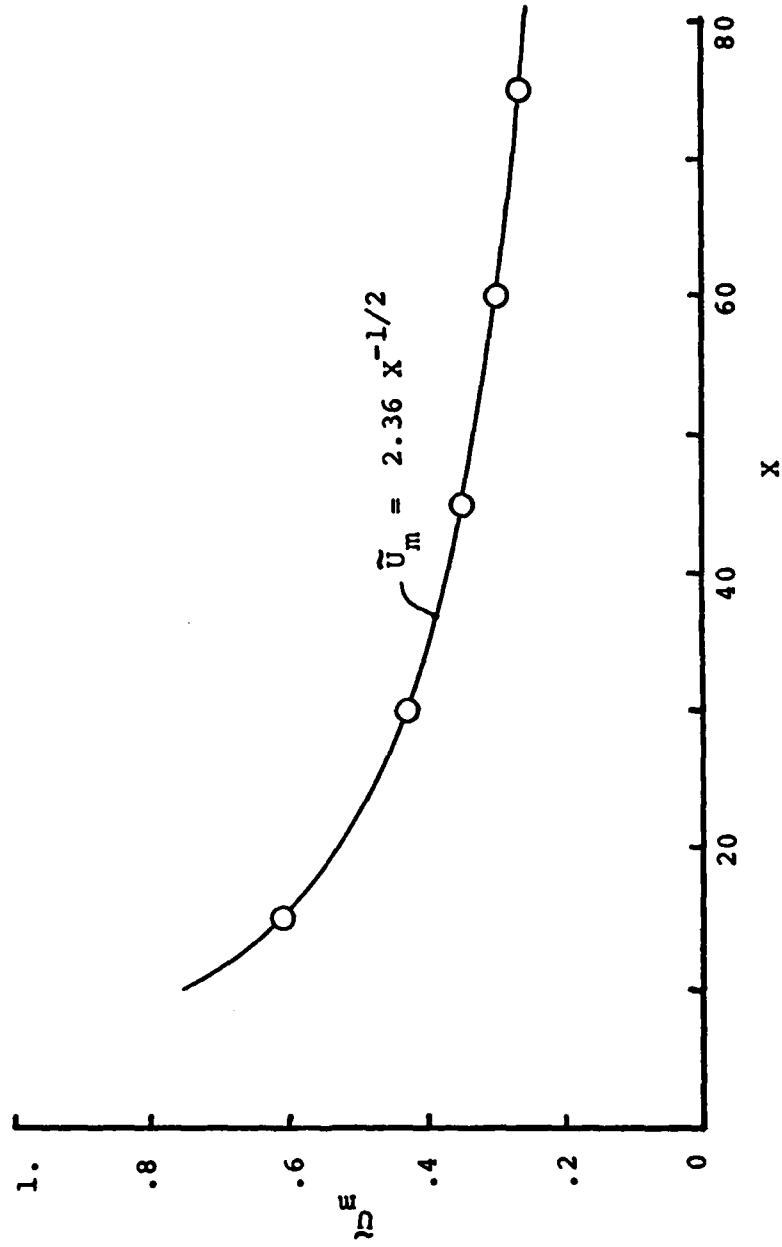
The collapse of the calculated profiles, from the various transverse planes onto the reduced coordinate,  $Y/B$ , supports the manner in which the self-preserving characteristic of real jet flows was incorporated into the formulation of the model. Transverse distributions of all other calculated flow properties exhibit the same degree of collapse and consequently, only the representative distribution from  $X = 45$  is given for those (tabulated results will be given in Oler & Goldschmidt (1980)).

From Figure 5-4, it is noted that the vortex street model accurately represents the mean longitudinal velocity distribution and spreading rate  $\beta$  determined from experimental measurements. To further verify the capability of the model to duplicate similarity scaling, the variation of the mean centerline velocity,  $U_m(X)$ , with respect to  $X$  is given in Figure 5-5. From Figure 2-3, it was shown that

$$U_m(x/D)/U_o = 2.36 * (x/D)^{-1/2}$$

$$\tilde{U}_m(X) = C_U * X^{-1/2} \quad (5.41)$$

with which the model agrees. It should be recalled that the similarity coefficient,  $C_U$ , was chosen such that  $\tilde{U}_m(45) = 2.36 * (45)^{-1/2}$ . The coefficient was held constant for all other calculations and the mean centerline velocities illustrated in Figure 5-5 are the results.

Figure 5-5  $\tilde{U}_m(x)$  vs.  $x$

As noted in Section II.B.3, Moallemi (1980) has observed that the velocity vector of the potential flow beyond the jet boundary actually has a negative longitudinal component. Experiments with the numerical simulation have demonstrated that this phenomenon may be a consequence of the finite axial length over which the mean velocity gradients are strong enough to maintain a coherent vortex-like large scale structure.

The original approach taken for the numerical simulation was to extend the vortex street far enough downstream such that the furthest vortices had a negligible effect on the calculation of local flow properties. The implicit assumption was that self-preservation would be maintained for  $0 < X < \infty$ . While theoretically appealing, that assumption is only approximately true in real flows.

Figure 5-6 illustrates the effect of a finite length of the vortex street and Figure 5-7 magnifies the effect on the potential outer flow.\* It is apparent that the longitudinal component of the velocity vector approaches zero from negative values in the limit as the streamwise length of the vortex street goes to infinity.

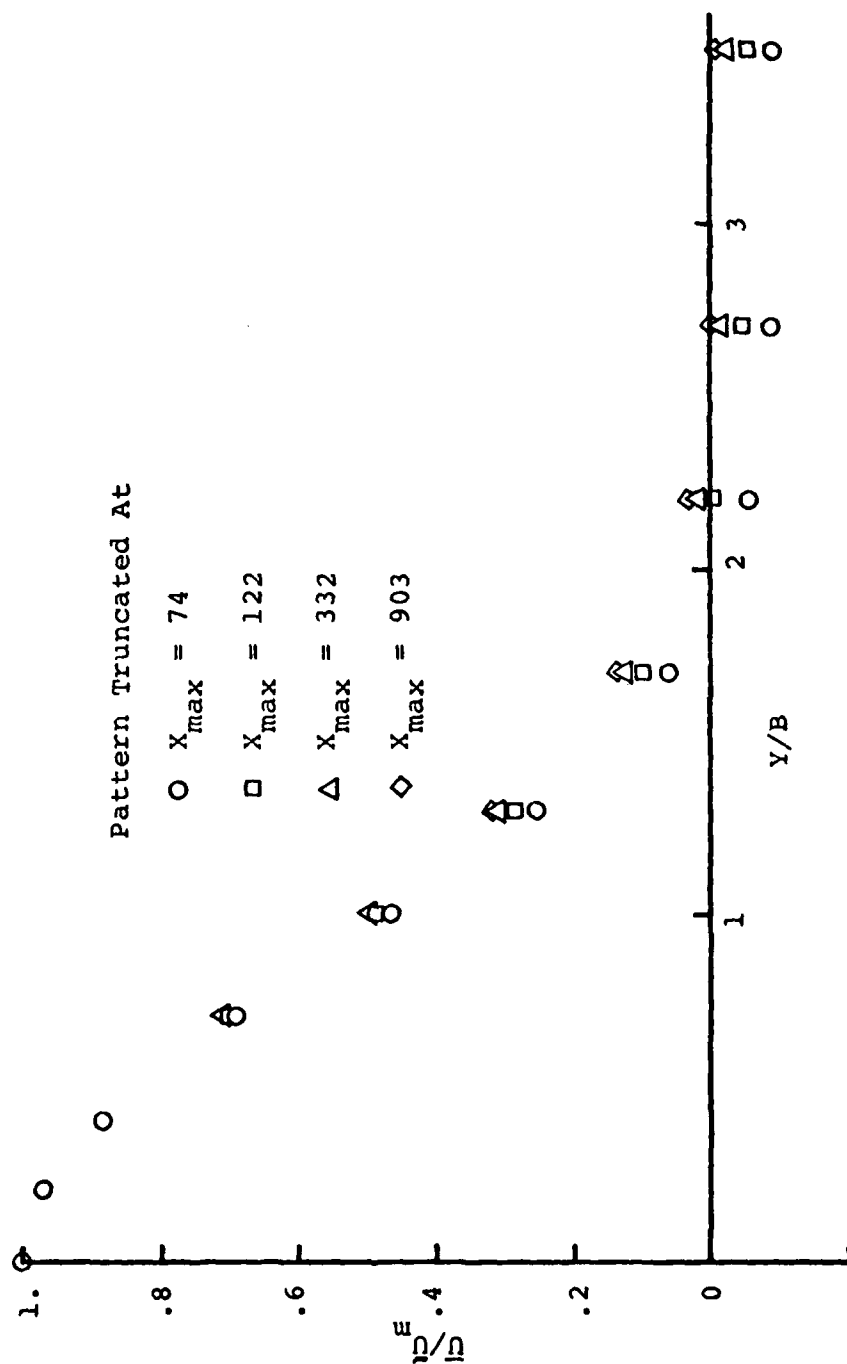
The surprising implication of these results is that there may be local deviations from perfect similarity due to the influence (or rather the lack of it) of coherent structures much further downstream.

## 2. Mean Lateral Velocities

The mean lateral velocities were calculated numerically by

---

\* The numerical simulation does not provide any indication of interface position. However, the maximum extent of the intermittent region may be inferred from experimentally based expectations of its relationship to the mean velocity profile.

Figure 5-6  $U(X, Y/B) / \bar{U}_m(X)$  vs.  $Y/B$  for Various  $X_{\max}$

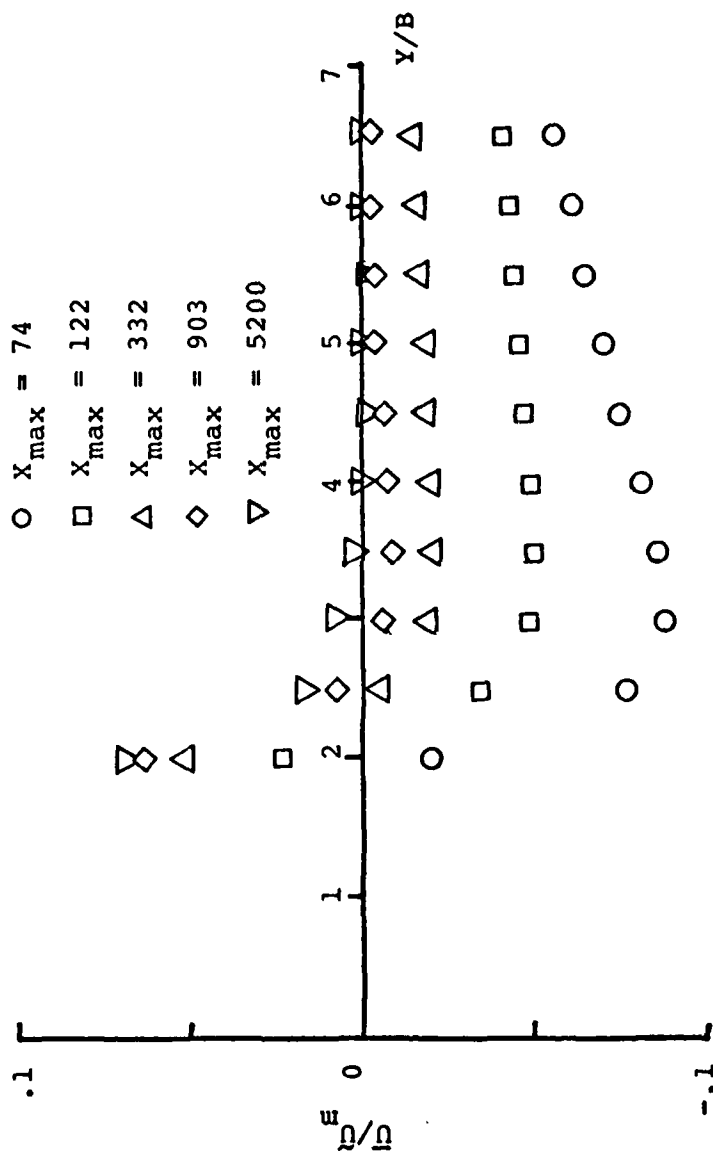


Figure 5-7 Enlargement of Figure 5-6



$$\bar{V}(X, Y, \tilde{t}) = \frac{1}{\tilde{T}} \int_0^{\tilde{T}} V(X, Y, \tilde{t}) d\tilde{t} . \quad (5.42)$$

Figure 5-8 illustrates the resulting transverse distributions,  $\bar{V}(X, Y/B)/U_m(X)$  vs.  $Y/B$ . Again, the self-preserving variation of length and velocity scales calculated by the model are evident.

The distribution of mean lateral velocity may also be calculated from knowledge of the mean velocity profile and conservation of mass. Continuity requires

$$\frac{\partial \bar{U}(X, Y)}{\partial X} + \frac{\partial \bar{V}(X, Y)}{\partial Y} = 0$$

or

$$\bar{V}(X, Y) = - \int_0^Y \frac{\partial \bar{U}(X, Y)}{\partial X} dY . \quad (5.43)$$

From similarity for the plane jet,

$$\frac{\bar{U}(X, Y/B)}{\tilde{U}_m(X)} = f(Y/B) \quad (5.44)$$

and

$$\frac{\bar{V}(X, Y/B)}{\tilde{U}_m(X)} = g(Y/B) . \quad (5.45)$$

Substituting Eqs. 5.44 and 5.45 into Eq. 5.43 yields

$$\tilde{U}_m(X) g(\eta) = B(X) \int_0^\eta \frac{\partial}{\partial X} [f(\eta) \tilde{U}_m(X)] d\eta$$

$$\begin{aligned} \text{or} \quad g(\eta) = & - \left[ \frac{B(X)}{\tilde{U}_m(X)} \frac{d\tilde{U}_m(X)}{dX} + \frac{dB(X)}{dX} \right] \int_0^\eta f(\eta) d\eta \\ & + \frac{dB(X)}{dX} \eta f(\eta) \end{aligned} \quad (5.46)$$

where  $\eta = Y/B$ .

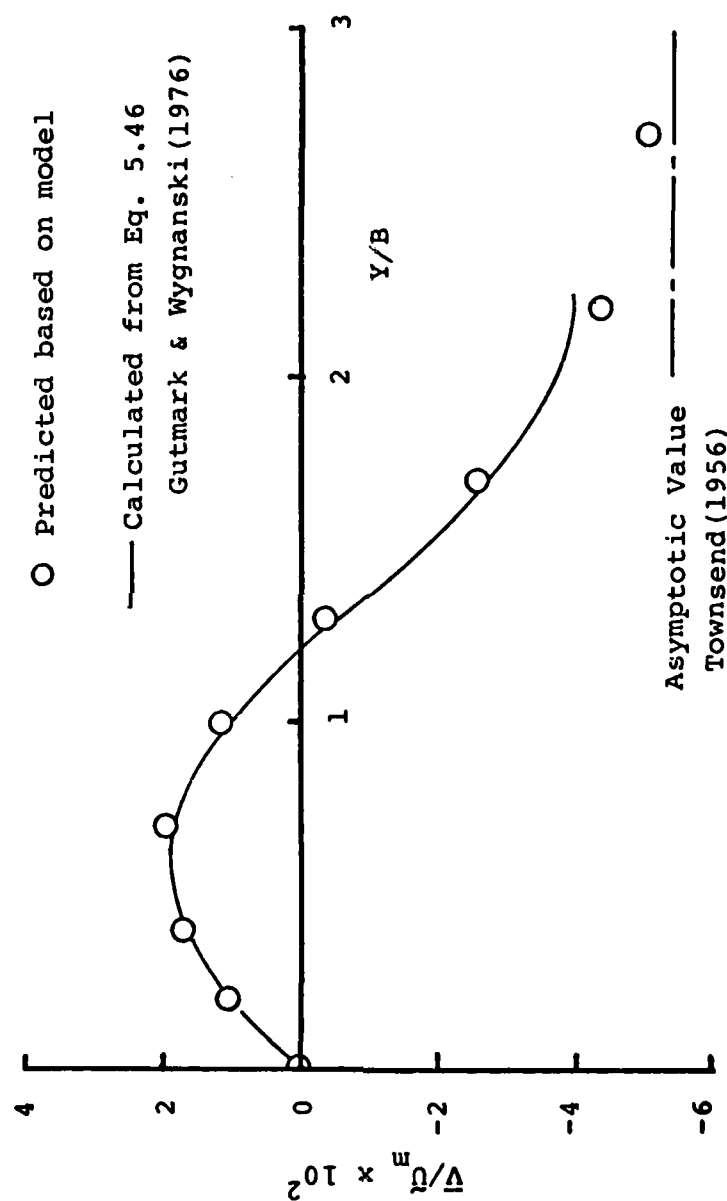


Figure 5-8  $\bar{V}(x, y/B)/\bar{U}_m(x)$  vs.  $y/B$

This procedure has been followed by Gutmark & Wygnanski (1976) and the results are given in Figure 5-8 for comparison with the distribution calculated by the vortex street model. From the agreement of the two analyses evidenced by Figure 5-8, it is verified that the simulated flow satisfies conservation of mass requirements.

Extension of the integral limit of Eq. 5.46 yields the lateral velocity at infinity or the entrainment velocity,  $V_e(X)$ , i.e.

$$\frac{V_e}{\tilde{U}_m} = g(\infty) = - \left[ \frac{B(X)}{\tilde{U}_m(X)} \frac{d\tilde{U}_m(X)}{dX} + \frac{dB(X)}{dX} \right] \int_0^\infty f(\eta) d\eta \quad (5.47)$$

Townsend (1976) has shown that  $g(\infty) = .054$  which is the asymptotic value indicated in Figure 5-8.

### 3. Reynolds Stress Distributions

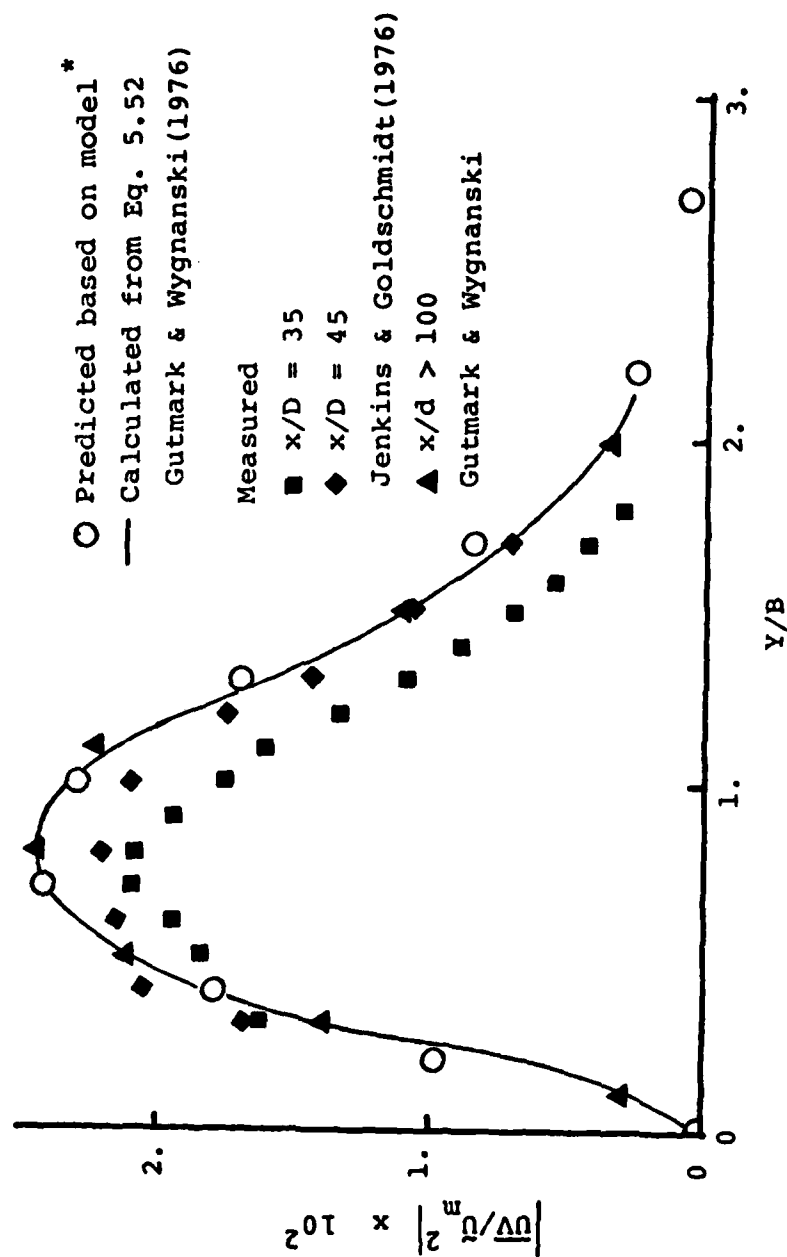
Local values of the Reynolds stress were calculated by

$$\overline{UV}(X,Y) = \frac{1}{\tilde{T}} \int_0^{\tilde{T}} \{ [U(X,Y,\tilde{t}) - \bar{U}(X,Y)] [V(X,Y,\tilde{t}) - \bar{V}(X,Y)] \} d\tilde{t}. \quad (5.48)$$

The resulting distributions of  $\overline{UV}(X,Y)/\tilde{U}_m(X)^2$  are given in Figure 5-9.

Also given in the figure are experimentally determined distributions of the Reynolds stress by Jenkins (1974) and Gutmark & Wygnanski (1976). By plotting on the reduced coordinate,  $Y/B$ , the distributions exhibit reasonable agreement.

The Reynolds stress distribution may also be calculated from the mean velocity profile, continuity equation, and streamwise component of the Navier-Stokes equations. With the appropriate boundary layer



\*Note that the absolute value of the Reynolds stress is given due to the fact that the model yields the wrong sign (see Section VI.B).

Figure 5-9  $\left| \frac{uv}{c^2} \right| \times 10^2$  vs.  $y/B$

approximations for plane jet flows (see Townsend (1956)), the Reynolds averaged X-component of the Navier-Stokes equations becomes

$$\bar{U}(X,Y) \frac{\partial \bar{U}(X,Y)}{\partial X} + \bar{V}(X,Y) \frac{\partial \bar{U}(X,Y)}{\partial Y} = - \frac{\partial \bar{UV}(X,Y)}{\partial Y} . \quad (5.49)$$

Utilizing the continuity equation given by Eq. 5.43, Eq. 5.49 may be rewritten as

$$\bar{U}(X,Y) \frac{\partial \bar{U}(X,Y)}{\partial X} - \frac{\partial \bar{U}(X,Y)}{\partial Y} \int_0^Y \frac{\partial \bar{U}(X,Y)}{\partial X} dY = - \frac{\partial \bar{UV}(X,Y)}{\partial Y} \quad (5.50)$$

Since the jet is self-preserving,

$$\frac{\bar{UV}(X,Y/B)}{\tilde{U}_m(X)^2} = q(Y/B) = q(\eta) \quad (5.51)$$

and Eq. 5.44 may be used to write Eq. 5.50 in terms of the mean velocity profile  $f(\eta)$ . After some simplification, the result is

$$\begin{aligned} \frac{dq(\eta)}{d\eta} = & \left[ \frac{B(X)}{\tilde{U}_m(X)} \frac{d\tilde{U}_m(X)}{dX} + \frac{dB(X)}{dX} \right] \frac{df(\eta)}{d\eta} \int_0^\eta f(\eta) d\eta \\ & - \frac{B(X)}{\tilde{U}_m(X)} \frac{d\tilde{U}_m(X)}{dX} f(\eta)^2 \end{aligned} \quad (5.52)$$

Integration of Eq. 5.52 will then yield the Reynolds stress distribution  $q(\eta)$ . This procedure has been utilized by

Gutmark & Wygnanski (1976) with the results given in Figure 5-9.\*

From Figure 5-9, it is noted that the Reynolds stress calculated by the vortex street model is in close agreement with measurements and that derived from the Navier-Stokes equation. The capability of the model to duplicate experimentally determined self-preserving mean longitudinal profiles and simultaneously satisfy the requirements of the continuity and Navier-Stokes equations provides substantial support for the hypothesized structure.

#### 4. Velocity Fluctuation Intensities

Calculations of the velocity fluctuation intensities were made using

$$\frac{U'(X,Y)}{\tilde{U}_m(X)} = \frac{1}{\tilde{U}_m(X)} \left\{ \frac{1}{T} \int_0^T [U(X,Y) - \bar{U}(X,Y)]^2 d\tilde{t} \right\}^{1/2} \quad (5.53)$$

and

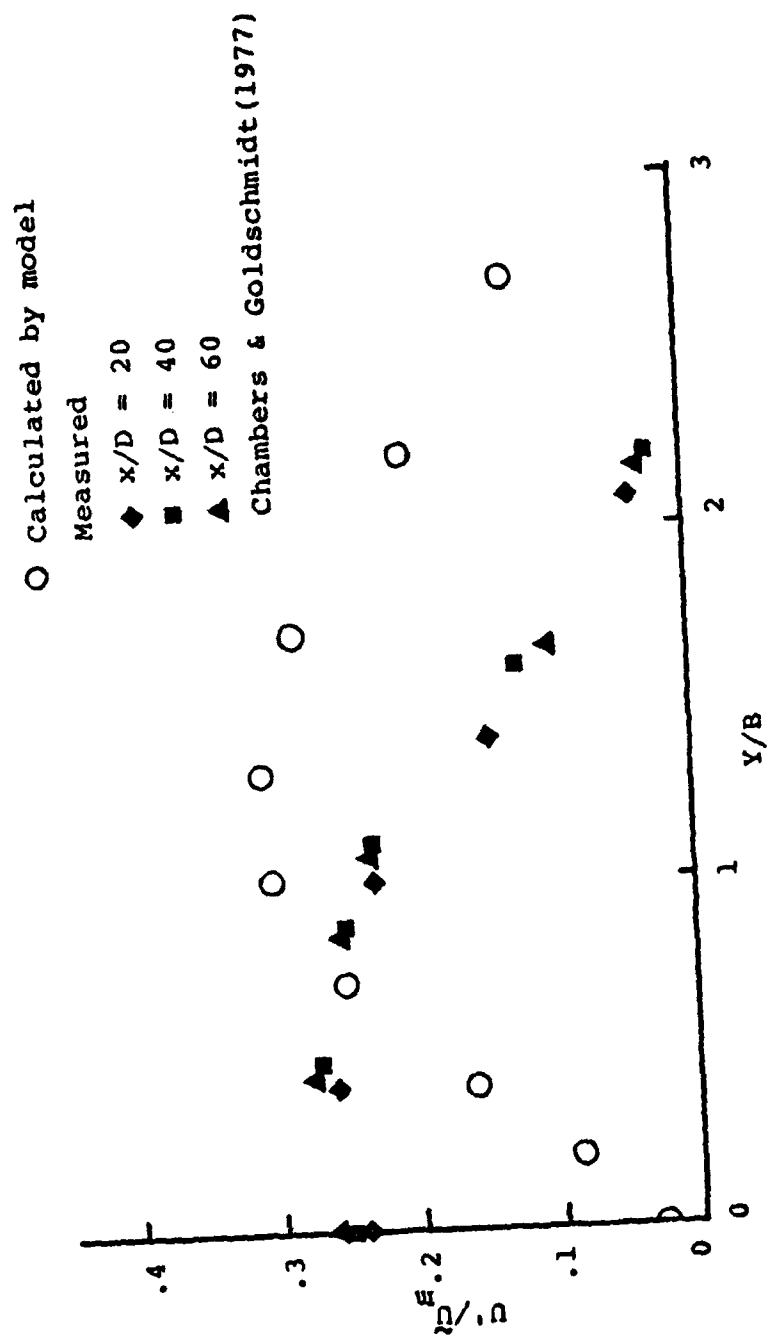
$$\frac{V'(X,Y)}{\tilde{U}_m(X)} = \frac{1}{\tilde{U}_m(X)} \left\{ \frac{1}{T} \int_0^T [V(X,Y) - \bar{V}(X,Y)]^2 d\tilde{t} \right\}^{1/2}. \quad (5.54)$$

The resulting distributions together with experimentally determined ones are given in Figures 5-10 and 5-11.

Not surprisingly, it is in these properties that the vortex street model, as applied, fails to generate accurate representations of the real flow. Although the calculated distributions are qualitatively reasonable, the magnitude of the lateral fluctuations are about twice the experimental values and the longitudinal fluctuations near the axis are much lower than the experimentally determined ones.

---

\* The integration could have also been carried out with the present data giving similar results.

Figure 5-10  $u'(x, y/B) / \bar{u}_m(x)$  vs.  $y/B$

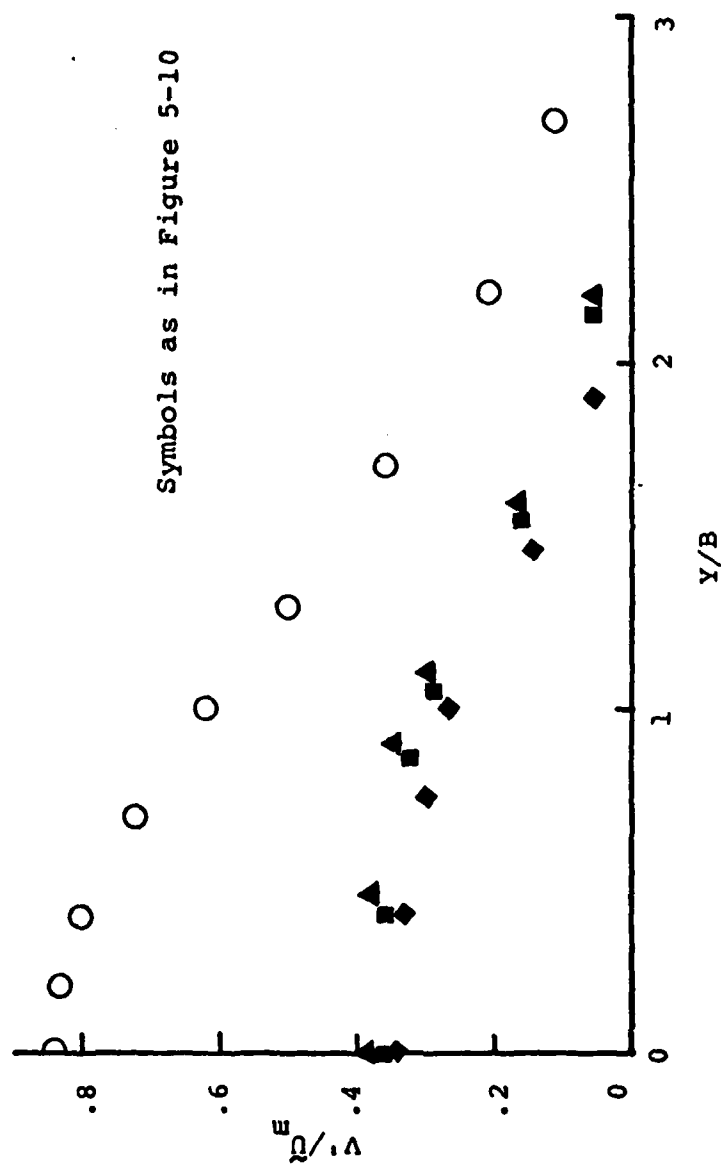


Figure 5-11  $v'(x, y/B) / \bar{U}_m(x)$  vs.  $y/B$



These problems are directly related to the total neglect of the small scale turbulence and the simplicity of the Rankine vortex model. The extremely high values of the lateral fluctuation levels are a result of the linear superposition of the velocities induced at the mid-point between adjacent counter-rotating vortices on opposite sides of the centerline. In these regions, the total velocities are approximately twice what either vortex would induce alone. Undoubtedly, the inclusion of small scale turbulent diffusion effects would prohibit the unreasonably high local strain rates calculated by the current vortex street model.

There are two approaches that might be utilized in order to account for the small scale turbulent effects. The first is to attempt to model the local large scale/small scale interaction, energy exchange and energy dissipation by the small scales, which is not a trivial task. The second and more simplistic approach would be to modify the basic Rankine vortex vorticity and velocity distributions into nonaxisymmetric ones that accounted for local variations of the turbulent momentum transport.

Neither approach was adopted in the currently reported research since the large scales were of principal interest and the Rankine vortex was apparently sufficient to demonstrate their effect on mean velocities and Reynolds stress production. The key question concerning the reported fluctuation intensities is whether or not they are critical to the apparent accuracy of the calculated  $\bar{U}$ ,  $\bar{V}$  and  $\overline{UV}$  distributions. This problem is considered in Section E.

##### 5. Limitations of the Model

Due to the manner in which the numerical simulation was formulated, several of the experimental turbulent flow properties either cannot be calculated or their calculation

yields meaningless results. The primary missing ingredients in the formulation are the effects of random "jitter" in the coherent structural pattern and the effects of the random small scale turbulent velocity fluctuations.

For instance, the turbulent kinetic energy equation cannot be evaluated since there is no representation of the small scales which receive energy from the large scales or the even smaller scales which provide the eventual viscous dissipation of the energy. Similarly, nothing may be inferred concerning the turbulent energy spectra since the model only represents one frequency component.

Although qualitative agreement with the experimentally determined correlation map of Figure 4-5 is obvious for the hypothesized structure, the simulation does not give a realistic corresponding pattern. The regions of positive and negative correlations would have calculated correlation coefficients of  $\pm 1$  since the simulation is perfectly deterministic.

While the vortex street structure would determine the overall interface geometry, the exact location cannot be simulated without the small scale effects that actually delineate the interface.

#### E. The Mechanisms of Entrainment and Reynolds Stress Production

Considering that the effects of the random small scale turbulence were not included in the numerical simulation of the vortex street model, the capability of the model to represent growth rates, velocity decay rates, mean velocity profiles and the averaged Reynolds stress profile is remarkable. It is especially surprising that the calculation of these properties was not affected by the inability of the model to duplicate the experimental distributions of velocity fluctuation intensity. Browand & Weidman (1976) noted the invariance of mean flow properties and Reynolds

stress distributions with respect to Reynolds number (and the associated small scales) in a plane mixing layer. The explanation which they offered was that these properties are controlled solely by the large scales since only they are unaffected by the magnitude of the Reynolds number. The same explanation may be offered for the success of the vortex street model where it represents the limiting case in which the small scales are totally absent. The question then becomes one of explaining the manner in which the large structures do generate the observed jet properties.

The relationship between the calculated mean flow properties and the streamwise development of the jet was investigated by modifying the numerical model. In the modification, the vortex street was represented as a parallel flow with identical and equally spaced vortices extending up and downstream to infinity. This is the pattern that an observer located at a fixed location would predict having only the structural information available at that point. The calculation results duplicated the experimental mean longitudinal velocity profile but calculated zero distributions of mean lateral velocity and Reynolds stress. The conclusion drawn from this experiment is that the global development of the large structures is critically important to local mean flow properties.

Insight into the effects of the streamwise development of the vortex street on entrainment and Reynolds stress production is gained from examination of the instantaneous longitudinal velocity profiles given in Figure 5-12. The analogous distributions for the parallel flow representation are given in Figure 5-13. The most obvious difference between the parallel and developing vortex streets is the lack of symmetry of the distributions at  $\tilde{t} = \tilde{T}/4$  and  $\tilde{t} = 3\tilde{T}/4$  for the developing pattern.

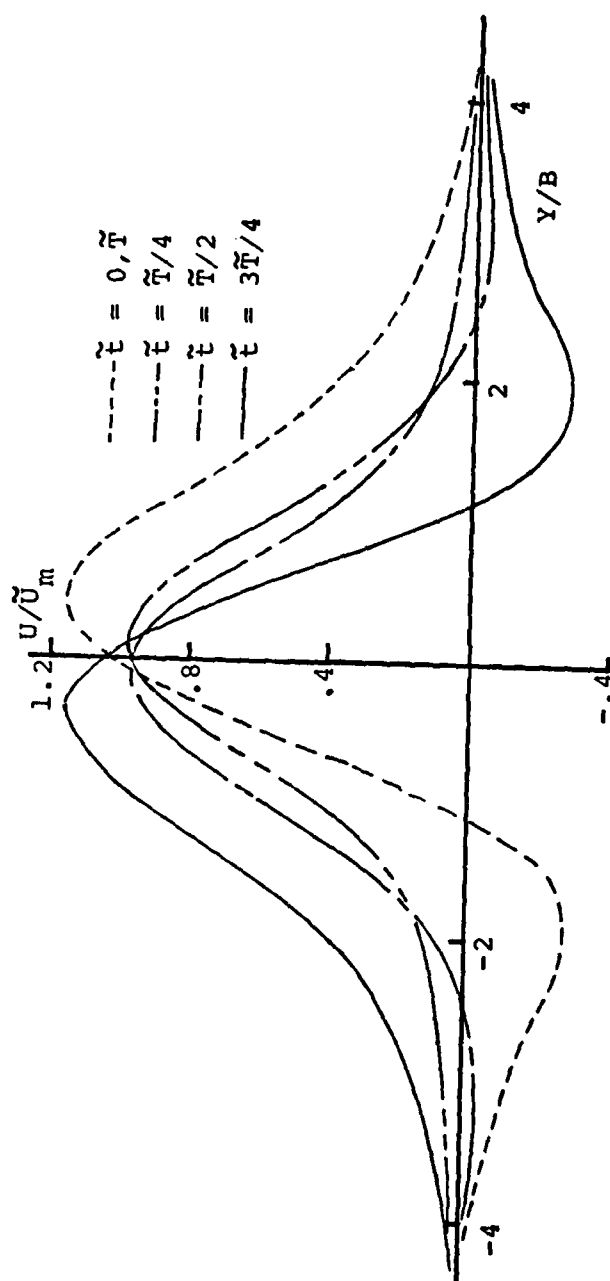


Figure 5-12  $U(x, y/B; t)/\tilde{U}_m(x)$  : A Spreading Jet

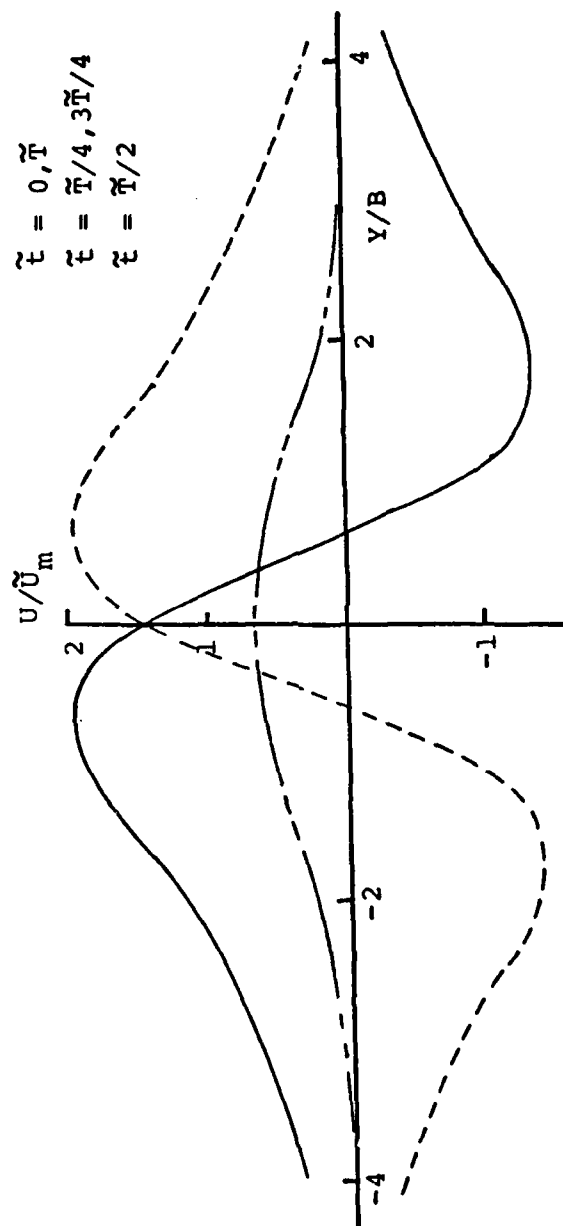


Figure 5-13  $U(X, Y/B; \tilde{\tau})/\tilde{U}_m(X)$  : A Parallel Flow Jet

The significance of the difference is clarified by comparing the time histories of the longitudinal and lateral velocity fluctuations and Reynolds stress at a fixed point,  $(X, Y)$ . Plots of this type are given in Figure 5-14. The fixed point  $(X = 45, Y/B = 0.7)$  for this case corresponds to the lateral location where the maximum Reynolds stress production occurs. The key feature to be noted from the figure is the slight decrease in the phase lag between the longitudinal and lateral fluctuations. Apparently, the phase change is a direct consequence of the spreading rate and the key to nonzero time averaged entrainment and Reynolds stress production.

The dependence of the lateral velocity and Reynolds stress distributions on the spreading rate is implied by the continuity and Navier-Stokes equations when expressed in terms of similarity variables. From Eq. 5.46 the distribution of  $\bar{V}(X, Y/B)/\tilde{U}_m(X)$  is given by

$$g(\eta) = - \left[ \frac{B(X)}{\tilde{U}_m(X)} \frac{d\tilde{U}_m(X)}{dX} + \frac{dB(X)}{dX} \right] \int_0^\eta f(\eta) d\eta + \frac{dB(X)}{dX} \eta f(\eta) \quad (5.55)$$

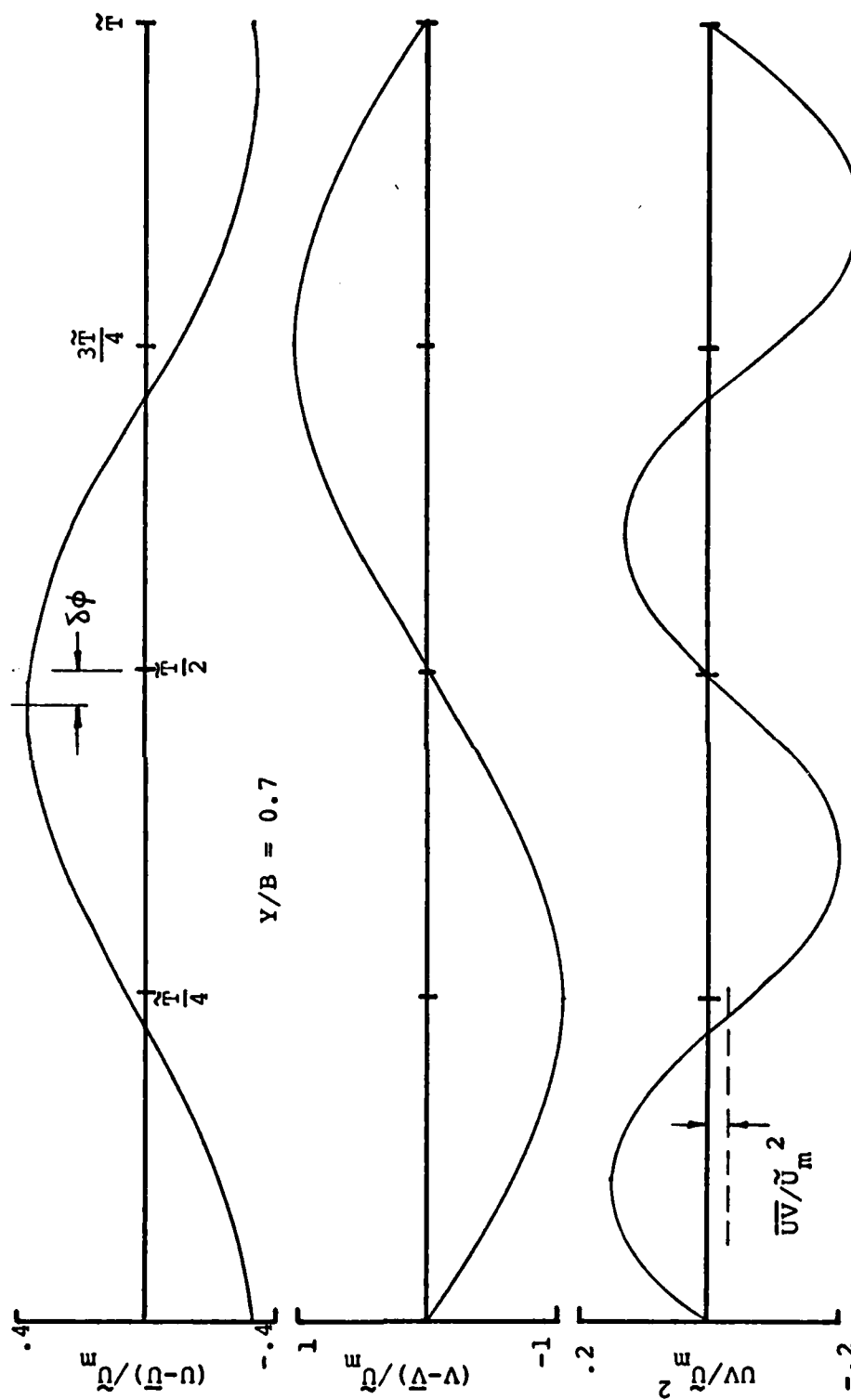
where  $\eta = Y/B$  and

$$f(\eta) = U(X, Y/B)/\tilde{U}_m(X) .$$

Substituting Eq. 5.40 for  $B(X)$  and Eq. 5.41 for  $\tilde{U}_m(X)$  yields

$$g(\eta) = \beta \left[ -\frac{1}{2} \int_0^\eta f(\eta) d\eta + \eta f(\eta) \right] \quad (5.56)$$

Eq. 5.56 illustrates that the lateral velocities are scaled directly by the growth rate,  $\beta$ .

Figure 5-14 Temporal Relationships Between  $U$ ,  $V$  and  $UV$

Substituting for  $B(X)$  and  $\tilde{U}_m(X)$  in the streamwise Navier-Stokes equation given by Eq. 5.52 yields

$$q(\eta) = \overline{UV}(X,Y) / \tilde{U}_m(X)^2$$

$$q(\eta) = \frac{\beta}{2} \int_0^\eta \left\{ f(\eta)^2 + \frac{df(\eta)}{d\eta} \int_0^\eta f(\eta) d\eta \right\} d\eta \quad (5.57)$$

Again, the growth rate is noted to determine the magnitude of the Reynolds stress distribution.

The growth rate,  $\beta$ , is an experimentally determined coefficient approximately equal to 0.1 for plane jet flows. There has been no purely theoretical analysis reported which was capable of predicting  $\beta$ . Since its value was incorporated into the vortex street model as a scaling length, it is possible to use the model as a means of postulating the flow fields which would result for varying values of  $\beta$ . The only restriction is that the accompanying velocity scale be compatible. Conservation of momentum provides the desired relationship. Consider

$$\frac{d}{dX} \int_{-\infty}^{\infty} \overline{U}(X,Y)^2 dY = 0 \quad (5.58)$$

Since the flow is self-preserving, Eq. 5.58 may be rewritten as

$$\frac{d}{dX} \{ \tilde{U}_m(X)^2 B(X) \int_{-\infty}^{\infty} f(\eta)^2 d\eta \} = 0$$

or

$$\tilde{U}_m^2(X) B(X) = \text{constant} \quad (5.59)$$



Substituting Eqs. 5.41 and 5.42 for  $B$  and  $\tilde{U}_m$ , respectively, yields

$$C_U^2 \beta = (2.36)^2 * 0.1 \quad (5.60)$$

where the constant has been determined from the naturally occurring flow.

Figures 5-15 through 5-17 illustrate distributions of  $\bar{U}$ ,  $\bar{V}$  and  $\overline{UV}$  calculated by the vortex street model for a wide range of jet growth rates. For comparison, the corresponding distributions calculated from Eqs. 5.56 and 5.57 are also given.

From data similar to that shown in Figure 5-14, the phase change,  $\delta\phi$ , was determined for each widening rate with the results given in Figure 5-18. Surprisingly,  $\delta\phi$  and  $\beta$  are approximately linear with respect to one another.

In a remarkably insightful publication, Townsend (1979) has postulated that the global flow development introduces the same type of phase shift effect between the velocity components in a two-dimensional wake. He noted that the velocity product of fluctuations represented by sinusoids exactly  $180^\circ$  out of phase would not on the average generate a nonzero Reynolds stress. If from the overall flow development, a slight phase change was introduced, a nonzero product would result. The present results substantiate that effect.

The distributions of the fluctuating velocity intensities for the various widening rates are given in Figures 5-19 and 5-20. It is noted that they are scaled by  $\tilde{U}_m$  and are not dependent on  $\beta$ . Consequently, it is apparent that the capability of the vortex street model to generate realistic distributions of entrainment velocity and Reynolds stress is not dependent on the corresponding fluctuation intensity distributions.

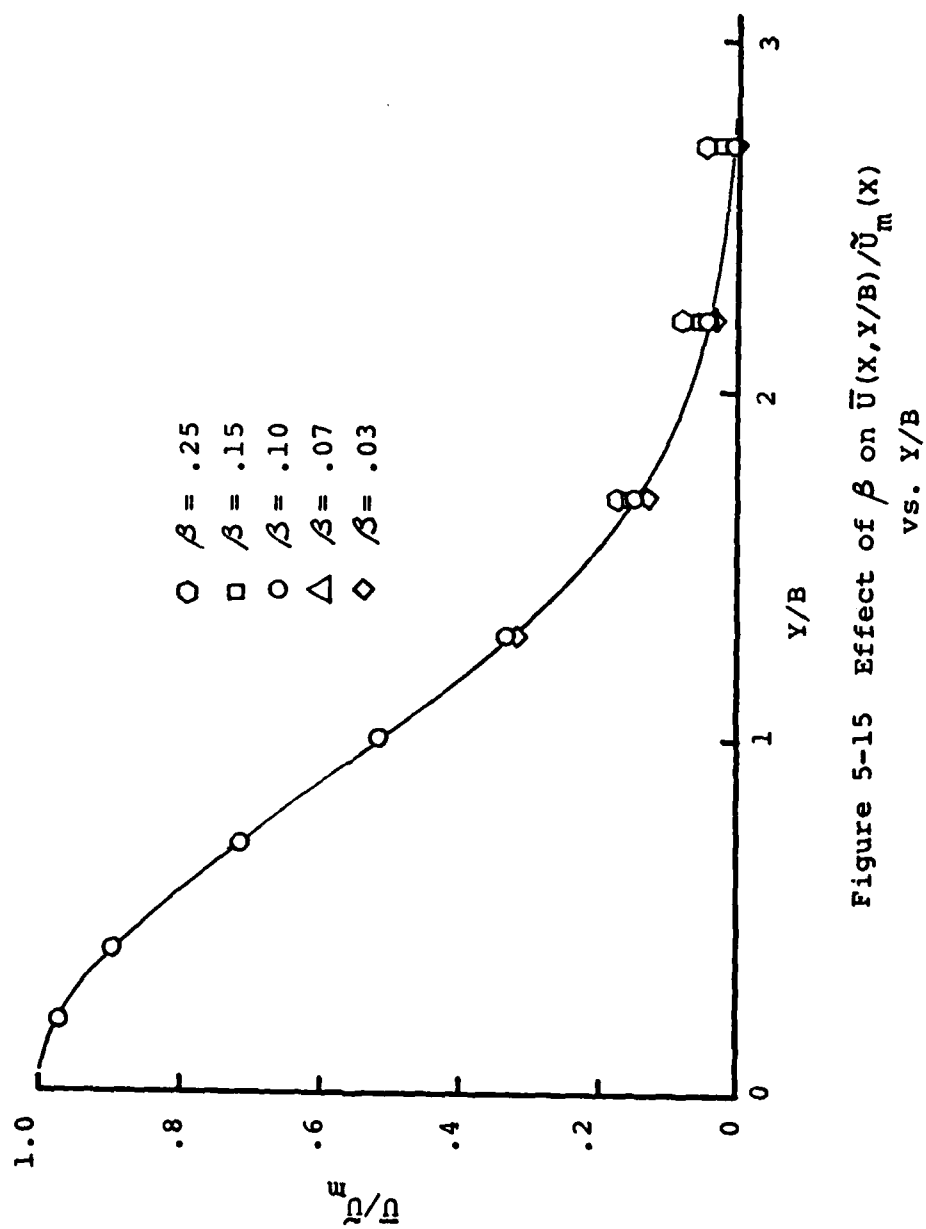


Figure 5-15 Effect of  $\beta$  on  $\bar{U}(x, y/B) / \bar{U}_m(x)$  vs.  $y/B$

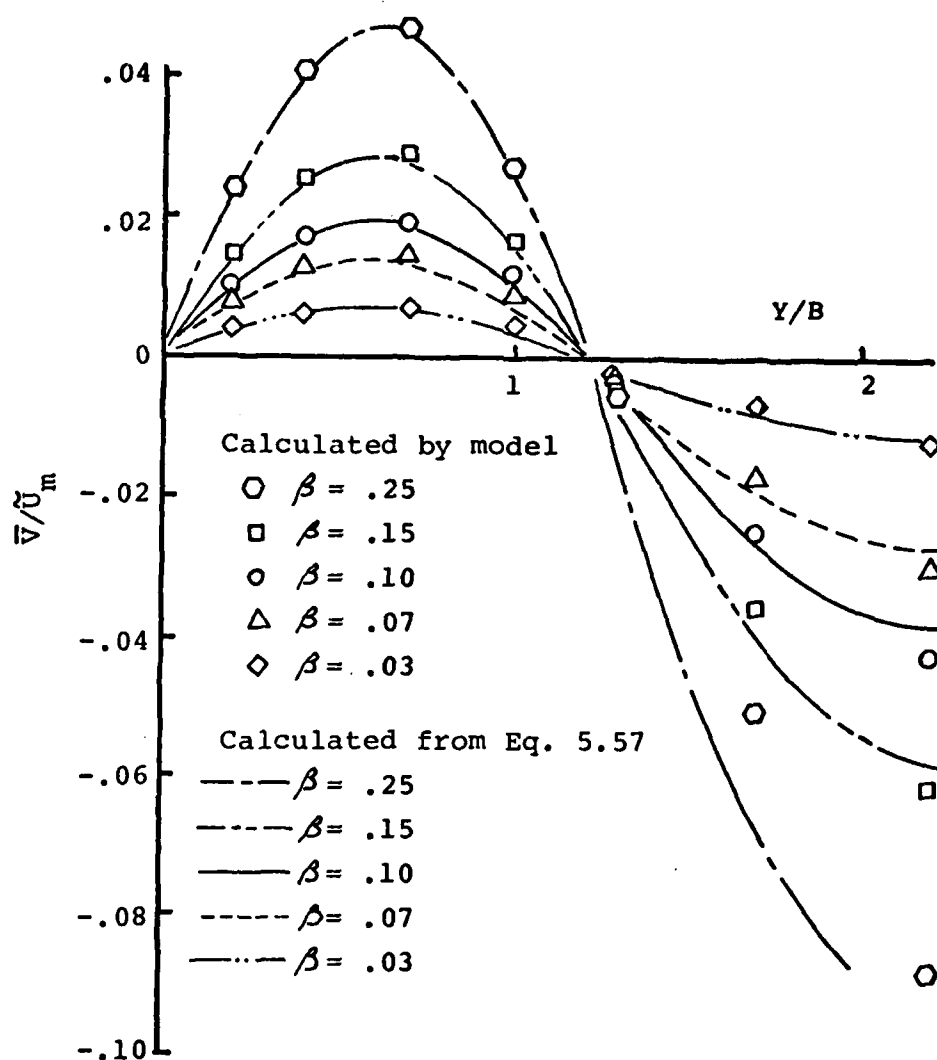


Figure 5-16 Effect of  $\beta$  on  $\bar{V}(X, Y/B)/\tilde{U}_m(X)$  vs.  $Y/B$

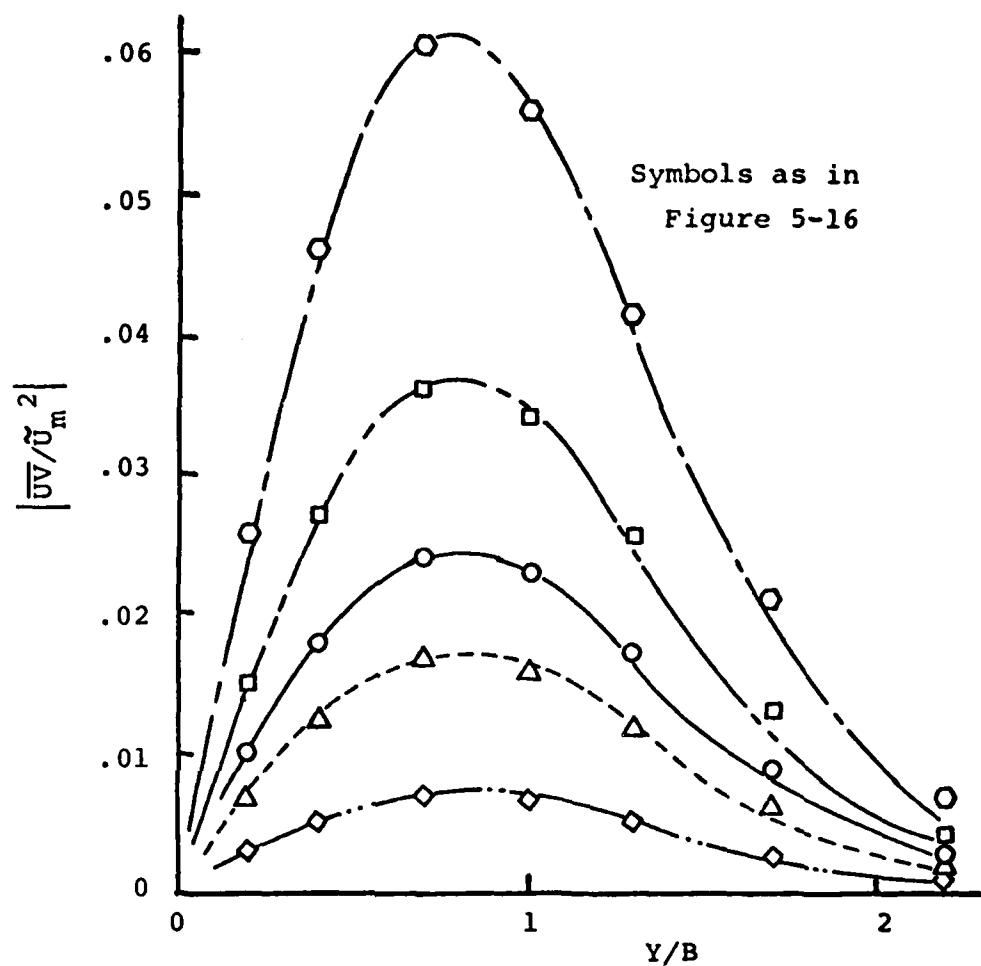


Figure 5-17 Effect of  $\beta$  on  $|\overline{UV}(X, Y/B)/\tilde{u}_m(X)^2|$  vs.  $Y/B$

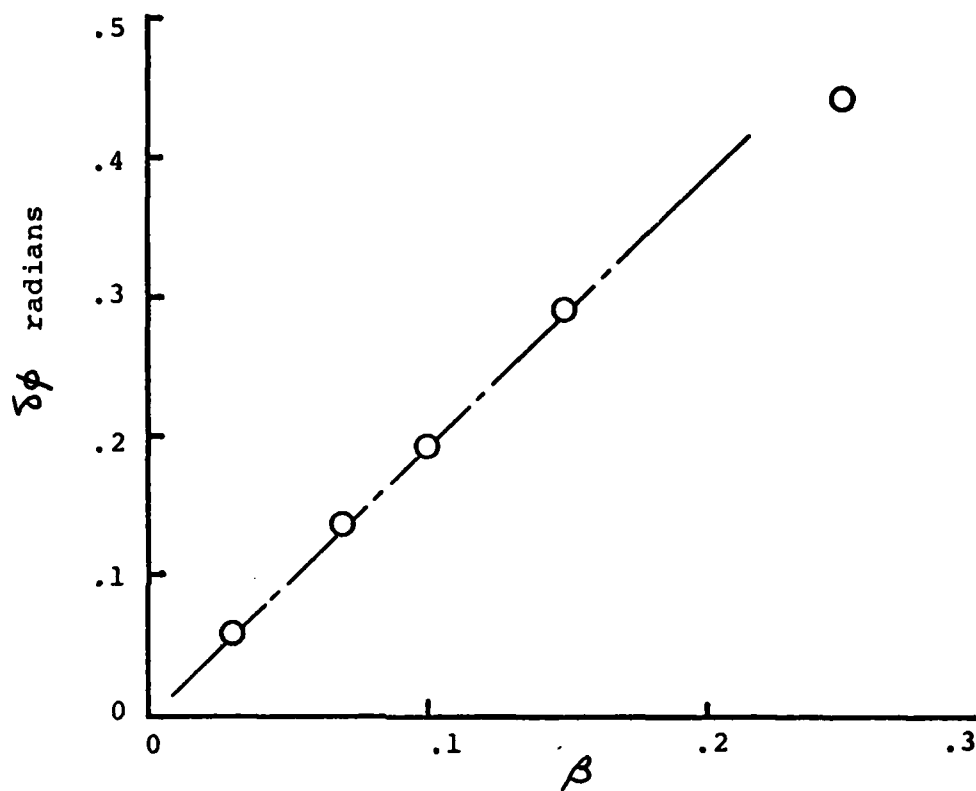


Figure 5-18  $\delta\phi$  vs.  $\beta$

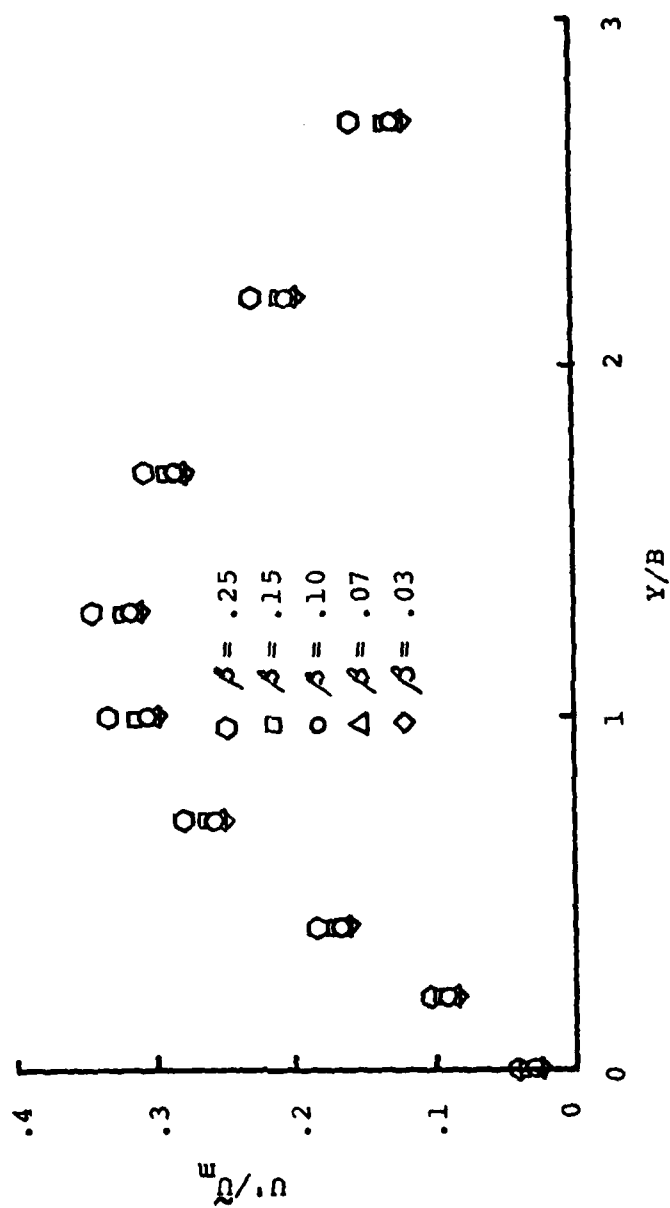


Figure 5-19 Effect of  $\beta$  on  $u'(X, Y/B)/\bar{u}_m(X)$  vs.  $Y/B$

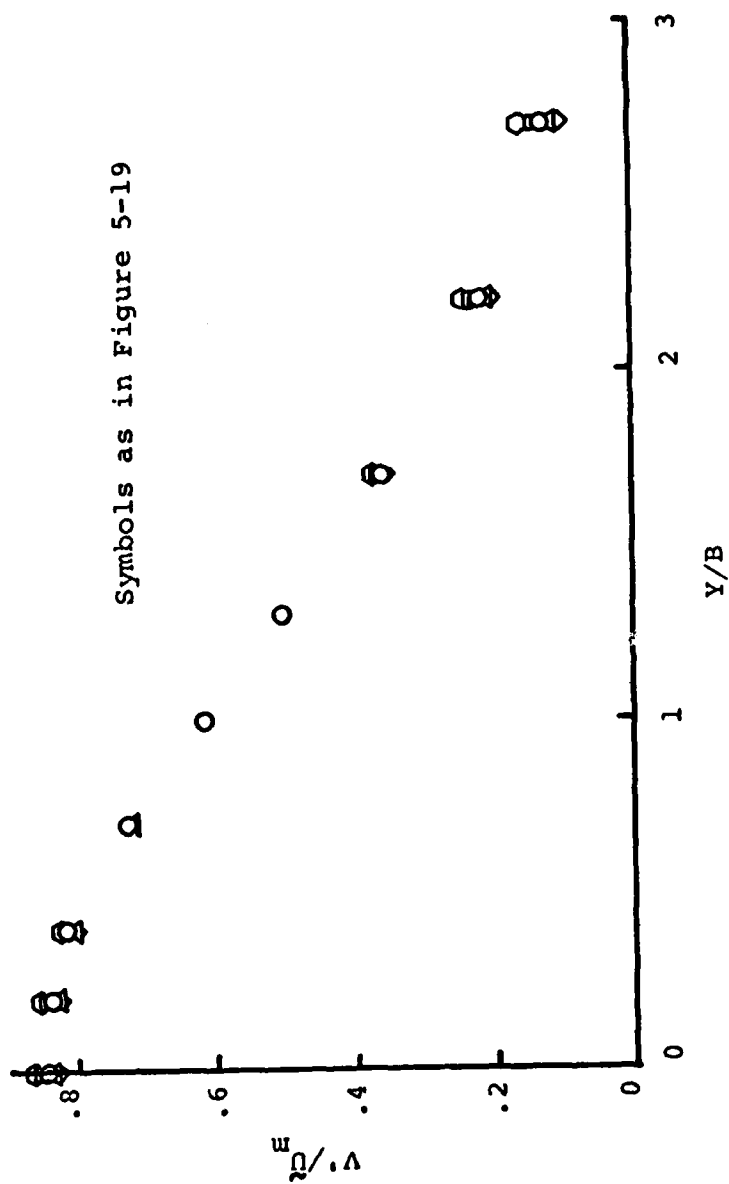


Figure 5-20 Effect of  $\beta$  on  $V'(X, Y/B)/\bar{U}_m(X)$  vs.  $Y/B$

The fluctuation intensity, mean velocity, and Reynolds stress profiles are related, however. For a given approximate model of the individual vortices making up the vortex street, there is a corresponding set of similarity constants,  $C_H$ ,  $C_R$  and  $C_L$ , which optimize the agreement with the mean longitudinal velocity profile ( $C_L$  is fixed from experimental observations). The accuracy with which the corresponding Reynolds stress and lateral velocity profiles may be calculated is apparently directly related to the accuracy with which the associated mean velocity profile is duplicated and independent of the associated fluctuation intensities. The inaccuracy of the fluctuation intensities is therefore an unavoidable side effect of utilizing a simplistic vortex model such as the axisymmetric Rankine vortex.

#### G. Summary

A numerical simulation of the vortex street model for the large scale structures of a turbulent plane jet has been described. The formulation includes the effects of streamwise flow development through the expression of geometry and vortex parameters in terms of similarity length and velocity scales.

The calculation results indicate that the hypothesized structure is capable of giving virtually exact representations of the growth rate, velocity decay rate, mean velocity profiles and Reynolds stress distributions of real jet flows. Although the qualitative shapes of the fluctuation intensity profiles were in agreement with experimentally determined ones, the magnitudes were considerably in error. It was argued that this was a consequence of the failure to include the effects of the small scale turbulence.

A key feature of the combined calculated mean velocity and Reynolds stress profiles was that taken together, they demonstrated compatibility with the requirements of the



two-dimensional continuity and the Navier-Stokes equations. This capability is particularly notable considering the simple kinematic representation of the flow field.

Detailed examination of the relationship between instantaneous Reynolds stress and the velocity fluctuations revealed that the downstream development of the jet flow is critical to the local entrainment and Reynolds stress production rates. This dependence on the growth rate is implicit in the continuity and Navier-Stokes equations. The model successfully represents cases in which the growth rate is different from that occurring naturally in plane jets. The strongest outward indication of the effect of a nonzero growth rate is the introduction of a change in the phase relationship between the longitudinal and lateral velocity fluctuations.

In Section V.A , it was noted that an alternative representation of the vortex model might have been the superposition of the structure onto an otherwise homogeneous mean flow. From the preceding analysis, it is apparent that this would have upset the balance between the longitudinal mean velocity profile and the requirements of continuity and the Navier-Stokes equations. It is necessary for the large scale structures to possess sufficient energy to duplicate the mean longitudinal velocity profile before the appropriate accompanying lateral velocity and Reynolds stress distributions can be generated.

## CHAPTER VI

### CONCLUSIONS AND RECOMMENDATIONS

The primary focus of the research which has been reported was to gain insight into the characteristics and importance of the large scale structures in the similarity region of a two-dimensional turbulent jet. This was motivated by experimental indications early in the program of a vortex street type of coherent eddying pattern. The vortex street model was then adopted as a working hypothesis for the interpretation of the experimental and numerical analysis that followed.

#### A. Conclusions Based on Experimental Results

Several conclusions relative to the hypothesized structure may be drawn from the experimental results which have been reported.

1. Every experimental indication points to the fact that the concept of structural similarity is applicable to the large structures of a fully developed jet. Support for this conclusion is drawn from the similarity scaling of the intermittent region and the integral length scales. In addition, the streamwise variation of the interface crossing frequency is compatible with similarity considerations.
2. Comparison of the interface crossing frequency (measured using a rationally defined hold time variation) with the previously reported "flapping" frequencies indicates that the interface geometry and underlying structure are related. Further comparisons

with reported "flapping" frequency measurements indicate a structural frequency constant,  $f_s b/U_m \approx 0.1$  for all plane jet flows. This suggests a universal instability mode which leads to the vortex street structure.

3. Two point correlations within the turbulent velocity field yield the same spatial relationships which would be expected of a vortex street-like structure. These include a characteristically antisymmetric instantaneous longitudinal velocity profile, streamwise periodicity and coherence over substantial distances. It is not clear how these patterns develop within the initial and transition regions (i.e.,  $0 < x/D < 10$ ). This is one area of suggested further research.
4. Utilizing similarity concepts and relationships based upon the premise of a vortex-like structure, the convective velocity of the structural pattern was determined from flow visualization experiments. The result is that the pattern (i.e., the vortex centers) travels at approximately one-half the local mean centerline velocity.
5. Efforts at determining the extent of two-dimensionality characteristic of the large vortex-like structures led to inconclusive results. Comparison of axial and vertical integral length scales within the intermittent region suggest at least limited two-dimensionality. The same is not true for the integral scales of the turbulent velocity field. There is, however, an indication from the vertical correlation measurements that a vortex-like structure may exist which is more complex than the hypothesized structure, yet still substantially coherent in the vertical direction. It is suggested that this feature be investigated further possibly utilizing numerically applied pattern

recognition techniques such as those used by Blackwelder (1977) in the two-dimensional turbulent boundary layer.

B. Conclusions Based on the Numerical Simulation

Based upon the results of the experimental investigation, a numerical simulation of a two-dimensional jet formed from a vortex street was evaluated. The following conclusions were reached:

1. A vortex street model is quite capable of duplicating experimentally determined mean velocity profiles, growth rates, velocity decay rates and Reynolds stress distributions but fails to calculate intensities, spectra and correlations.
2. Flow properties calculated by the numerical simulation satisfy the two-dimensional approximations of the fundamental conservation requirements expressed by the continuity and Navier-Stokes equations.
3. It is evident that the key feature of the vortex street model, as formulated, is the inclusion of the effects of global flow development on locally measured or calculated flow properties.
4. As a consequence of the flow development, a change in the phase relationship between longitudinal and lateral velocity components is introduced. It is suggested that this feature be verified experimentally in plane jet flows which have different spreading rates due to acoustic forcing or some other form of external excitation.
5. The numerical simulation suggests that increasingly negative longitudinal velocity components at the jet edges are a consequence of the finite length of streamwise structural coherence. This could possibly be verified by examining the effect on the outer flow of artificially disrupting the structure at

increasingly shorter downstream lengths.

6. The effects of smaller random scales of turbulence were not included in the simulation and unrealistic distributions of flow properties directly related to them are the consequence. It is suggested that the vortex street simulation serve as a starting point for the modeling of the large scale/small scale interactions and turbulent-nonturbulent interface.
7. The most astonishing implication of the model is that entrainment and Reynolds stress production, which are key elements of any free turbulent shear flow, are actually consequences of the coherent or nonturbulent aspects of the flow. This is actually a question of semantics which serves to illustrate the type of redefinition of fundamental turbulence concepts which must result from the increasingly convincing indications of the importance of coherent structures in turbulence.
8. As noted on page 95, the model predicts a negative distribution of Reynolds stress although a positive distribution is required by the Navier-Stokes equation. This problem is clearly indicated in Figure 5-14. A thorough search has been made for a simple sign error in the algorithm but none was found. The possibility then arises that the hypothesis of a vortex street structure in plane jets is invalid. This is difficult to accept due to the experimental evidence and the capability of the model to calculate  $\bar{U}$ ,  $\bar{V}$  and  $|\overline{UV}|$ . It is suggested that there are some subtle aspects of the mean flow effects and energy transport processes which have not been properly accounted for in the model and that further research be made in this area.

LIST OF REFERENCES

## LIST OF REFERENCES

- Ajagu, C. O. and Geldschmidt, V. W., 1976; "Fold-over, Intermittency and Crossing Frequency of a Plane Jet Interface With and Without an Acoustic Disturbance," Herrick Lab Rept. HL 76-22, School of Mechanical Engineering, Purdue University.
- Anderson, P., LaRue, J. C., and Libby, P. A., 1977; "Turbulence Measurements of a Two-Dimensional Helium Jet in a Moving Airstream," Project SQUID Technical Rept. UCSD-9-PU.
- Antonia, R. A., 1972; "Conditionally Sampled Measurements Near the Outer Edge of a Turbulent Boundary Layer," JFM, 56, 1, p. 1.
- Antonia, R. A. and Atkinson, J. D., 1974; "Use of a Pseudo-Turbulent Signal to Calibrate an Intermittency Measuring Circuit," J. Fluid Mech., 64, 4, p. 679.
- Barsoum, M. L., Kawall, J. G., and Keffer, J. F., 1978; "Spanwise Structure of the Plane Turbulent Wake," Phys. Fluids, 21, 2, pp. 157-161.
- Becker, H. A. and Massaro, T. A., 1968; "Vortex Evolution in a Round Jet," JFM, 31, 3, pp. 435-448.
- Bevilaqua, P. M. and Lykoudis, P. S., 1971; "Mechanism of Entrainment in Turbulent Wakes," AIAA J., 9, 8, pp. 1657-1659.
- Blackwelder, R., 1977; "On the Role of Phase Information in Conditional Sampling," Phys. Fluids, 20, 10, pp. 5232-5242.
- Bradbury, L. J. S., 1965; "The Structure of a Self-Preserving Turbulent Plane Jet," JFM, 23, 1, pp. 31-64, 1965.
- Bradshaw, P., 1976; "Interacting Shear Layers in Turbo-machines and Diffusers," A Project SQUID Workshop - Turbulence in Internal Flows, (Murthy, S.N.B., Ed.), pp. 35-64, Hemisphere Publishing.

- Bradshaw, P., Ferriss, D. H., and Johnson, R. F., 1964; "Turbulence in the Noise Producing Region of a Circular Jet," JFM, 19, 4, pp. 591-624.
- Browand, F. K. and Weidman, P. D., 1976; "Large Scales in the Developing Mixing Layer," JFM, 76, 1, pp. 127-144.
- Brown, G. L. and Roshko, A., 1971; "The Effect of Density Difference on the Turbulent Mixing Layer," Turbulent Shear Flows, AGARD-CP-93, pp. 23(1-12).
- Brown, G. L. and Roshko, A., 1974; "On Density Effects and Large Structure in Turbulent Mixing Layers," JFM, 64, 4, pp. 775-816.
- Bruun, H. H., 1977; "A Time Domain Analysis of the Large Scale Flow Structure in a Circular Jet," JFM, 83, 4, pp. 641-671.
- Cervantes de Gortari, J. G., 1978; "An Experimental Study of the Flapping Motion of a Turbulent Plane Jet," Ph.D. Thesis, Purdue University.
- Chambers, F. W., 1977; "Acoustic interaction With a Turbulent Plane Jet," Ph.D. thesis, School of Mechanical Engineering, Purdue University.
- Chandrsuda, C., Mehta, R. D., Weir, A. D. and Bradshaw, P., 1978; "Effect of Free-Stream Turbulence on Large Structure in Turbulent Mixing Layers," JFM, 85, 4, pp. 693-704.
- Corrsin, S. and Kistler, A. L., 1954; "Free Stream Boundaries of Turbulent Flows," NACA Rept. 1244.
- Crow, S. C. and Champagne, F. H., 1971; "Orderly Structure in Jet Turbulence," JFM, 48, 3, pp. 547-591.
- Davies, P. O. A. L., and Yule, A. J., 1975; "Coherent Structures in Turbulence," JFM, 69, 3, pp. 513-537.
- Dimotakis, P. E. and Brown, G. L., 1976; "The Mixing Layer at High Reynolds Number: Large Structure Dynamics and Entrainment," JFM, 78, 3, pp. 535-560.
- Everitt, K. W. and Robins, A. G., 1978; "The Development and Structure of Turbulent Plane Jets," JFM, 88, 3, pp. 563-568.



- Ffowcs Williams, J. E. and Kempton, A. J., 1978; "The Noise from the Large-Scale Structure of a Jet," JFM, 84, 4, pp. 673-694.
- Fiedler, H. E. and Head, H. R., 1966; "Intermittency Measurements in the Turbulent Boundary Layer," JFM, 25, 4, p. 719.
- Foss, J. F., 1977; "THE VORCOM, Part 2; Demonstration Vorticity Measurements," Third Annual Report to NASA Langley, Dept. of Engineering Research, Michigan State University.
- Freymuth, P. and Uberoi, M. S., 1973; "Temperature Fluctuations in the Turbulent Wake Behind an Optically Heated Sphere," Phys. Fluids, 16, 2, p. 161.
- Fuchs, H. V., 1972; "Space Correlations of the Fluctuating Pressure in Subsonic Turbulent Jets," J. of Sound and Vibration, 23, 1, pp. 77-99.
- Goldschmidt, V. W. and Bradshaw, P., 1973; "Flapping of a Plane Jet," Phys. Fluids, 16, 3, pp. 354-355.
- Gortler, H., 1942; ZAMM, 22, pp. 244-254.
- Grant, H. L., 1958; "The Large Eddies of Turbulent Motion," JFM, 4, pp. 149-190.
- Gutmark, E. and Wygnanski, I., 1976; "The Planar Turbulent Jet," JFM, 73, 3, pp. 465-495.
- Hedley, T. B. and Keffer, J. F., 1974; "Turbulent/Non-turbulent Decisions in an Intermittent Flow," JFM, 64, 4, p. 625.
- Heskestad, G., 1965; "Hot Wire Measurements in a Plane Turbulent Jet," Trans. of ASME J. Appl. Mech., 32, 4, pp. 721-734.
- Hinze, J. O., 1975; Turbulence, McGraw-Hill, Inc., N.Y.
- Hooker, S. G., 1936; "On the Action of Viscosity in Increasing the Spacing Ratio of a Vortex Street," Proc. Roy. Soc., 154, pp. 67-89.
- Jenkins, P. E., 1974; "Study of the Intermittent Region of a Two-dimensional Plane Jet," Ph.D. thesis, School of Mechanical Engineering, Purdue University.

- Jenkins, P. E. and Goldschmidt, V. W., 1974; "Study of the Intermittent Region of a Two Dimensional Plane Jet," Herrick Lab Report. HL 74-75, School of Mechanical Engineering, Purdue University.
- Kaplan, R. E. and Laufer, J., 1968; "The Intermittently Turbulent Region of the Boundary Layer," Proceedings 12th International Conference of Applied Mechanics, p. 26, Stanford University.
- Kibens, V. and Kovasznay, L. S. G., 1970; "Detection of the Turbulent/Nonturbulent Interface," Interim Tech. Report 1, Department of Mechanics, The Johns Hopkins University (U. S. Army Research Office - Durham) DA-31-124-ARO-D-313.
- Ko, N. W. M. and Davies, P. O. A. L., 1971 ; "The Near Field Within the Potential Cone of Subsonic Cold Jets," JFM, 50, 1, pp. 49-78.
- Kohan, S. M., 1969; "Some Studies of the Intermittent Region and the Wall Region of a Two Dimensional Plane Wall Jet," Ph.D. Thesis, Stanford University.
- Kovasznay, L. S. G., 1977; "The Role of Large Scale Coherent Structures in Turbulent Shear Flows," Proceedings: Fifth Biennial Symposium on Turbulence, pp. 379-389, University of Missouri - Rolla.
- Lamb, H., 1945; Hydrodynamics, Dover Publications, New York.
- Lau, J. C. and Fisher, M. J., 1975; "The Vortex Street Structure of Turbulent Jets," JFM, 67, 2, pp. 299-337.
- Lau, J. C., Fisher, M. J. and Fuchs, H. V., 1972; "The Intrinsic Structure of Turbulent Jets," J. of Sound and Vibration, 22, 4, pp. 379-406.
- Laufer, J., 1975; "New Trends in Experimental Turbulence Research," Annual Review of Fluid Mechanics, 7, pp. 307-326.
- LaRue, J. C., 1974; "Detection of the Turbulent - Nonturbulent Interface in Slightly Heated Turbulent Shear Flows," Phys. Fluids, 17, 8, p. 1513.
- Liepmann, H. W. and Laufer, J., 1947; "Investigation of Free Turbulent Mixing," NACA TN 1257.

- Liu, J. T. C., 1974; "Developing Large-Scale Wavelike Eddies and the Near Jet Noise Field," JFM, 62, 3, pp. 437-464.
- Mattingly, G. E. and Criminale, W. O., 1971; "Disturbance Characteristics in a Plane Jet," Phys. Fluids, 14, 11, pp. 2258-2264.
- Merkine, L. and Liu, J. T. C., 1975; "On the Development of Noise Producing Large-Scale Wavelike Eddies in a Plane Turbulent Jet," JFM, 70, 2, pp. 353-368.
- Moallemi, K., 1980; "Visualization and Characterization of a Two-Dimensional Turbulent Jet," M.S. Thesis, School of Mechanical Engineering, Purdue University. (to be published)
- Mollo-Christensen, E., 1971; "Physics of Turbulent Flow," AIAA J., 9, 7, pp. 1217-1228.
- Moum, J. W., Kawall, J. G., and Keffer, J. F., 1979; "Structural Features of the Plane Turbulent Jet," Phys. Fluids, 22, 7, pp. 1240-1244.
- Oler, J. W. and Goldschmidt, V. W., 1978; "Self-preserving and Detection Characteristics of the Turbulent-Non-turbulent Interface in a Plane Jet," Herrick Laboratories Rept. HL 78-21, School of Mechanical Engineering, Purdue University.
- Oler, J. W. and Goldschmidt, V. W., 1979; "The Use of Microprocessors for Continuous Real Time Digital Formulation of the Intermittency Function," Proceedings, Symposium on Turbulence, University of Missouri - Rolla.
- Oler, J. W. and Goldschmidt, V. W., 1980; "Coherent Structures in Turbulent Plane Jets," Herrick Laboratories Rept. HL 80, School of Mechanical Engineering, Purdue University.
- Ott, E. S. and Goldschmidt, V. W., 1972; "Convective Velocities in a Turbulent Plane Jet," Herrick Laboratories Rept. HL 72-33, Department of Mechanical Engineering, Purdue University.
- Pao, H. P. and Kao, T. N., 1977; "Vortex Structure in the Wake of a Sphere," Phys. Fluids, 20, 2, pp. 187-191.
- Papailiou, D. D. and Lykoudis, P. S., 1974; "Turbulent Vortex Streets and the Entrainment Mechanism of the Turbulent Wake," JFM, 62, 1, pp. 11-31.

- Perry, A. M. and Lim, T. T., 1978; "Coherent Structures in Coflowing Jets and Wakes," JFM, 88, 3, pp. 451-463.
- Pui, N. K. and Gartshore, I. S., 1979; "Measurements of the Growth Rate and Structure in Plane Turbulent Mixing Layers," JFM, 91, 1, pp. 111-130.
- Reichardt, H., 1943; J. Royal Aero. Soc., 47, p. 167.
- Roshko, A., 1954; "On the Development of Turbulent Wakes From Vortex Streets," NACA Rept. 1191.
- Roshko, A., 1976; "Structure of Turbulent Shear Flows: A New Look," AIAA J., 14, 10, pp. 1349-1357.
- Schaefer, J. W. and Eskinazi, S. 1959; "An Analysis of the Vortex Street Generated in a Viscous Fluid," JFM, 6, 2, pp. 241-260.
- Takaki, R. and Kováczsnay, L. S. G., 1978; "Statistical Theory of Vortex Merger in the Two Dimensional Mixing Layer," Phys. of Fluids, 21, 2, 1978.
- Taneda, S., 1959; "Downstream Development of the Wakes Behind Cylinders," J. of the Physics Soc. of Japan, 14, pp. 843-848.
- Thomas, R. M., 1973; "Conditional Sampling and Other Measurements in a Plane Turbulent Wake," J. Fluid Mech., 57, 3, p. 549.
- Townsend, A. A., 1949; "The Fully Developed Turbulent Wake of a Circular Cylinder," Australian Journal of Scientific Research, Series A(2), p. 451.
- Townsend, A. A., 1956; The Structure of Turbulent Shear Flow, Cambridge University Press.
- Townsend, A. A., 1979; "Flow Patterns of Large Eddies in a Wake and in a Boundary Layer," JFM, 95, 3, pp. 515-537.
- Weir, A. D. and Bradshaw, P., 1975; "Resonance and Other Oscillations in the Initial Region of a Plane Turbulent Jet," Imperial College Report 75-07.
- Winant, C. D. and Browand, F. K., 1974; "Vortex Pairing: The Mechanism of Turbulent Mixing-Layer Growth at Moderate Reynolds Number," JFM, 63, pp. 237-255.

- Wooldridge, C. E. and Wooten, D. C., 1971; "A Study of the Large Scale Eddies of Jet Turbulence Producing Jet Noise," AIAA 9th Aerospace Sciences Meeting, No. 71-154, New York, NY.
- Wyganski, I. and Fiedler, H., 1969; "Some Measurements in the Self-Preserving Jet," JFM, 64, 4, p. 679.
- Wyganski, I. and Fiedler, H., 1970; "The Two Dimensional Mixing Region," JFM, 41, 2, p. 327.
- Wyganski, I. and Gutmark, E. 1971; "Lateral Motion of the Two-Dimensional Jet Boundaries," Phys. Fluids, 14 7, pp. 1309-1311.
- Wyganski, I., Oster, D., Fiedler, H., and Dziomba, B., 1979; "On the Perseverance of a Quasi-Two-Dimensional Eddy Structure in a Turbulent Mixing Layer," JFM, 93. 2. pp. 325-335.
- Young, M. F., 1973; "A Turbulence Study: Convective Velocities, Energy Spectra, and Turbulence Scales in a Plane Air Jet," M.S. Thesis, School of Mechanical Engineering, Purdue University.

## APPENDICES

## APPENDIX A

## LITERATURE REVIEW - TURBULENCE DETECTION

In principle, the formulation of the intermittency function and the measurement of the intermittency fraction and interface crossing frequency are straightforward. However, in practice, the procedure is difficult due to the sensitivity of  $I(\vec{r}, t)$  to the choices made for the original indicator signal, threshold and hold time. Most variations on Townsend's original intermittency circuit have been conceived with the intent of overcoming these difficulties. What follows is a summary of the techniques that have been utilized and reported in the literature.

A. The Intermittency Indicator Signal,  $S(\vec{r}, t)$ 

Different choices for  $S(\vec{r}, t)$  have been tried by several investigators for the purpose of clarifying the determination of  $\tau_h$  and  $C$  by increasing the turbulent-non-turbulent contrast of  $S(\vec{r}, t)$ . A representative sample of these different types of signals are tabulated later in the chapter in Table 1.

Townsend's choice for  $S(\vec{r}, t)$  was the rectified time derivative of the streamwise component of the velocity fluctuation. As would be expected, the fluctuation intensities are appreciably greater in turbulent than in nonturbulent regions. The contrast is enhanced by taking the time derivative which favors the high frequency fluctuation components characteristic of the turbulent regions. This type of signal has been utilized by Corrsin and Kistler (1955), Fiedler and Head (1966), Wygnanski and

Fiedler (1969), Thomas (1973), Antonia and Atkinson (1974) and Ajagu and Goldschmidt (1976).

The rectified time derivative of the instantaneous uv Reynolds' stress component was found to give a more distinct turbulent-nonturbulent contrast by Antonia (1972).

As suggested by Corrsin and Kistler, the seemingly ideal choice for  $S(\vec{r}, t)$  is the instantaneous vorticity. With the exception of recent advances made by Foss (1977), the practical difficulties of constructing a probe to sense even a single component of the vorticity vector have been prohibitive. Kibens and Kovasznay (1970) have, however, utilized a signal that is approximately proportional to the transverse vorticity component by forming  $\delta u / \delta y$  from the differential output of two parallel probes separated by a small transverse distance. This signal was differentiated with respect to time and rectified to form  $S(\vec{r}, t)$ . Jenkins and Goldschmidt (1974) have also used this procedure.

There is an inherent difficulty in the use of the velocity fluctuation, its spatial or time derivatives or any similar flow property which fluctuates between positive and negative values as a basis for  $S(\vec{r}, t)$ . This difficulty is due to the frequent threshold crossings that are not related to an interface passage but are instead a result of the fluctuating signal crossing zero. The occurrence of these extraneous threshold crossings increases the difficulty in choosing  $\tau_h$  and adds to the uncertainty of intermittency measurement.

To avoid the zero crossing problem, Kaplan and Laufer (1968) defined  $S(\vec{r}, t)$  as the variance of the time derivative of the velocity fluctuation from its short time mean value. The time interval over which the mean value was formed was chosen to be small compared to the expected burst and void lengths and centered over the instant of interest so that the past and future were weighted equally.



Wyganski and Fiedler (1970) found that the number of non-interface related threshold crossings could be reduced by forming  $S(\vec{r}, t)$  from the sums of the rectified first and second derivatives of the velocity fluctuation.

A similar effect was achieved by Fiedler and Head (1966) who used the sum of the rectified time derivative of the velocity fluctuation signal phase shifted by a time interval that was small compared to burst and void durations with the original unshifted but rectified signal. Hedley and Keffer (1974) approached this problem by forming  $S(\vec{r}, t)$  from the sum of the squares of time derivatives of the longitudinal and transverse components of the fluctuating velocity vector.

A different approach to the "zero crossing" problem is to base  $S(\vec{r}, t)$  on the detection of a marked species transported within the turbulent fluid so that the indicator signal will contain only positive deviations from the reference level. The advantage of having only positive deviations is obvious. The disadvantage is the uncertainty as to the contamination of the flow field by the tracked scalar. Freymuth and Uberoi (1973), LaRue (1974), Barsoum, Kawall and Keffer (1978) and Jenkins and Goldschmidt (1974) have utilized the measurement of temperature in slightly heated turbulent flows for this purpose. A helium marked jet has been investigated by Anderson, LaRue and Libby (1977) while Fiedler and Head (1966) revealed the intermittent characteristics of a smoke filled boundary layer by illuminating it and observing the alternating light and dark patches with a high resolution optical system.

### B. The Intermittency Detection Parameters, C and $\tau_h$

The greatest uncertainty in forming  $I(\vec{r}, t)$  is in defining the criteria for selecting the threshold\*, C, and hold time  $\tau_h$ . Most investigators have achieved satisfactory results by considering each parameter separately.

The optimum choice for the threshold is the minimum value which is still above the inherent "noise" contained in the nonturbulent portions of  $S(\vec{r}, t)$ . Wygnanski and Fiedler (1969), Antonia (1972), Kaplan and Laufer (1968), and LaRue (1974), have found that this level was most easily determined through subjective inspections of  $S(\vec{r}, t)$  and the  $I(\vec{r}, t)$  which resulted from a particular choice of C as shown by oscilloscope or computer plotted traces. Jenkins and Goldschmidt (1974), and Ajagu and Goldschmidt (1976), determined C by observing the variation  $\gamma$  and  $F_\gamma$  for a range of thresholds. Although  $\gamma$  systematically decreased for increasing C, the rate of variation of  $F_\gamma$  decreased markedly for thresholds above a value which was interpreted as the optimum value. A similar approach was taken by Hedler and Keffer (1974) using the variation of the average nonturbulent time interval as the critical threshold dependent property.

Kibens and Kovasznay (1970), found that the optimum choice for the intermittency of  $I(\vec{r}, t)$  was a function of the intermittency and the ratio of the zone averaged rms levels of the turbulent and nonturbulent portions of  $S(\vec{r}, t)$  which was defined as the signal to noise ratio. Since the intermittency and signal to noise ratio are themselves dependent on C, calibration plots for the optimum C were determined

---

\* The threshold is typically defined as either the percentage of some characteristic measured flow property (peak or rms) or alternately as an absolute voltage level. The hold time is always given in units of time.

from analysis of an artificial turbulence signal with known intermittency properties. An iteration procedure could be used to find  $C$  by assuming a value of  $\gamma$  and the  $S/N$  ratio and picking the optimum threshold from the calibration plots. The measured  $\gamma$  and  $S/N$  were compared to the assumed values and additional iterations made accordingly.

The hold time is typically determined from estimations of the minimum expected length scale,  $\ell_{\min}$ , of the eddy structure associated with interface deformations.  $\tau_h$  is then approximately equal to  $\ell_{\min}/U_c$  where  $U_c$  is the convection velocity. Hedley and Keffer (1974), and LaRue (1974), expressed  $\ell_{\min}$  as an integer multiple of the Kolmogoroff length,  $\ell_k$ . Kibens and Kovaszny (1970), Jenkins and Goldschmidt (1974), and Antonia and Atkinson (1974), found that  $\tau_h$  could be expressed in terms of a characteristic frequency defined as  $F_{ch} = \dot{S}(\vec{r}, t)/S(\vec{r}, t)$ .

A completely different approach was adopted by Ajagu and Goldschmidt (1976), who chose  $\tau_h$  as the minimum value that would allow measurement of an intermittency equal to one in a fully turbulent zone for the range of thresholds which were used. Unlike other investigators who based  $\tau_h$  on the measurement of local properties so that it had a nonconstant value, Ajagu and Goldschmidt (1976) were able to use a constant  $\tau_h$  over a wide portion of the self-preserving region of a plane jet.

The most involved procedure for the determination of  $\tau_h$  and  $C$  was developed by Antonia and Atkinson (1974). They considered the optimum choice of  $\tau_h$  and  $C$  to be functionally related to each other as well as to the intermittency and  $S/N$  ratio. Using calibration plots derived from the analysis of artificial turbulent signals,  $C$  and  $\tau_h$  were determined through an iteration procedure similar to that of Kibens and Kovaszny.

A partial tabulation of a few of the intermittency measurement procedures is given in Table A-1. The uncertainty of the measurement process is attested to by the wide variety of techniques.

Table A-1. Turbulence Detection Techniques

Investigator	$S(\vec{r}, t)$	C	$\tau_H$
Antonia (1972)	$\frac{\partial^2 uv}{\partial t^2}$	(*)	(*)
Antonia & Atkinson (1974)	$\frac{\partial u}{\partial t}$	iterative scheme using calibration plots of $\gamma$ vs. C vs. $\tau_H$	
Hedley & Keffer (1974)	$\frac{\partial^2 u}{\partial t^2} + \frac{\partial^2 v}{\partial t^2}$ plus $\frac{\partial^2 v}{\partial t^2}$	calibration plots of average nonturbulent zone durations vs. C	$28 \epsilon_k / U_c$
Kaplan & Laufer (1968)	$\frac{\partial u}{\partial t} - \frac{\partial u}{\partial t}$	(*)	application of $\tau_H$ is implicit in definition of $S(\vec{r}, t)$
Kibens & Kovaszny (1970)	$\frac{\partial^2 u}{\partial y \partial t}$	iterative scheme using calibration plots of C vs. $\gamma$	$\frac{2\pi}{\omega \text{ char.}}$
LaRue (1974)	$\theta(t)$	(*)	$3 \epsilon_k / U_c$

\* determined from subjective comparisons of  $S(\vec{r}, t)$  and resulting  $I(\vec{r}, t)$

## APPENDIX B

## THE DIGITAL INTERMITTENCY MEASUREMENT TECHNIQUE

Although the plane jet apparatus is located in the R. W. Herrick Laboratories, the analysis of the early intermittency data was done on a General Automation mini-computer located in the mechanical engineering stochastic laboratory. For this reason, the raw turbulence indicator signal was recorded on an Ampex FM tape recorder and later played back for digitization and analysis. A block diagram of the data acquisition and analysis equipment is given in Figure B-1.

Analysis of the digitally recorded data was accomplished by subroutine DTECTR under the control of the main routine TDAP. Listings of these routines are given at the end of this section. The logic for the application of the threshold (designated as LEVEL in DTECTR) and hold time (designated as HOLDTM) may be given in three rules:

1. Data samples (DATA(1)) greater than LEVEL are identified as being part of turbulent bursts while samples below LEVEL represent voids or the intervals separating bursts.
2. All bursts and voids must have durations greater than the hold time to be valid, i.e., a burst must last longer than the hold time before it may interrupt an otherwise continuous void and vice versa.
3. A conflicting case may arise for rule #2 when a series of short bursts are separated by short voids with neither the bursts nor voids longer than the hold time. For this case, the short bursts and voids are counted

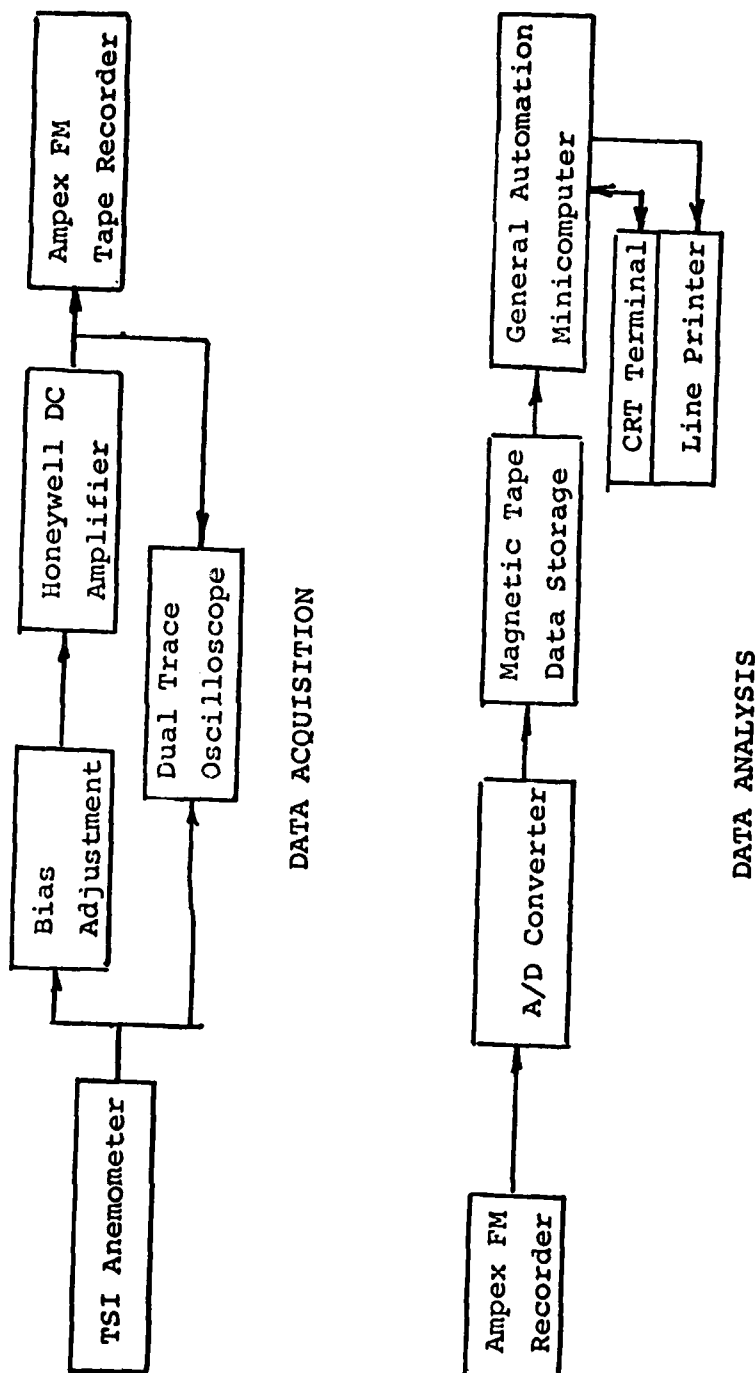


Figure B-1 The Digital Intermittency Analysis Technique

as a single burst provided the total duration is then greater than the hold time.

A flow chart describing the implementation of these rules and an example of their application is given in Figure 3-3.



Table B-1 Program TDAP

```

TDAP  -TURB. DATA ANALYSIS PROGRAM      1 4 M F J#0
DIMENSION Y(30), FREQ(30), HEIGHT(2), THRHL(30)
REAL INTERM(30), MXFREQ, NSET
INTEGER STRIVE, NFILE(30), OPTION
INTEGER HLADR, LABX(4), LABY1(8), LABY2(10)
DATA HEADER /0/
DATA LABEX / 'Y' ., ., 'B' ., 2/
DATA LABY1 / 'IN', 'TE', 'RM', 'IT', 'TE', 'NC', 'Y' ., 1/
DATA LABY2 / 'CR', 'OS', 'SI', 'NG', 'F', 'RE', 'QU', 'EN', 'CY

99 CONTINUE
  WRITE(7.107)
  READ(7.999) NFILES
  IF(NFILES.EQ.0)GO TO 98
  WRITE(7.101)
  READ(7.999) HOLDTM
  WRITE(7.111)
  READ(7.999) DT
  WRITE(7.108)
  READ(7.999) NSET
  NN=NFILES+2
  WRITE(7.109)
  DO 9 I=3.NN
    J=I-2
    WRITE(7.110) J
    READ(7.999) Y(I),NFILE(I),THRHL(I)
  9 CONTINUE

CALCULATE INTERMITTENCY & CROSSING FREQ. DISTRIBUTIONS
  DO 10 I=3.NN
    CALL D$OPEN
    ILENGH = STRIVE(NFILE(I),14,0,0,-1)
    CALL D$OPEN
    CALL DTECTR(DT,HOLDTM,THRHL(I),NSET,INTERM(I),FREQ(I))
  10 CONTINUE

NORMALIZE THE CROSSING FREQ. DISTRIBUTION
  MXFREQ = 0.0
  DO 11 I=3.NN
    IF(FREQ(I) .GT. MXFREQ) MXFREQ = FREQ(I)
  11 CONTINUE

  DO 12 I = 3.NN
    FREQ(I) = FREQ(I) / MXFREQ
  12 CONTINUE

```

Table B-1 cont.

## WRITE THE RESULTS

```

WRITE(5.102)
WRITE(5.103) D1. HOLDTM. MXFREQ
WRITE(5.104)
WRITE(5.105) ( Y(I).THRHLDD(I). INTERM(I). FREQ(I). I=3.NI

```

## PLOT THE RESULTS

```

WRITE(7.106)
READ(7.999) OPTION

IF ( OPTION .LT. 0 ) GO TO 99
IF ( OPTION .NE. 1 ) GO TO 13
Y(1)=0.0
Y(2)=2.0
INTERM(1) = 0.0
INTERM(2) = 1.0
FREQ(1) = 0.0
FREQ(2) = 1.0
LABLX(1) = 'Y'
LABLY1(1) = 'IN'
HEIGHT(1) = 5.0
HEIGHT(2) = 5.0
CALL JPLOT(1.NFILES,-1.1,HEADER,Y,LABLX,-999.0,INTERM,LABL
% -999.0,HEIGHT,-1.0)
LABLY2(1) = 'CR'
HEIGHT(1) = 5.0
HEIGHT(2) = 0.0
CALL JPLOT(0.NFILES,-1.1,HEADER,Y,LABLX,-999.0,FREQ,LABLY
% -999.0,HEIGHT,-1.0)
GO TO 99

13 CONTINUE
HEIGHT(1) = 5.0
HEIGHT(2) = 5.0
LABLX(1) = 0
LABLY1(1) = 0
CALL JPLOT(0.NFILES,-1.1,HEADER,Y,LABLX,999.0,INTERM,LABL
% HEIGHT,-1.0)
HEIGHT(1) = 5.0
HEIGHT(2) = 0.0
LABLY2(1) = 0
CALL JPLOT(0.NFILES,-1.1,HEADER,Y,LABLX,999.0,FREQ,LABLY2
% HEIGHT,-1.0)

GO TO 99

98 CONTINUE

```

## Table B-1 cont.

```

101 FORMAT(' HOLDTM?')
102 FORMAT(///' INTERMITTENCY & CROSSING FREQ. DISTRIBUTIONS'
103 FORMAT(/4X.'DT = '.E11.3,4X.'HOLD TIME = '.E11.3,/4X.
      X'MAX CROSSING FREQ = '.E11.3//)
104 FORMAT(/9X.'Y/B',8X,'THRHL'D',5X,'INTERMITTENCY',3X,'CR.
105 FORMAT(4(3X.E11.3))
106 FORMAT(//'          1 - PLOT ON A NEW PAGE'//.
      X          ' ENTER:  0 - PLOT ON SAME PAGE'//.
      X          '          -1 - CONTINUE W/O PLOT')
107 FORMAT(' NFILES?')
108 FORMAT(' NSET? ')
109 FORMAT(' Y(I) , NFILE(I), THRHL'D(I) ')
110 FORMAT(1X,I3)
111 FORMAT(' DT? ')
999 FORMAT(V)

```

END

Table B-2 Program DTECTR

```

** DTECTR -TURB BURST DETECTION ROUTINE      1 4 S F JWO R PRIE
SUBROUTINE DTECTR(DT,HOLDTM,LEVEL,NSET,INTERM,FREQ)
DIMENSION DATA(3)
REAL LEVEL,INTERM,NSET,ILE,ITE,I
J = 1
I = 0.0
TURBTM = 0.0

FIND THE FIRST TURB BURST
1 CONTINUE
I = I + 1.0
IF(I .GT. NSET) GO TO 901
CALL VSREAL(DATA,IER)
IF(IER .NE. 0) GO TO 950
IF(DATA(1) .GT. LEVEL) GO TO 1
ILE = I

FIND THE TRAILING EDGE
2 CONTINUE
I = I + 1.0
IF(I .GT. NSET) GO TO 902
CALL VSREAL(DATA,IER)
IF(IER .NE. 0) GO TO 950
IF(DATA(1) .LE. LEVEL) GO TO 2
ITE = I

LOOK FOR THE NEXT BURST AND VERIFY THAT INTERVENING VOID
IS LONGER THAN HOLDTM
3 CONTINUE
I = I + 1.0
IF(I .GT. NSET) GO TO 903
CALL VSREAL(DATA,IER)
IF(IER .NE. 0) GO TO 950
IF(DATA(1) .GT. LEVEL) GO TO 3
VOIDTM = (I - ITE) * DT
IF(VOIDTM .LT. HOLDTM) GO TO 2

VERIFY THAT PREVIOUS TURB BURST WAS LONGER THAN HOLDTM
BURSTM = (ITE - ILE) * DT
IF(BURSTM .LT. HOLDTM) GO TO 4

INCREMENT J - INDEX AND ADD BURST LENGTH TO TOTAL
J = J + 1
TURBTM = TURBTM + BURSTM

BEGIN CALCULATION FOR NEW BURST PROSPECT
4 CONTINUE
ILE = I
GO TO 2

```

## Table B-2 cont.

```
COMPLETE SEARCH
981 CONTINUE
  J = J
  GO TO 910
982 CONTINUE

  ITE = I
983 CONTINUE
  TURBTM = TURBTM + (ITE - ILE) * DT
910 CONTINUE

  CALCULATE INTERMITANCY AND CROSSING FREQ
  INTERM = TURBTM / (NSET * DT)
  FREQ = J / (NSET * DT)

  WRITE THE RESULTS
  WRITE(7,101) LEVEL,INTERM,FREQ,J
101 FORMAT(' THRLD = '.F6.3.3X,'INTERM = '.E10.3.3X,'CR FRE
  % E10.3.3X,'J = '.I5)
  GO TO 950
102 FORMAT(' LAS INPUT ERROR - IER = '.I3)
950 CONTINUE
  WRITE(5,102) IER
960 CONTINUE
  RETURN
  END
```

## APPENDIX C

### THE HYBRID INTERMITTENCY INSTRUMENT

In an effort to overcome the inconvenience of performing data acquisition and data analysis at two different locations, an alternate means of formulating the intermittency function,  $I(\vec{r}, t)$ , was devised. The resulting hybrid instrument has the virtues of low cost and convenience inherent with analog instrumentation while retaining much of the precision of a larger digital computer. To the author's best knowledge, the instrument represents the first application of a computer of any size for the continuous and real-time formulation of the intermittency function.

#### 1. The Hardware

A block diagram of the basic elements of the intermittency detection instrument is given in Figure C-1. They consist of a hot wire anemometer, DC signal conditioning circuits, the threshold circuit and an RCA Cosmac micro-computer.

The DC signal conditioning circuits consist of a reverse biasing circuit to remove the DC component of  $S(\vec{r}, t)$  and a DC amplifier. Application of  $C$  to  $S(\vec{r}, t)$  is accomplished with an operational amplifier comparator. With  $S(\vec{r}, t)$  at the negative input and a variable  $C$  at the positive input, a square wave,  $G(\vec{r}, t)$  is available at the output.  $S(\vec{r}, t)$ ,  $C$  and  $G(\vec{r}, t)$  are all available as outputs to an oscilloscope which facilitates the adjustment of  $C$ .

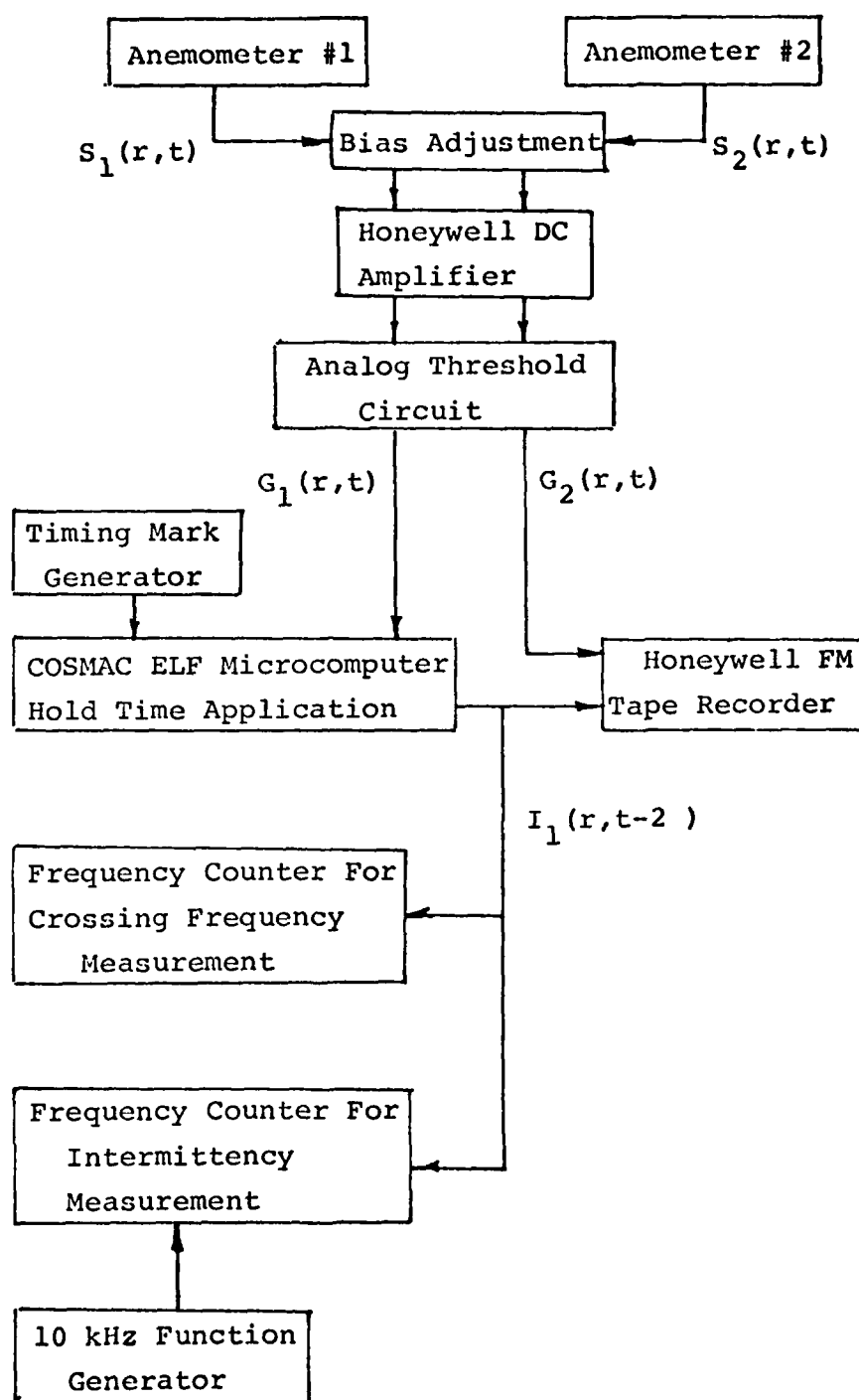


Figure C-1 The Hybrid Intermittency Analysis Technique

The microcomputer is based on the RCA Cosmac family of microprocessor integrated circuits using an eight bit data bus and 16 bit address bus. Operating system firmware is contained in 1/4K ROM and 3K RAM is available for user programs. An audio cassette interface is utilized for program storage and retrieval. The intermittency circuit is interfaced to the microcomputer via one bit of a parallel input/output port. Since  $G(\vec{r}, t)$  is available to the microcomputer as a logic level signal, an analog to digital converter is unnecessary and  $G(\vec{r}, t)$  is merely sensed at intervals controlled by the external clock.

## 2. The Software

Rules #2 and #3 of Appendix B for the formulation of  $I(\vec{r}, t)$  concern the application of the hold time and are repeated below:

2. All bursts and voids must have a duration greater than  $\tau_h$  to be included in  $I(\vec{r}, t)$ .
3. For the conflicting case where a series of short bursts are separated by short voids, all of which are less than  $\tau_h$ , a single uninterrupted burst will result in  $I(\vec{r}, t)$  provided that the total duration is then longer than  $\tau_h$ .

The difficulty in applying the rules is that they require future knowledge of the fate of each burst and void before  $I(\vec{r}, t)$  can be formulated. Rule 2 requires the ability to "look ahead"  $\tau_h$  msecs. While Rule 3 requires as much as  $2\tau_h$  msecs. of future knowledge to determine the instantaneous state of  $I(\vec{r}, t)$ .

The "look ahead" capability has been incorporated into the present system through the use of a circular data buffer and the allowance of a constant time lag between input  $G(\vec{r}, t)$  and output  $I(\vec{r}, t - 2\tau_h)$ . Figure C-2 illustrates the concept of a circular data buffer. The three data pointers are allowed to step through 256 consecutive bytes of memory



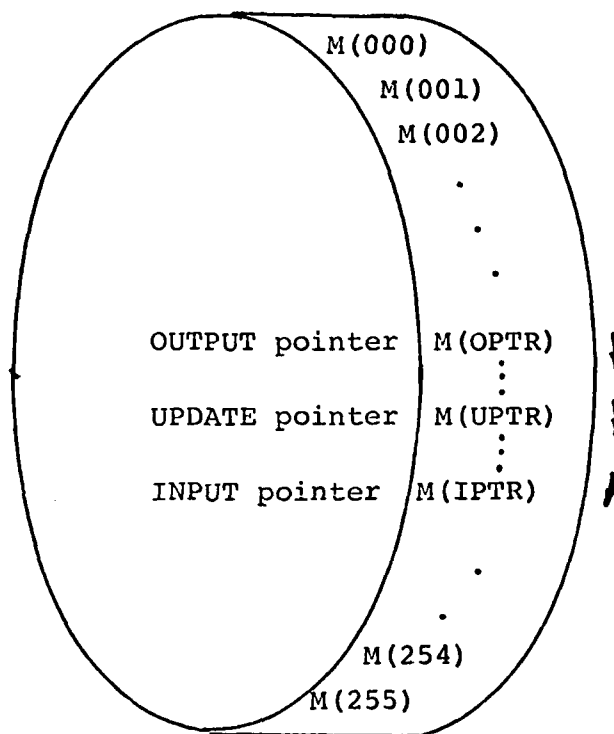


Figure C-2 The Circular Data Buffer

which serve as a data buffer. As each pointer reaches the end of the buffer, MEMORY(255), it is automatically reset to MEMORY(0) and allowed to step through the buffer again in a circular manner.

At each clock pulse, new  $G(\vec{r}, t)$  data is input and stored at M(IPTR) and updated  $I(\vec{r}, t - 2\tau_h)$  data is output from M(OPTR). Following this, IPTR and OPTR are incremented so that they are ready for the next clock pulse while maintaining the same relative position. The output  $I(\vec{r}, t - 2\tau_h)$  always lags the input  $G(\vec{r}, t)$  by a constant  $2\tau_h$  msecs.

Following the input/output operations, the new  $G(\vec{r}, t)$  data is combined with previous information for the purpose of measuring burst and void durations and comparing them with  $\tau_h$ . If sufficient data is unavailable to determine the short term future of a burst or void, the analysis segment of the algorithm pauses and waits for the next clock pulse and additional  $G(\vec{r}, t)$  data. However, if sufficient information is available, completely formulated  $I(\vec{r}, t - n\Delta t)$  data is inserted into the buffer starting at the memory location pointed to by the UPDATE pointer. Although the UPDATE pointer is always bracketed by IPTR and OPTR, its relative position fluctuates depending on the random analysis sequence.

The machine language routine which performs the hold time application is given at the end of this section. A unique feature of the RCA 1802 microprocessor is an internal array of 16 general purpose registers which may be used interchangeably as memory pointers, program counters, or for temporary storage. Table C-1 gives the register assignments used in the analysis routines. The entry point for the routine is at label "INITIAL" or (04 00) and it is in this section that the registers are initialized.

Table C-1 Register Assignments

REGISTER	ASSIGNMENT
0	
1	UPDATE routine program counter
2	Stack pointer
3	MAIN routine program counter
4	TAP routine program counter
5	IPTR - Input buffer pointer
6	OPTR - Output buffer pointer
7	UPTR - Update buffer pointer
8.1	Constant - Buffer page number
8.0	NB - Burst counter
9.1	Temporary storage for I(t)
9.0	NV - Void counter
A.1	Constant - 01
A.0	Constant - 00

The analysis program is made up of a main routine, MAIN, at (0500) and two subroutines, TAP (Turbulence Analysis Program) and UPDATE at (0518) and (0570), respectively. MAIN performs the functions of monitoring the external clock and input/output control. The actual application of  $\tau_h$  is done by TAP which has multiple entry and exit points depending on the instantaneous status of the analysis. Once the bursts and voids have been analyzed by TAP, UPDATE performs the function of modifying the data buffer in accord with the results. For additional information concerning the machine language programming, the reader is referred to the RCA 1802 Users Manual.

### 3. Limitations

The precision with which  $\tau_h$  is applied to  $G(\vec{r}, t)$  is limited by the resolution with which the duration of the bursts and voids may be determined. Therefore, it is desirable to operate the external sampling clock at the highest possible frequency compatible with the data handling capacity of the microcomputer. Each possible sequence of instructions that the microcomputer could be required to perform during a single sampling interval  $\Delta T$  was examined and the time required for their execution was determined. The maximum sampling frequency could then be chosen according to the longest execution time requirement. It is possible to increase the timing resolution by increasing the microcomputer machine cycle speed, thereby improving its data handling capacity and allowing a higher sampling frequency. The microcomputer utilized in the present experiment was operated at a machine cycle frequency of .25 Mhz.

Table C-2 lists the values for  $\tau_h$  and the sampling interval  $\Delta T$  used in making the measurements of  $\gamma(\vec{r})$  and  $F_Y(\vec{r})$ . The ratio  $\Delta T/\tau_h$  provides a measure of the relative precision with which the hold time could be applied. Due to the speed limitations of the microcomputer, this precision

Table C-2 Signal Analysis Timing Parameters

$x/D$	$\tau_h$ msec	$\Delta T$ msec	$\Delta T/\tau_h$
20	2.15	.54	.25
30	4.0	.67	.17
40	6.19	.77	.12
50	8.68	.87	.10
60	11.44	.95	.08

becomes progressively more critical at positions closer to the jet exit and accounts for the discrepancies evident in Figure C-3. Accordingly, the hybrid instrument was only used for measurements at  $x/D \geq 20$ .

4. A Microcomputer Delay Line

For correlations involving intermittency functions with relative time shifts, a second RCA based microcomputer was used to introduce the appropriate delay.

The input intermittency signal is sampled at 5 kHz rate with the data going into a circular data buffer at a location pointed to by the input pointer. At the same time, data from the buffer pointed to by the output pointer is output. As the input and output pointer are stepped through the buffer, the output signal is an image of the input but delayed by an amount determined from the separation between the pointers. The machine language program which accomplishes this function is given at the end of this section.

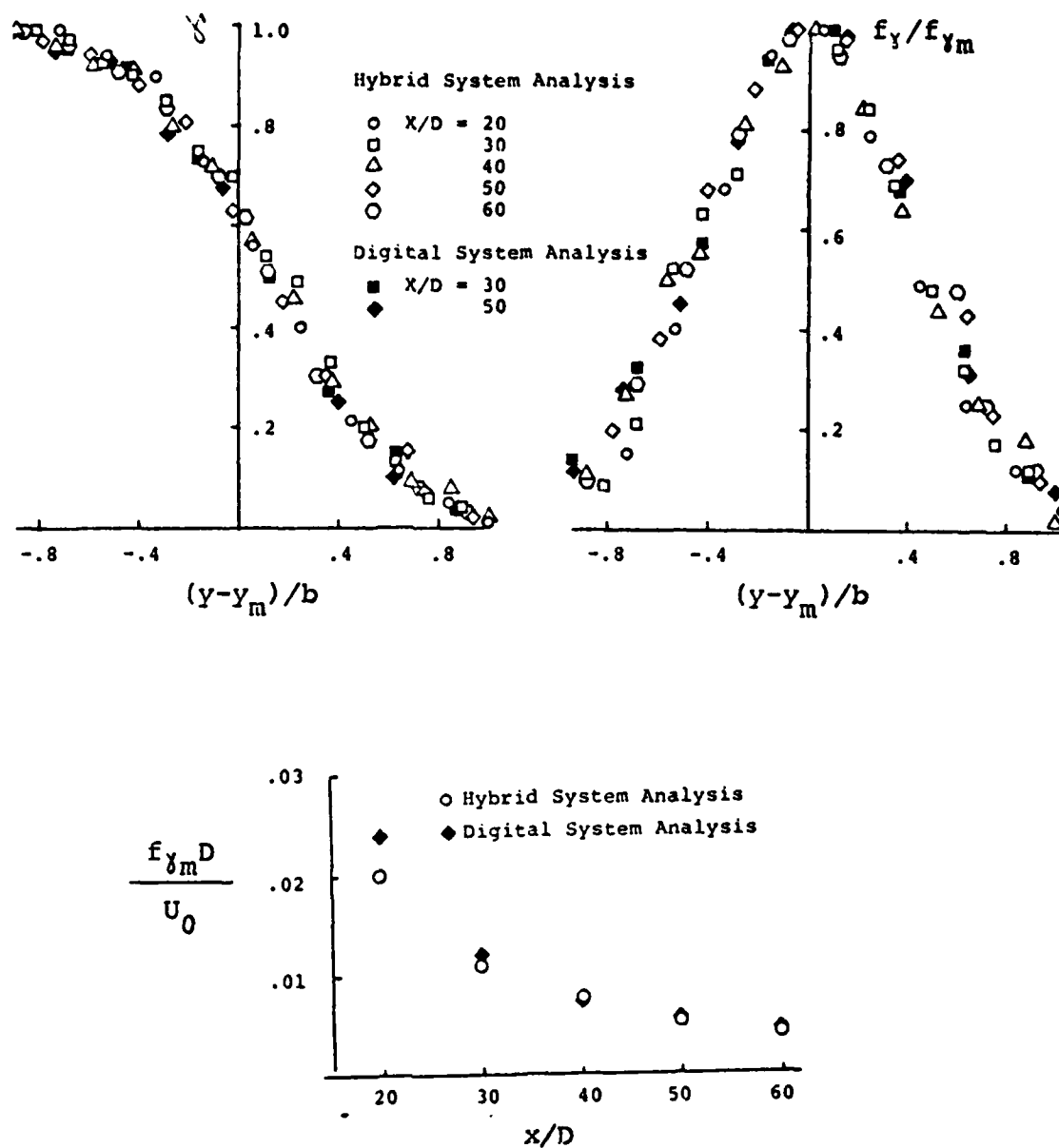


Figure C-3 Comparison of Hybrid and Digital Analysis Results

Table C-3  
TURBULENCE ANALYSIS ROUTINES

ADDRESS	CODE	LABEL	MNEM.	OPERAND	COMMENTS
04 00	F8 04	INITIAL	LDI	04	
02	B3		PHI	3	
03	B1		PHI	1	
04	F8 06		LDI	PC3	
06	A3	PC3	PLO	3	R3 = Program Ctr.
07	D3		SEP	3	
08	F8 03		LDI	03	
0A	B2		PHI	2	
0B	F8 FF		LDI	FF	
0D	A2		PLO	2	
0E	E2		SEX	2	R2 = Stack Ptr
0F	6C		INP	4	Input NHT
10	64		OUT	4	Display NHT
11	22		DEC	2	M(RX) = NHT
12	F8 31		LDI	31	
14	A1		PLO	1	R1 = UPDATE Program Ctr.
15	F8 05		LDI	05	
17	B4		PHI	4	
18	F8 19		LDI	19	
1A	A4		PLO	4	R4 = TAP Program Ctr.



Table C-3 cont.

ADDRESS	CODE	LABEL	MNEM.	OPERAND	COMMENTS
04 1B	F8 06		LDI	06	
1D	B5		B5		
1E	B6		B6		
1F	B7		PHI	7	
20	B8		PHI	8	
21	F8 30		LDI	30	
23	A5		PL0	5	R5 = IPTR
24	A7		PL0	7	R7 = UPTR
25	F8 00		LDI	00	
27	A6		PL0	6	R6 - OPTR
28	A8		PL0	8	R8.0 = NB
29	B9		PHI	9	
2A	A9		PL0	9	R9.0 = NV
2B	AA		PL0	A	RA.0 = Con- stant = 0
2C	F8 01		LDI	01	
2E	BA		PHI	A	RA.1 = Con- stant = 1
2F	C0 0400		LBR	MAIN	Jump to MAIN
05 00	3E 00	MAIN	BN3	MAIN	Wait for clock pulse
02	E6		SEX	6	
03	61		OUT1		Output M(OPTR); OPTR + 1

Table C-3 cont.

ADDRESS	CODE	LABEL	MNEM.	OPERAND	COMMENTS
05 04	E5		SEX	5	
05	69		INP1		Input data to M(IPTR)
06	E2		SEX	2	
07	04		SEP	4	Jump to TAP; D = G(t)
08	15		INC	5	IPTR + 1
09	98		GHI	8	
0A	85		PHI	5	
0B	B6		PHI	6	
0C	36 0C	WAIT	B3	WAIT	Wait until end of clock cycle, then repeat
0E	30 00		BR	MAIN	
05 18	03	B1	SEP	3	Return to MAIN
19	32 30	NTRB1	BZ	V2	If G(t) = 0, go to V2, otherwise, NB + 1
1B	18	B2	INC	8	
1C	88		GLO	8	
1D	F7		SM		
1E	3B 18		BL	B1	If NB < NHT, re- peat
20	9A		GHI	A	
21	B9		PHI	9	01 → 1 for UP- DATE

Table C-3 cont.

ADDRESS	CODE	LABEL	MNEM.	OPERAND	COMMENTS
05 22	88		GLO	8	NB → D
23	D1		SEP	1	Call UPDATE
24	8A		GLO	A	
25	A8		PL0	8	0 → NB
26	D3	B3	SEP	3	Return to MAIN
27	32 30	NTRB2	BZ	V2	If G(t) = 0, go to V2, otherwise, 01 → D
29	9A		GHI	A	
2A	D1		SEP	1	Call UPDATE, then repeat
2B	30 26		BR	B3	
2D	D3	V1	SEP	3	Return to MAIN
2E	3A 46	NTRV1	BNZ	B4	If G(t) = 0, go to B4, otherwise, NB + 1 and NV + 1
30	18	V2	INC	8	
31	19		INC	9	
32	89		GLO	9	
33	F7		SM		
34	3B 2D		BL	V1	If NV < NHT, re- peat
36	8A		GLO	A	
37	B9		PHI	9	00 → 1 for UPDATE
38	88		GLO	8	NB → D

Table C-3 cont.

ADDRESS	CODE	LABEL	MNEM.	OPERAND	COMMENTS
05 39	D1		SEP	1	Call UPDATE
3A	8A		GLO	A	
3B	A8		PLO	8	0 → NB
3C	A9		PLO	9	0 → NV
3D	D3	V3	SEP	3	Return to MAIN
3E	3A 1B	NTRV2	BNZ	B2	If G(t), to to B2
40	9A		GHI	A	NV = 01 → D
41	D1		SEP	1	Call UPDATE, then repeat
42	30 3D		BR	V3	
05 46	18	B4	INC	8	NB + 1
47	8A		GLO	A	
48	A9		PLO	9	0 → NV
49	07		LDN	7	If M(UPTR) = 1, go to B5
4A	3A 5A		BNZ	B5	
4C	88		GLO	8	
4D	F7		SM		
4E	3B 18		BL	B1	If NB < NV, go to B1, otherwise,
50	9A		GHI	A	
51	B9		PHI	9	01 → 1 for UPDATE
52	88		GLO	8	NB → D

Table C-3 cont.

ADDRESS	CODE	LABEL	MNEM.	OPERAND	COMMENTS
05 53	D1		SEP	1	Call UPDATE
54	8A		GLO	A	
55	A8		PLO	8	0 → NB
56	30 26		BR	B3	then go to B3
5A	9A	B5	GHI	A	
5B	B9		PHI	9	01 → 1 for UPDATE
5C	88		GLO	8	NB → D
5D	D1		SEP	1	Call UPDATE
5E	8A		GLO	A	
5F	A8		PLO	8	0 → NB
60	30 26		BR	B3	then go to B3
05 70	D4	UEXIT	SEP	4	Return to TAP
71	22	NTRU	DEC	2	RX - 1, Save NHT
72	52		STR	2	NB or NV → M(RX)
73	FE		SHL		
74	FE		SHL		Compute address for correct number of UPDATE opera- tions
75	F4		ADD		
76	FD BA		SDI	10	
78	A1		PLO	1	Jump to address

Table C-3 cont.

ADDRESS	CODE	LABEL	MNEM.	OPERAND	COMMENTS
05 79	17	U13	INC	7	
7A	98		GHI	8	
7B	87		PHI	7	UPTR + 1
7C	99		GHI	9	
7D	57		STR	7	I → M(UPTR)
7E	17	U12	INC	7	
			.		
			.		
			.		
			etc.		Sequence repeats for U12 - U1
			.		
			.		
			.		
05 B5	17	U1	INC	7	
B6	98		GHI	8	
B7	87		PHI	7	UPTR + 1
B8	99		GHI	9	
B9	57		STR	7	I → M(UPTR)
BA	12	U0	INC	2	Restore M(RX) = NHT
BB	30 70		BR	UEXIT	Go to UEXIT

Table C-4  
DELAY LINE ROUTINE

ADDRESS	CODE	LABEL	MNEM.	OPERAND	COMMENTS
10 00	F8 00	START	LDI	00	
02	B4		PHI	4	
03	A4		PLO	4	
04	E4		SEX	4	R4 = OPTR
05	7B		SEQ		Signal for input
06	3F 06	A1	BN4	A1	
08	6C		INP	C	
09	FA 0F		ANI	0F	
0B	54		STR	4	
0C	B5		PHI	5	Input and display
0D	64		OUT	4	High delay byte
0E	24		DEC	4	
0F	37 0F	A2	B4	A2	
11	37 11	A3	BN4	A3	
13	6C		INP	C	R5 = IPTR
14	64		OUT	4	Input and display
16	A5		PLO	5	Low delay byte
17	7A		REQ		
18	37 18	A4	B4	A4	
1A	3E 1A	LOOP	BN3	LOOP	Wait for clock pulse

Table C-4 cont.

ADDRESS	CODE	LABEL	MNEM.	OPERAND	COMMENTS
10 1C	E5		SEX	5	
1D	6F		INP	F	Input and display
1E	64		OUT	4	Current data
1F	E4		SEX	4	
20	67		OUT	7	Output delayed data
21	94		GHI	4	
22	FA 0F		ANI	0F	
24	84		PHI	4	
25	95		GHI	5	
26	FA 0F		ANI	0F	
28	85		PHI	5	
29	3F 1A		BN4	LOOP	Repeat unless delay change desired
2B	30 00		BR	START	



## APPENDIX D

### NUMERICAL SENSITIVITY STUDY

In the formulation of the numerically simulated vortex street structure given in Chapter V, it was necessary to choose values for four similarity proportionality constants and to select a model for the vortices. The effects of variations from the choices which were utilized in Chapter V are given in this appendix.

#### 1. Proportionality Constants

Of the four proportionality constants involved in the numerical simulation, the pattern wavelength coefficient,  $C_L$ , and the vortex strength coefficient,  $C_T$ , could be set directly from experimental observations. The choices for the offset distance coefficient,  $C_H$ , and vortex core radius coefficient,  $C_R$ , were based on less objective criteria. For these two parameters, the selection was based upon finding the optimum combination which would yield the best agreement between numerically calculated and experimentally determined distributions of  $\bar{U}$ ,  $\bar{V}$  and  $\bar{UV}$ . The values chosen were  $C_H = .05$  and  $C_R = .13$ .

To examine the sensitivity of the calculations to these parameters, they were repeated with  $\pm 25\%$  variations

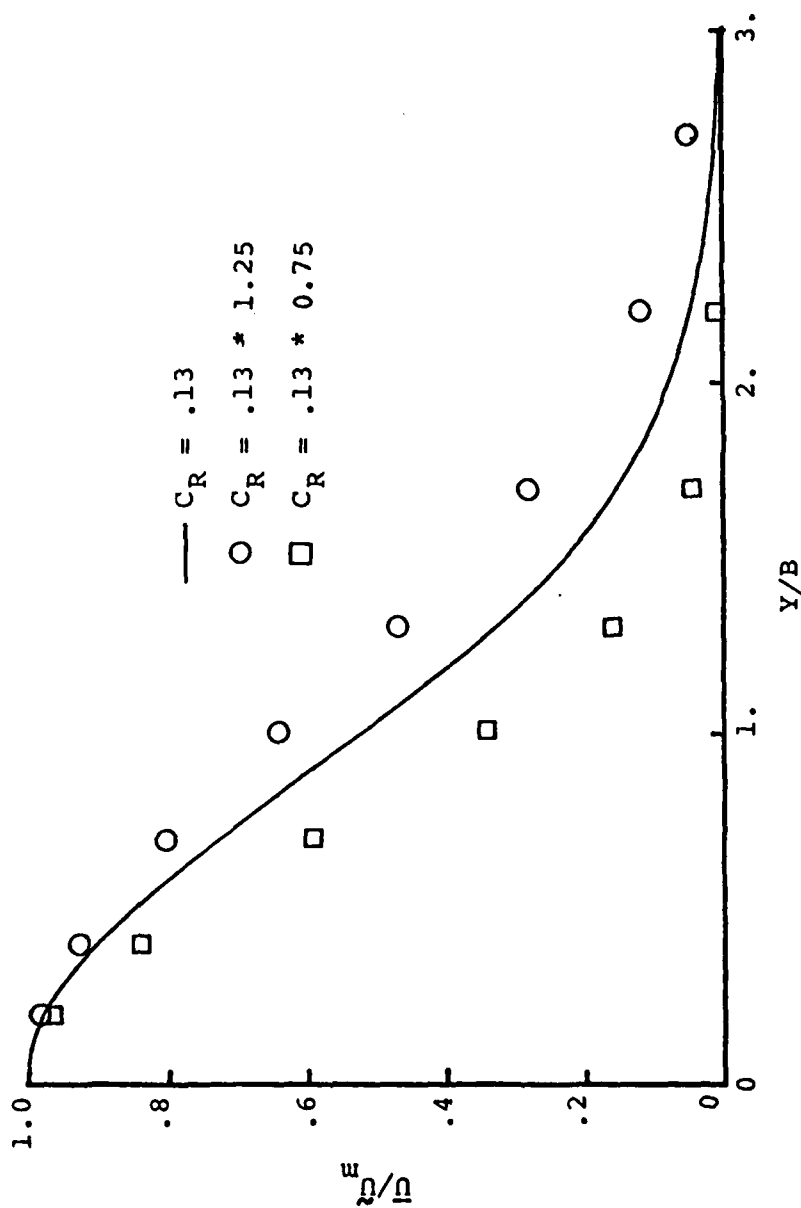
of the coefficients from their "optimum" values. Only one coefficient was varied for each case.

Figures D-1 through D-4 illustrate the sensitivity of the calculations to  $C_R$  and Figures D-5 through D-8 demonstrate the effects of variation of  $C_H$ . From the figures, it is noted that  $C_R$  has a comparatively stronger influence on the mean velocity profiles while the Reynolds stress and fluctuating intensities are more sensitive to  $C_H$ .

## 2. The Vortex Model

For the calculations described in Chapter V, a Rankine vortex was utilized to represent the individual vortices making up the vortex street. In the discussion of the results, it was argued that the capability of the model to calculate reasonable distributions of mean lateral velocity and Reynolds stress is a direct consequence of the model being able to calculate the mean longitudinal velocity accurately.

Figure D-9 illustrates the tangential velocity distribution for an alternate choice of the vortex model. In this representation, the induced velocity is exactly a potential vortex for  $r > r_c$  and solid body rotation for  $r < r_c$ . The discontinuity of the velocity derivative at  $r = r_c$  for the alternate choice should result in significant changes in the calculated results if it hampers the capability of the model to predict the mean longitudinal velocity.

Figure D-1 Sensitivity of  $\tilde{u}(x, y/B)/\tilde{u}_m(x)$  to  $C_R$

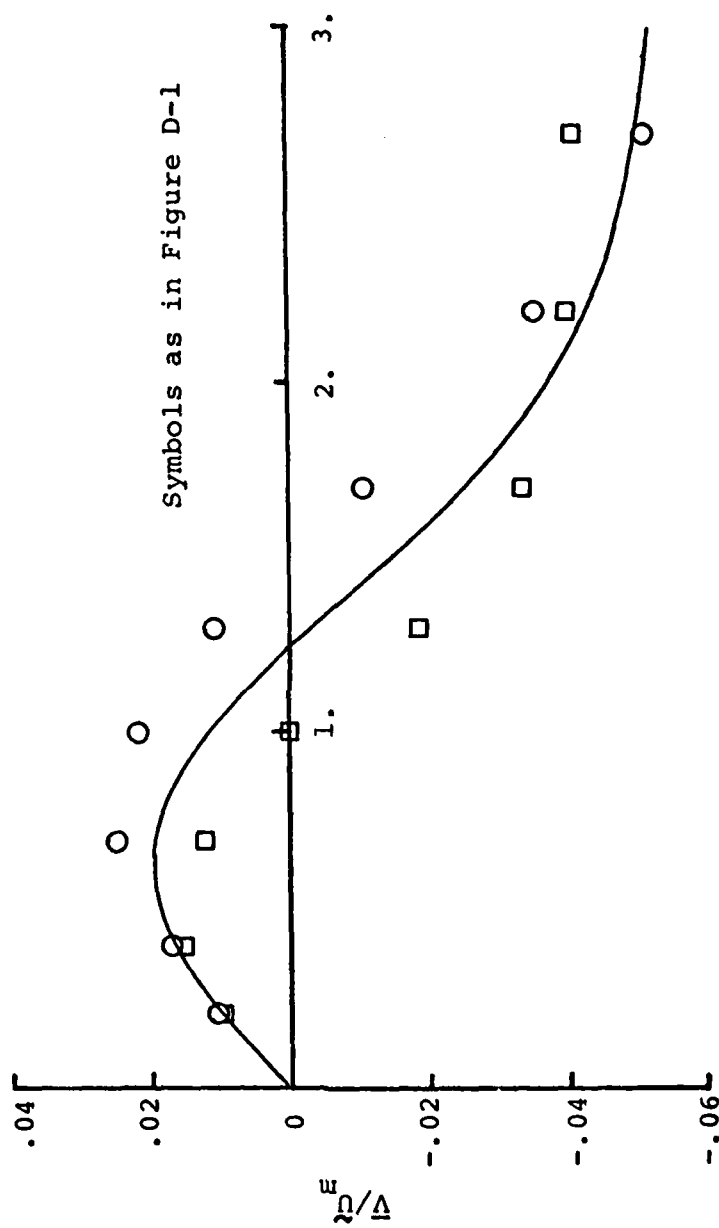


Figure D-2 Sensitivity of  $\bar{V}(x, y/B)/\bar{U}_m(x)$  to  $C_R$

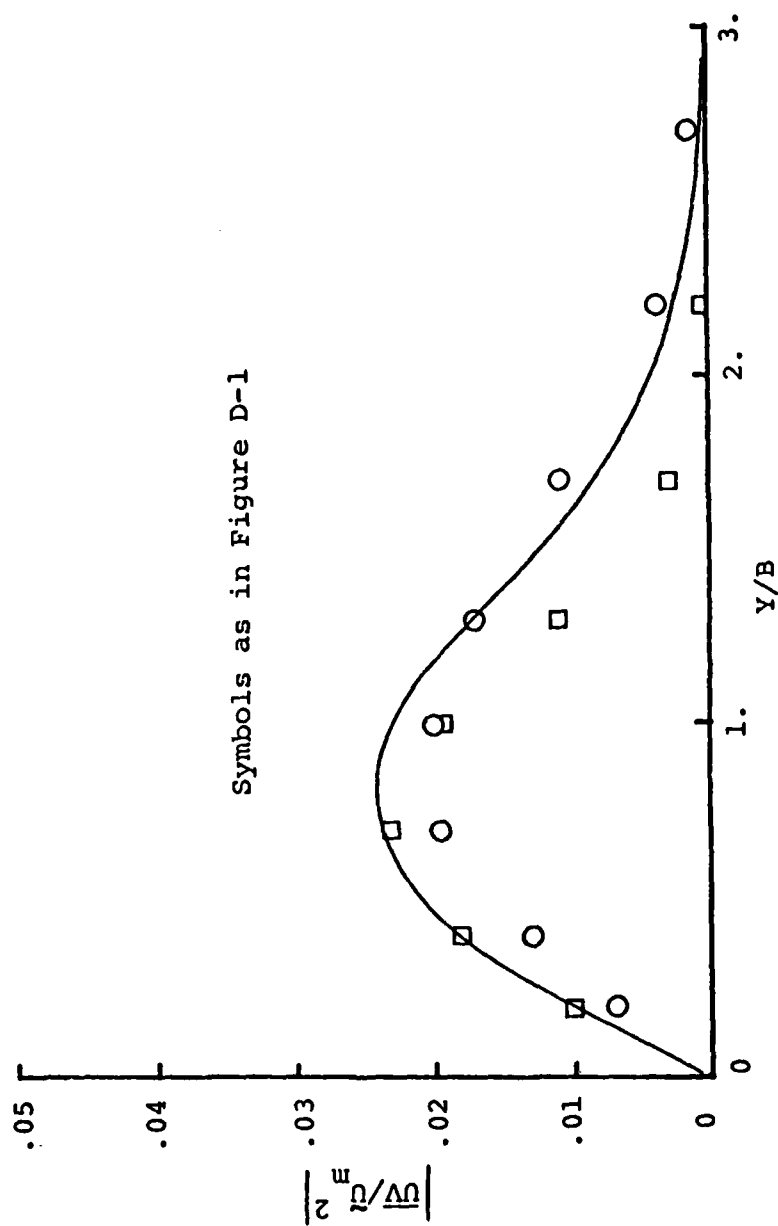


Figure D-3 Sensitivity of  $|\overline{uv}(x,y/B)/\tilde{u}_m^2(x)^2|$  to  $C_R$

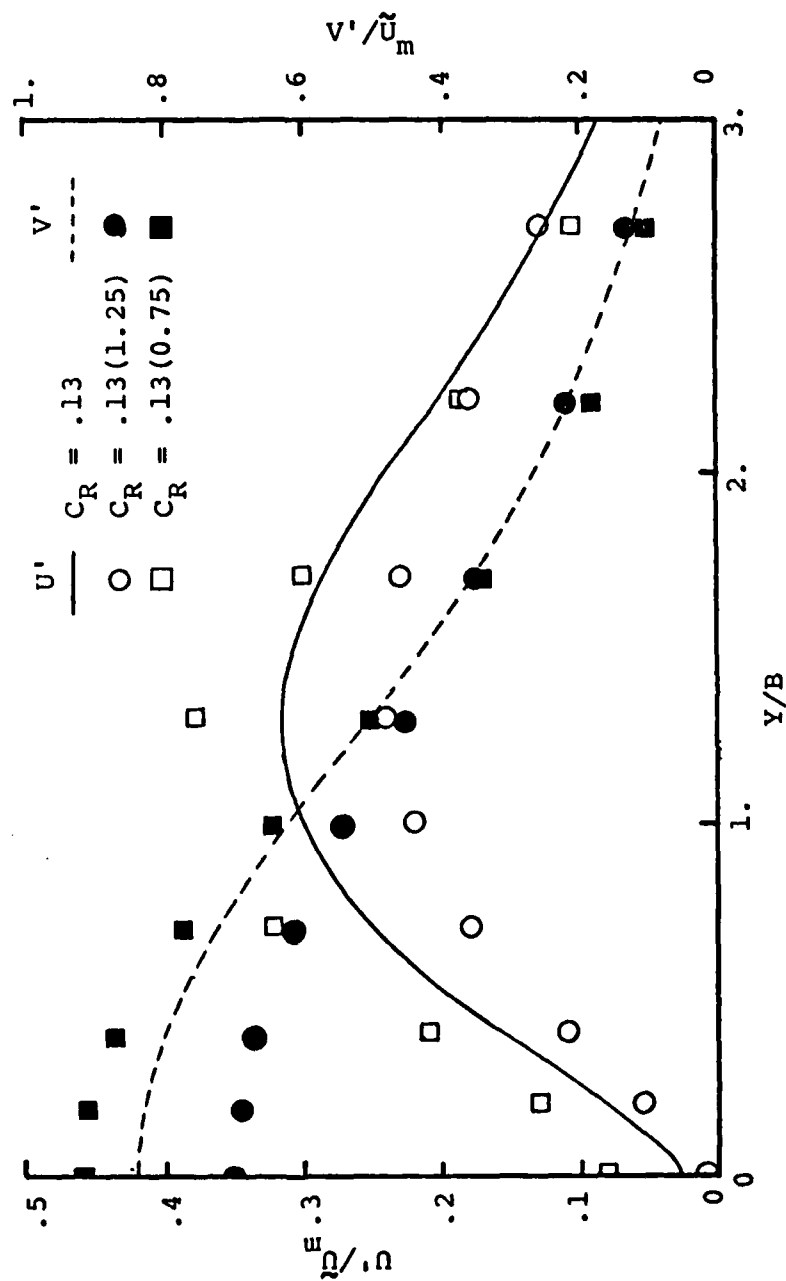


Figure D-4 Sensitivity of  $U'$  ( $X, Y/B$ ) and  $V'$  ( $X, Y/B$ ) to  $C_R$

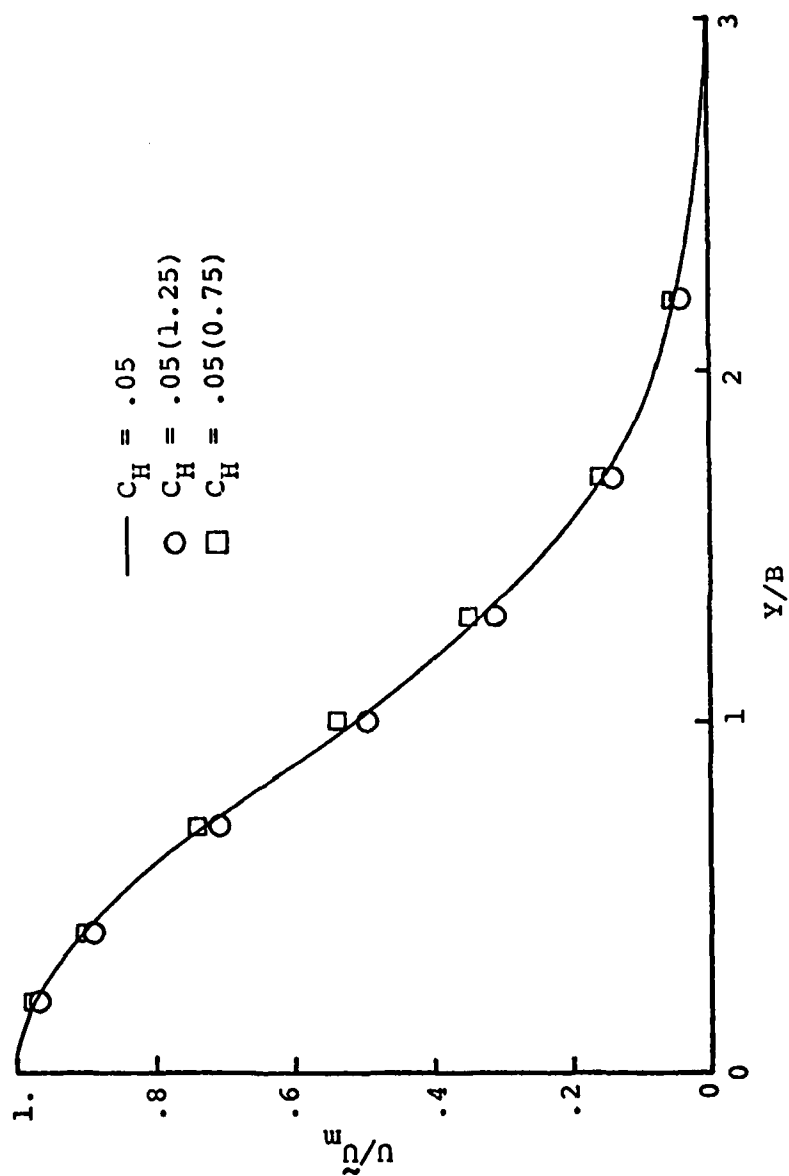


Figure D-5 Sensitivity of  $\bar{u}(x, y/B)/\bar{u}_m(x)$  to  $C_H$

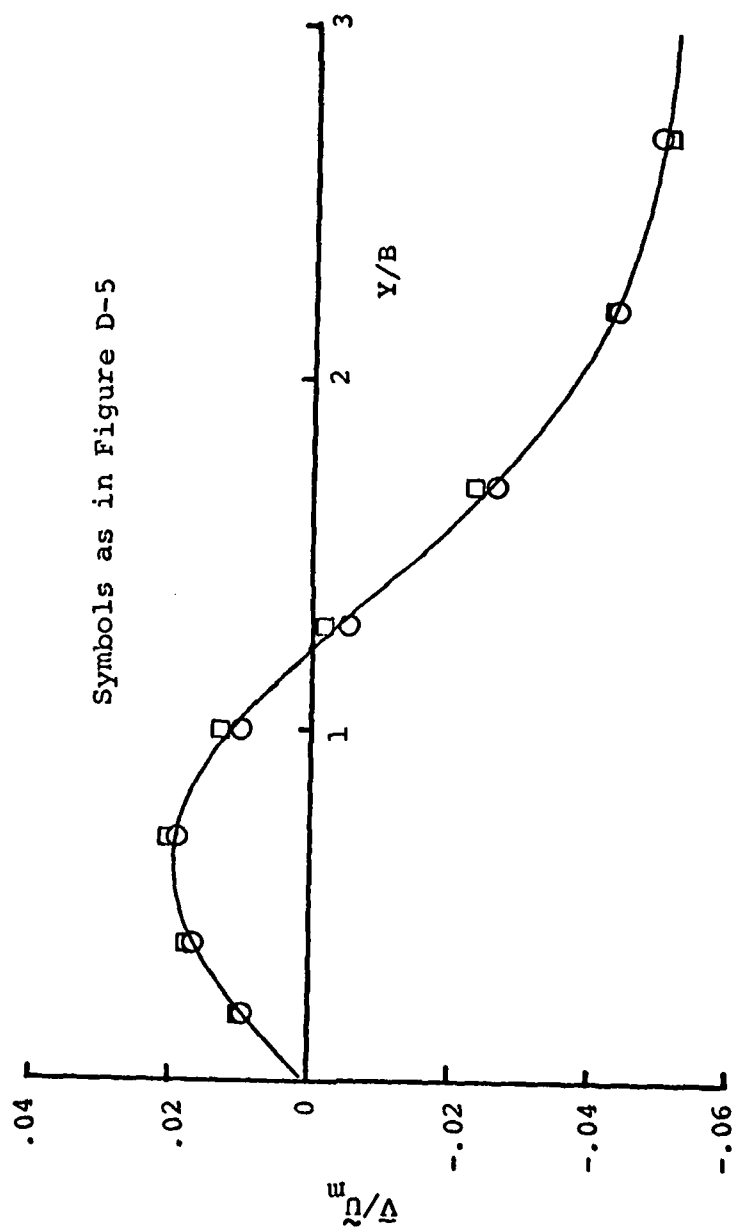


Figure D-6 Sensitivity of  $\bar{V}(x, y/B)/\tilde{U}_m(x)$  to  $C_H$



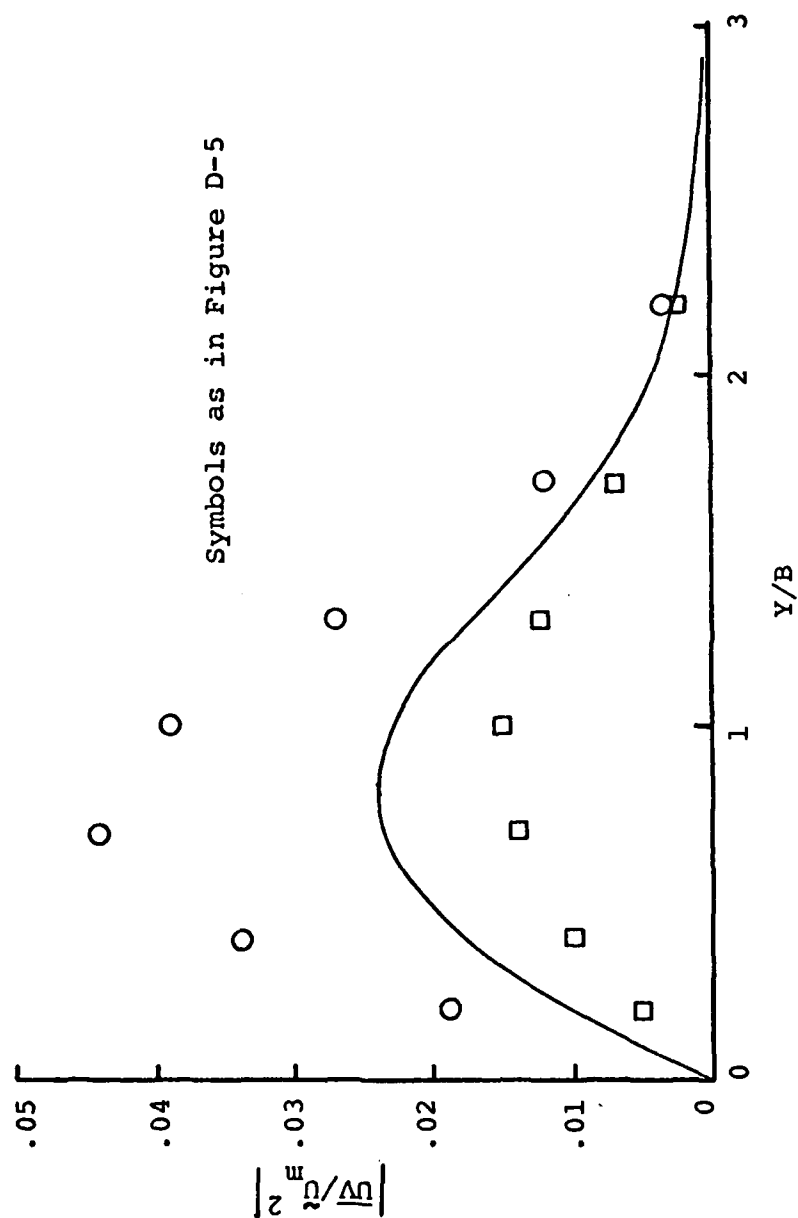
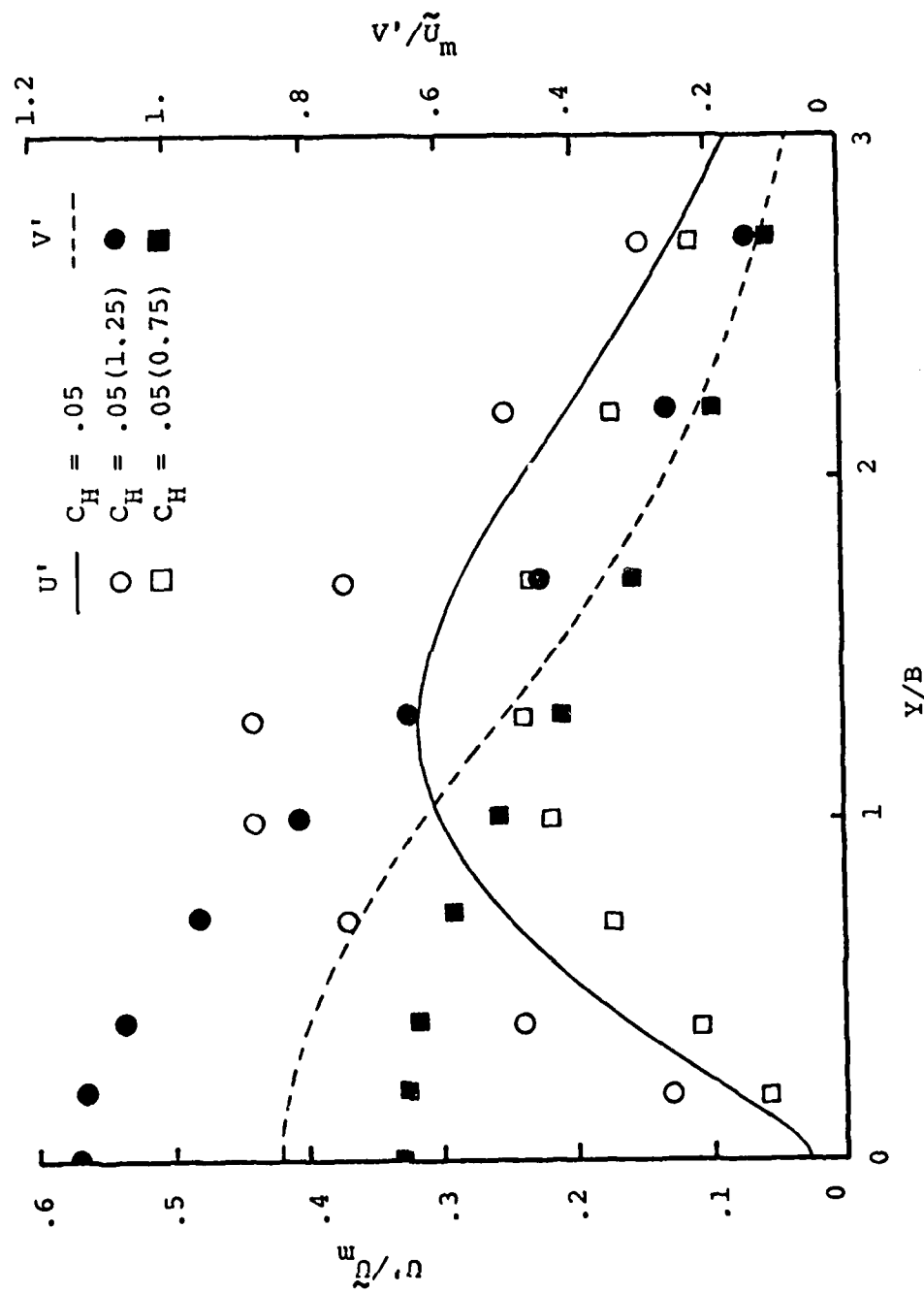


Figure D-7 Sensitivity of  $|\overline{uv}(x, y/B)/\tilde{u}_m(x)^2|$  to  $C_H$

Figure D-8 Sensitivity of  $U'$  ( $X, Y/B$ ) and  $V'$  ( $X, Y/B$ ) to  $C_H$

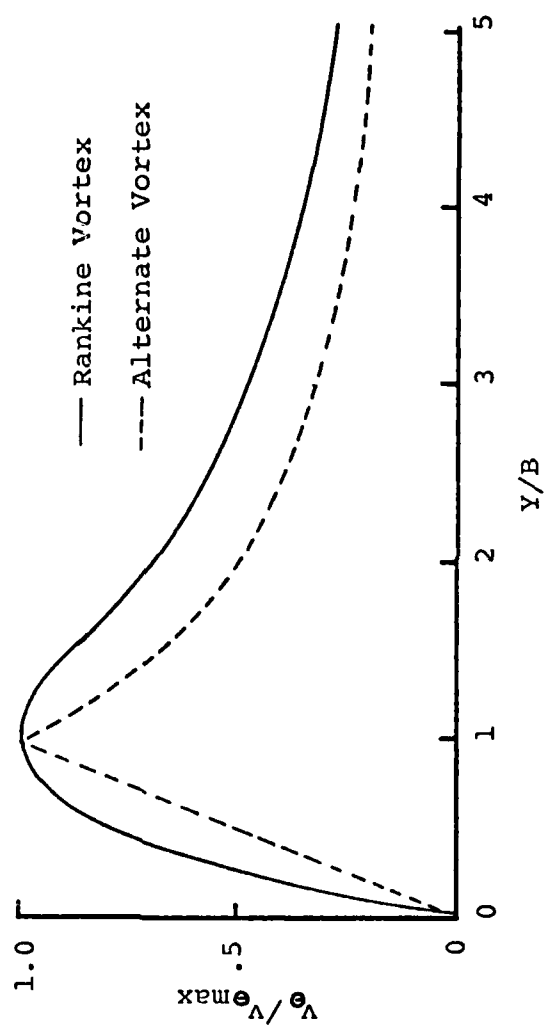


Figure D-9 Alternate Vortex Velocity Distribution

AD-A088 750

PURDUE UNIV LAFAYETTE IND RAY W HERRICK LABS F/G 20/4  
COHERENT STRUCTURES IN THE SIMILARITY REGION OF A TWO-DIMENSION--ETC(U)  
MAR 80 J W OLER, V W GOLDSCHMIDT N00014-75-C-1048  
HL-80-6 NL

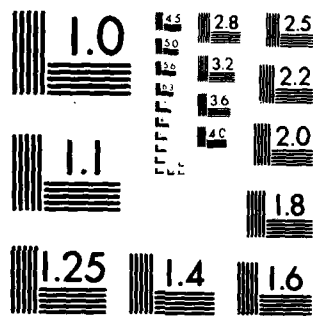
UNCLASSIFIED

3-3

By Hand



END  
DATE  
FILMED  
10 80  
DTIC



MICROCOPY RESOLUTION TEST CHART  
NATIONAL BUREAU OF STANDARDS 1963 A

The results of calculations utilizing the alternate vortex are given in Figures D-10 through D-13. For these calculations,  $C_L$  and  $C_H$  were held to the same values as for those with the Rankine vortex.  $C_T$  was set to 2.401 rather than 2.597 in order to match the experimentally determined mean centerline velocity. A value of  $C_R = .125$  instead of  $C_R = .130$  was needed to provide the expected spreading rate (i.e.,  $\bar{U}/\bar{U}_m = .5$  at  $Y/B = 1$ ).

From the results, it is noted that the subtle changes in the slope of the mean longitudinal velocity profile are associated with changes in the lateral velocity and Reynolds stress. The overall magnitudes are, however, approximately the same as for the calculations using Rankine vortices. The "saddle-back" distribution of the Reynolds stress might have been expected from the presence of the velocity derivative term in Eq. 5.57.

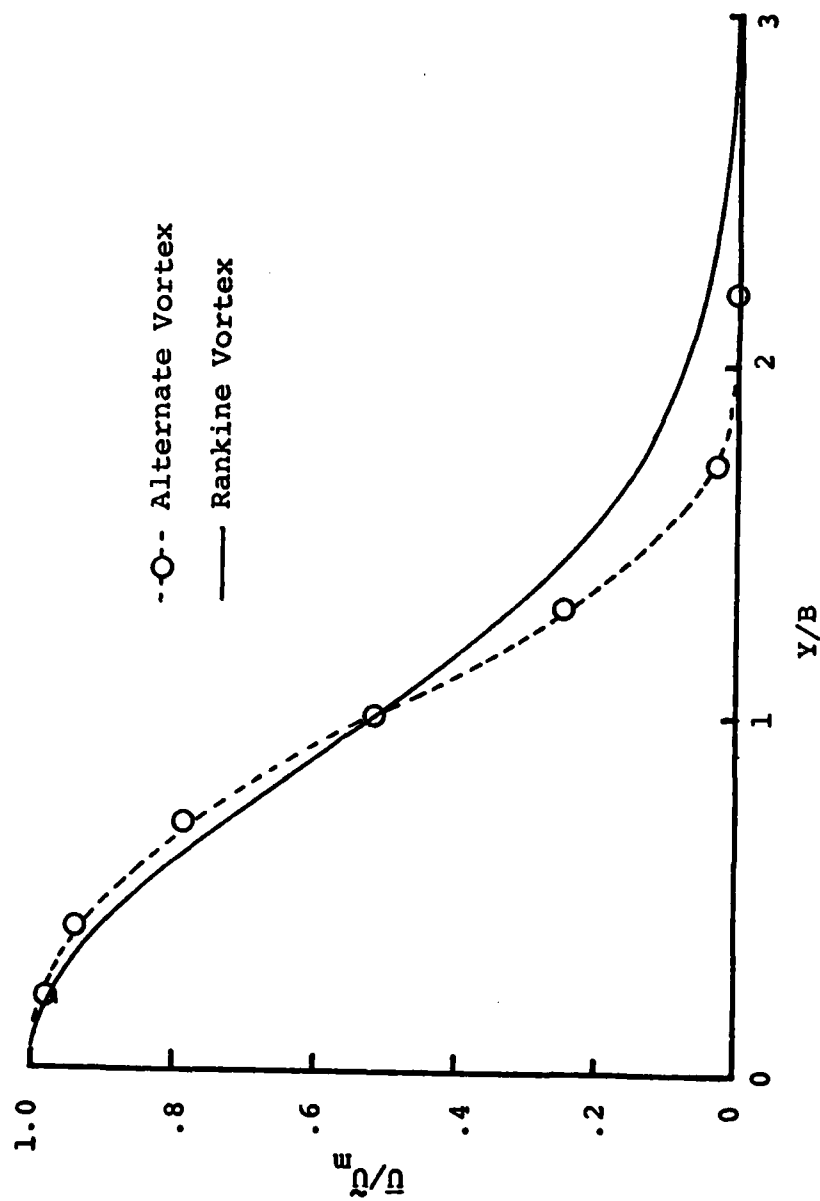


Figure D-10 Sensitivity of  $\bar{u}(x, y/B)/\bar{u}_m(x)$  to Vortex Model Choice

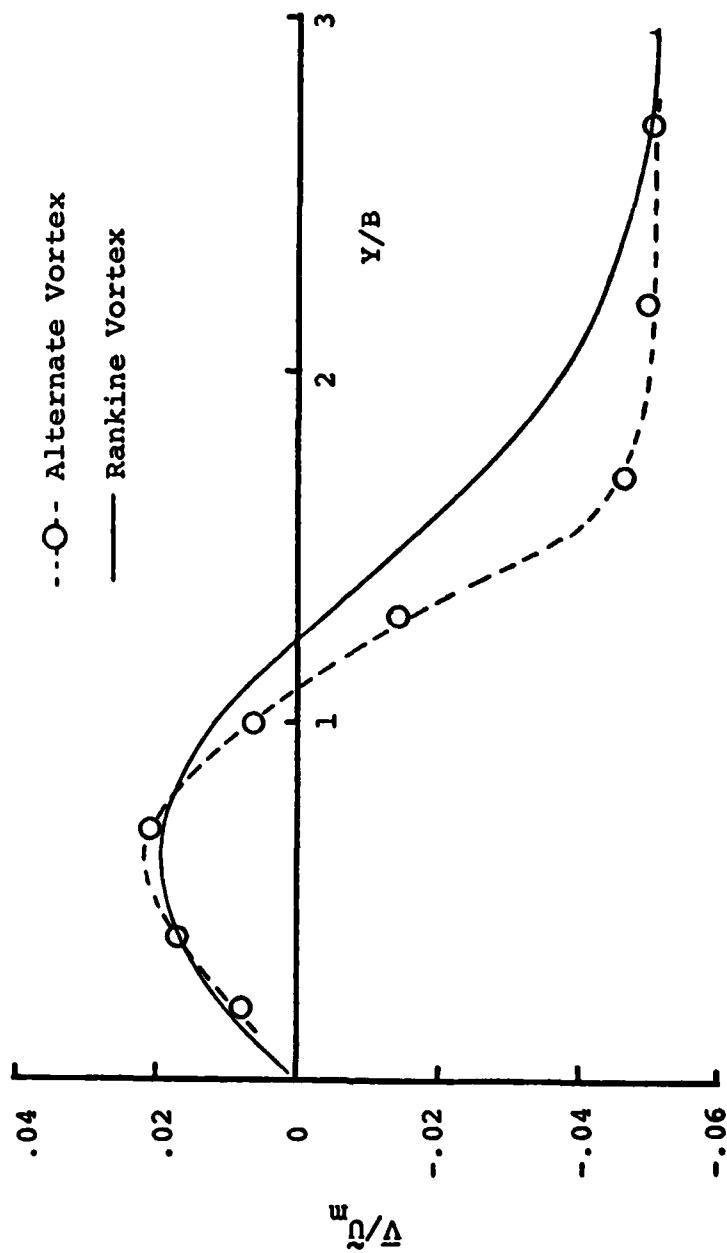


Figure D-11 Sensitivity of  $\bar{V}(x, Y/B)/\bar{U}_m(x)$  to Vortex Model Choice



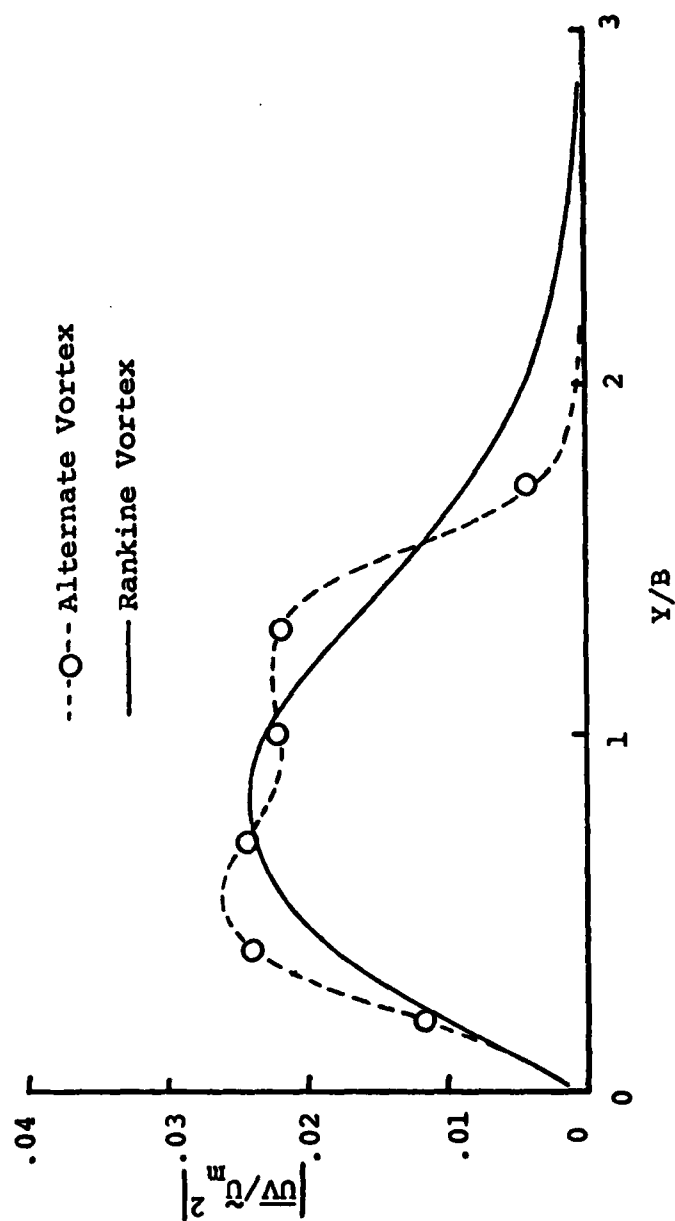


Figure D-12 Sensitivity of  $|\bar{U}(x, Y/B) - \bar{U}_m(x)|^2$  to Vortex Model Choice

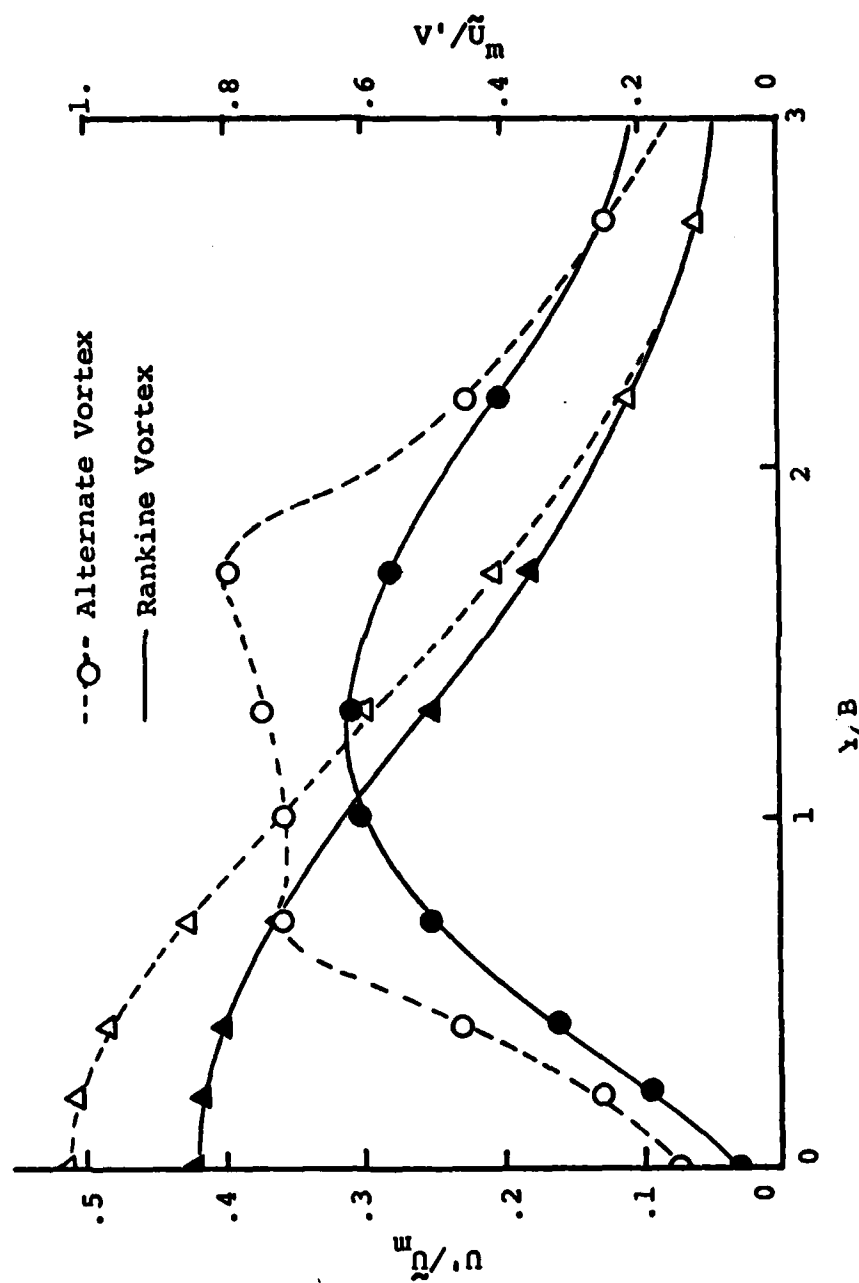


Figure D-13 Sensitivity of  $U' (X, Y/B)$  and  $V' (X, Y/B)$  to Vortex Model Choice

VITA

## VITA

James Walter Oler was born on September 3, 1950 in Tulia, Texas. After graduating from Tulia High School in 1969, he attended the University of Texas-Austin. There, he earned his B.S. and M.S. degrees in aerospace engineering during 1974 and 1976, respectively. From 1976 through 1980, he attended Purdue University where he earned the Doctor of Philosophy degree in mechanical engineering. After graduation, he went to Texas Tech University where he is currently serving as an assistant professor.